Towards the introduction of communication between metallo-supramolecular $[M_2L_3]^{2-}$ and $[M_2L_3]^{4+}$ assemblies.

A thesis submitted in partial fulfilment of the requirements for the degree of Masters of Science in Chemistry.

Lily M. Hermanspahn

University of Canterbury

2017

Acknowledgements

Firstly I would like to thank my supervisor, Professor Paul E. Kruger for his support, guidance and encouragement throughout the duration of my Masters thesis. To Dr Chris Fitchett I would also like to extend my thanks in particular for helpful discussion during group meetings. I would also like to thank Dr Jas S. Ward for his assistance in the lab, X-ray crystallography and for his general help towards my project.

To all the past and present members of the Kruger group, I would like to thank you for your friendship and support throughout the last two years. You have helped create a friendly lab environment, given encouragement and great advice both outside and within the lab environment. Thank you in particular to Sarah Jamieson, who has been a support since first year. I would also like to thank other people within the department for their friendship and support, in particular Anna Farquhar, Samantha Bodman, Andrew Flanagan, and Nic Bason.

I would also like to acknowledge the Academic Staff within the department who have taught me throughout the years. Also to the chemistry technicians who help the chemistry department run smoothly, in particular Wayne Mackay and Rob McGregor for their help with fixing any broken gear. I would additionally like to thank Dr Matt Polson, Dr Marie Squire and Dr Amelia Albrett for their help in particular with X-ray crystallography, NMR and Mass Spec. analysis. I would like to acknowledge Boujemaa Moubaraki, Professor Keith Murray and Benjamin Wilson for doing the magnetic characterisation. To the University of Canterbury I would like to thank for awarding me with a Masters Scholarship to assist with my studies.

Lastly I would like to thank all my family and friends in particular my parents for their continued love and support throughout the duration of my studies.

Atom colour scheme

Black: Carbon

Red: Oxygen

Blue: Nitrogen

Yellow: Sulphur

Purple: Potassium

Light Orange: Phosphorus

Green: Calcium

Pink: Rubidium

Dark Orange: Iron

Mauve: Cobalt

Light green: Nickel

Abstract

In this thesis the construction of a number of supramolecular entities was undertaken with the intention to probe their spin-crossover properties. The introduction of communication between metal complexes within the crystal lattice through non-covalent interactions was investigated in an attempt to probe cooperativity of any spin crossover (SCO). The coordination of two distinct ligands to create supramolecular $[M_2L_3]$ assemblies was investigated. Sulfonated helicates $[Fe(OH_2)_6][Fe_2\mathbf{L3}_3]$, $[Co(OH_2)_6][Co_2\mathbf{L4}_3]$, $[Ni(OH_2)_6][Ni_2\mathbf{L4}_3]$, $K_2[Fe_2\mathbf{L3}_3]$, $Ca[Fe_2\mathbf{L3}_3]$ and $[Fe(OH_2)_6]_{0.2}Rb_{1.6}[Fe_2\mathbf{L3}_3]$ were constructed from the precursor ligand 6,6'-oxy-*bis*(3-aminobenzenesulfonic acid). Preliminary investigations in the occurrence of SCO were conducted on the $[Fe(OH_2)_6][Fe_2\mathbf{L3}_3]$ and $[Co(OH_2)_6][Co_2\mathbf{L4}_3]$ metallo-helicates. In conjunction, phosphate supramolecular assemblies $\mathbf{[}Fe_2\mathbf{L5}_3]^{4+}$, $[Zn_2\mathbf{L5}_3]^{4+}$, $[Fe_2\mathbf{L6}_3]^{4+}$, $[Co_2\mathbf{L6}_3]^{4+}$, $[Ni_2\mathbf{L6}_3]^{4+}$, $[Co_2\mathbf{L7}_3]^{4+}$, $[Ni_2\mathbf{L7}_3]^{4+}$ and $[Cu_2\mathbf{L7}_3]^{4+}$ were also synthesised from the precursor ligand *bis*(4-aminophenyl)phenyl phosphate, however, further refinement of the crystallisation process is needed before spin-crossover studies can take place.

Table of Contents

Chapter 1:

Introduction

1.1 Preamble and Scope

The basis for this project was to investigate whether sub communication and subsequent cooperativity could be introduced between spin-crossover (SCO) capable 1st row transition metal centres in supramolecular assemblies. The key assemblies investigated consisted of those derived from the pro-ligands 6,6'oxybis(3-aminobenzenesulfonic acid) and *bis*(4-aminophenyl) phenylphosphate which coordinate to metal centres through bidentate iminoimidazole sites, after imine condensation with imidazolecarboxyaldehydes. The key interactions which were predicted to promote communication between supramolecular units included hydrogen bonding and π-π interactions. The pro-ligands described above could introduce these interactions through the presence of sulfonate and pendant benzene groups respectively. Structural studies, investigations into the intermolecular interactions and magnetic measurements were conducted on the supramolecular assemblies.

A brief introduction to supramolecular chemistry is outlined below. Owing to the large contribution of work conducted by a number of chemists within the field of supramolecular chemistry it is impossible to report all the significant results that have been achieved thus far. Therefore the core aspects of supramolecular chemistry relevant to this project have been covered which include self-assembly, common interactions within supramolecular chemistry and the potential properties such as SCO.

1.2 Supramolecular Chemistry

Molecular chemistry focuses on the covalent interactions or bonds within a molecular species.[1] Supramolecular chemistry focuses on interactions "beyond the molecule" where at least two chemical species are linked together by intermolecular rather than covalent forces.[1] The study of supramolecular chemistry has been of great interest after significant progress within this field was made by Cram,[2] Lehn[3] and Pedersen[4]. Their work in the field of

supramolecular chemistry was recognised by their joint Nobel Prize in Chemistry in 1987 "for their development and use of molecules with structure specific interactions of high selectivity". Supramolecular chemistry involves the combination of smaller sub-units resulting in larger structures which are the result of non-covalent interactions such as: π-π, hydrogen bonding, electrostatic, dipolar and coordination bonding interactions.[5] The π-π and hydrogen bonding interactions are particularly relevant to this study to investigate intramolecular cooperativity between supramolecular units and are therefore discussed in greater detail below.

1.2.1 Hydrogen bonding in supramolecular chemistry

Hydrogen bonds are electrostatic interactions between hydrogen atoms bonded to an neighbouring electronegative group such as oxygen nitrogen or fluorine. Supramolecular architectures can be stabilised through hydrogen bonding if the ligand contains hydrogen bonding functionalities.[6] The directionality of the hydrogen bond is an important factor of hydrogen bonding, with the angle between bonded and neighbouring electronegative groups usually within the range of 140° and 180°.[7] The angle is thought to be dependent on the strength of the hydrogen bonds, with smaller angles corresponding to weaker bonds. The structure directing roles of hydrogen bonds are demonstrated in the supramolecular assembly between cyanuric acid and melamine, which forms H-bonded 2D sheets. (**Fig. 1.1**).[8] Furthermore hydrogen bonds have significant biological importance due to its role within DNA base pairing and protein folding.[9]

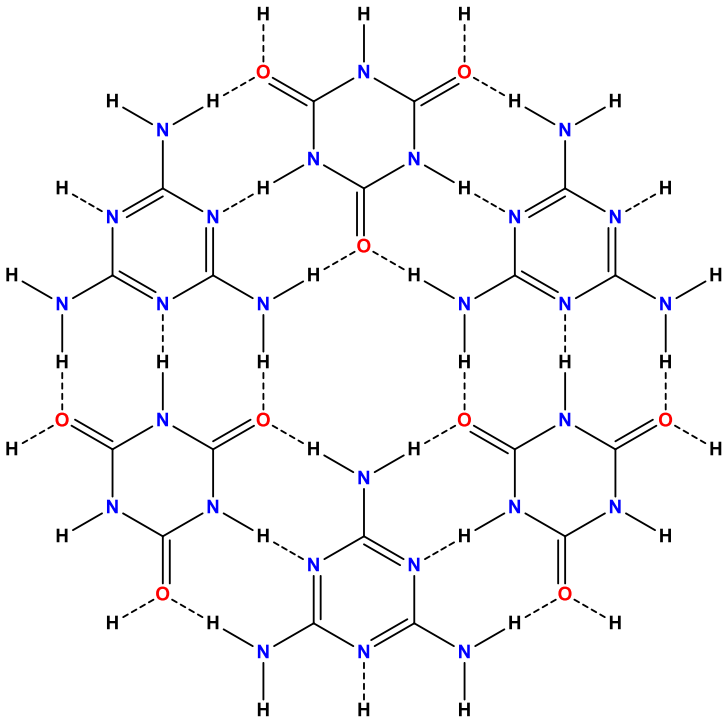

***Figure 1.1**: Supramolecular assembly through hydrogen bonds between cyanuric acid and melamine.*[8]

Guanidinium is known to have facile hydrogen bonding through its NH_2^+ groups with sulfonate and phosphate molecules. The incorporation of guanidinium salts into supramolecular structures has been reported in the literature.[10] It has been involved in the formation of 2-dimensional networks formed with guanidinium and sulfonate groups (**Fig. 1.2**).[11] Guanidinium has also been seen to cap the face of an edge-bridged tetrahedral cage formed by sulfonated ligands.[10] The high affinity of guanidinium for sulfonate groups makes guanidinium a good candidate for investigating communication between supramolecular structures formed with the sulfonated ligand 6,6'oxybis(3-aminobenzenesulfonic acid) used within this thesis.

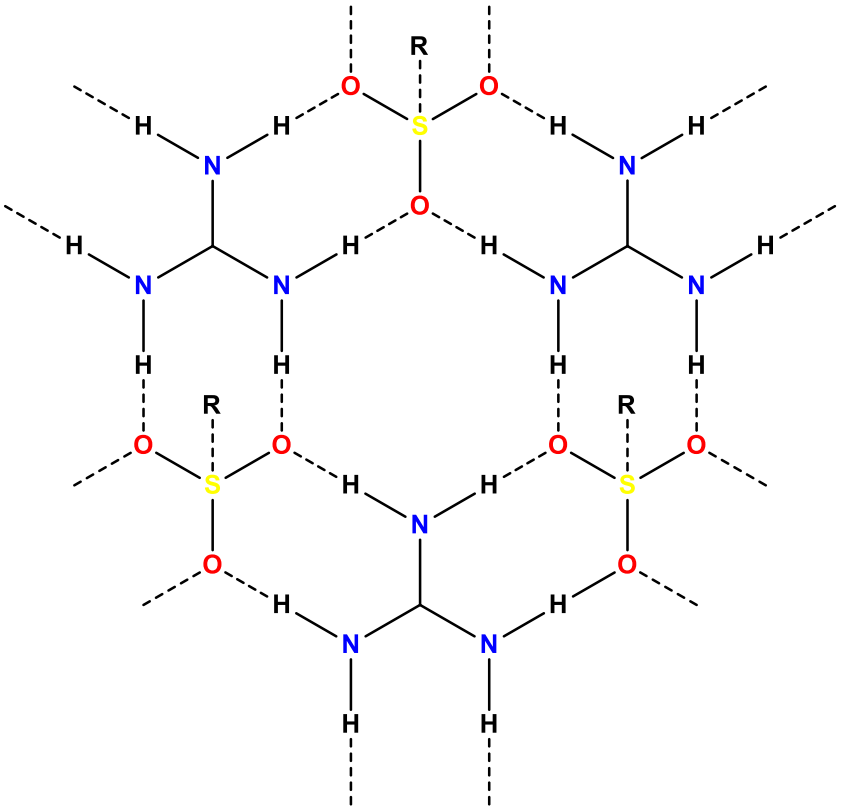

***Figure 1.2**: A 2-dimensional hydrogen bonding network formed with guanidinium and sulfonate groups.*[11]

1.2.1 π-π interactions in supramolecular chemistry

The interactions of π systems with one another are considerably weaker than other non-covalent interactions such as hydrogen bonding. These interactions are due to a quadrupole moment that is created from π electron density. In aromatic systems this generates a partial negative charge present above and below the face of the aromatic molecule and a partial positive charge around the edge.[12] Due to these electrostatic considerations centre-faced stacking (where aromatic systems are aligned directly on top of one another) is disfavoured as there is repulsion from the partial negative charges on the face of the molecule. Interactions between aromatic molecules are predominantly off-set parallel stacking or edge to face interactions where the electrostatic repulsion is minimised.[13] Substitution of different

functional groups onto the periphery of aromatic rings has shown to affect the electrostatic properties of the aromatic molecule. Electron-donating functional groups changes the electrostatics of the aromatic, decreasing the positive charge on the edge of the molecule.[12] Conversely, electron withdrawing groups substituted onto an aromatic ring result in the electron density to be drawn away from the centre of the molecule, allowing for face to face stacking to occur with an electron rich aromatic (**Fig. 1.3**).[14] The terms offset and edge to face stacking will be used to discuss the aromatic interactions within this study.

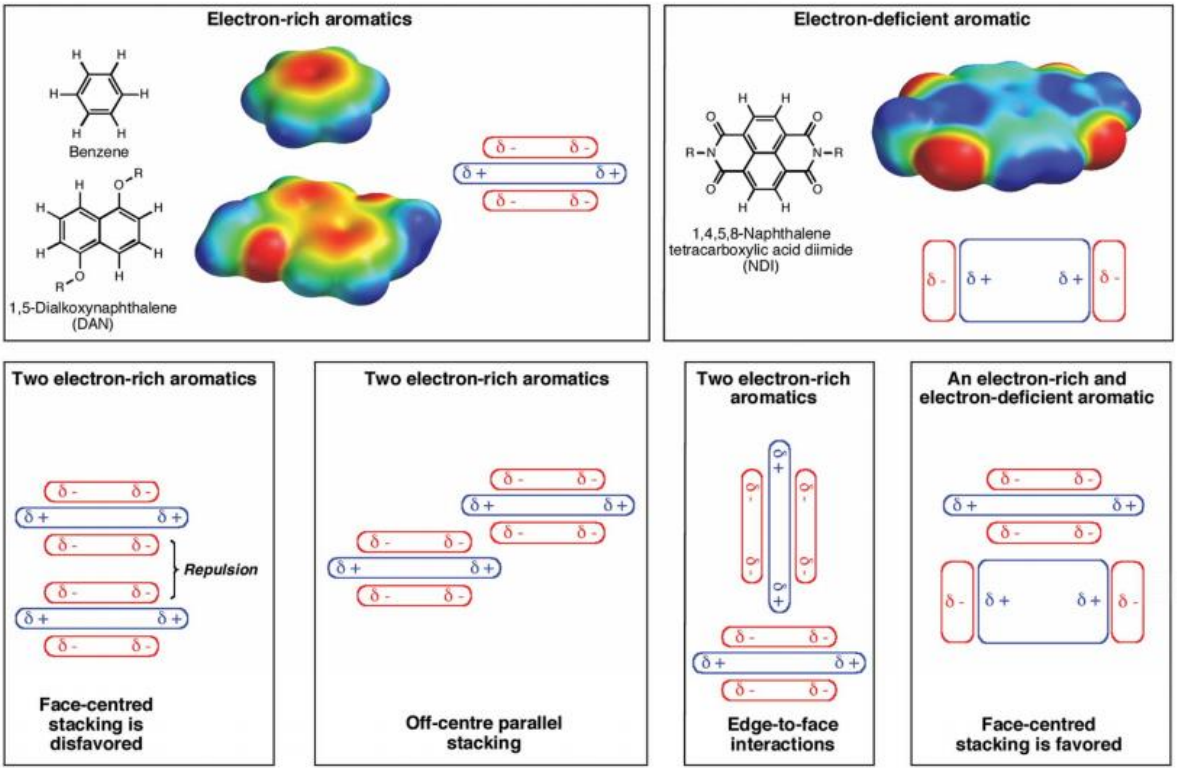

***Figure 1.3**: Schematic diagrams of the various interactions that can occur between aromatic electron rich and electron deficient molecules.*[14]

1.3 Metallo-supramolecular interactions and assemblies

Supramolecular assemblies which implement the strong coordination bonds formed between metal centres and ligands are termed metallo-supramolecular assemblies.[15] This involves the interaction of an electron poor metal centre with a ligand, which act as electron

acceptors and donors, respectively. One of the most common interactions involves nitrogen, *via* its lone pair, which can via a dative bond coordinate with the metal ion. Ligands are considered to be either hard or soft donors, dependant on the nature of the donor atoms. Ligands containing strongly electronegative donor atoms such as oxygen or nitrogen, have low polarizability and a small atomic radius. These are considered hard donors.[16] Those ligands containing donor atoms with low electronegivity, high polarizability and a large atomic radius, such as thiolates and phosphines are considered soft donors. The hard or soft nature of the ligand, influences the type of metal centre it coordinates to, with soft ligands coordinating to soft metals such as silver and hard ligands coordinating to hard metals such as iron or cobalt.

Monodentate coordination occurs when the ligand has one binding site and bidentate coordination occurs when multiple binding sites are on a ligand. Chelation is the formation of stabilised five, six or even seven membered rings between a bidentate ligand and the metal centre, stabilising the coordination interaction. The geometry of coordination often depends on the nature of the metal centre to which the ligands are coordinated which can direct the structure of the supramolecular assembly (**Fig. 1.4**). Though metal centres have preferred coordination geometries and oxidation states, their behaviour can be altered by the type or abundance of the ligand present.[17] Supramolecular structures within this thesis exhibit chelating bis-bidentate ligands that coordinate to the metal centres.

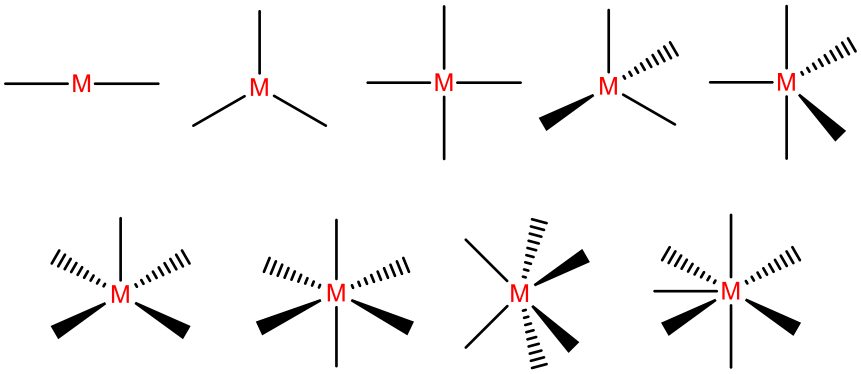

***Figure 1.4**: The metal coordination geometries commonly found in supramolecular complexes, from left to right: linear, trigonal planar, square planar, tetrahedral, trigonal bipyramid (top), square-based pyramidal, octahedral, trigonal prismatic, pentagonal bipyramidal (bottom).*[18]

Metallo-supramolecular assemblies consist of metal ions and ligands which can form a variety of polyhedral structures including helicates,[19] tetrahedra,[20] cubes,[21] truncated tetrahedra,[22] macrocycles,[23] cuboctahedron, pentagons[24] and numerous other architectures. These discrete molecules can form with the ligands either forming the edge, or the face of the polyhedra.[25] Interest in metallo-supramolecular assemblies has arisen due to their variability, ease of alteration and the potential applications they exhibit, which include: catalysis,[26] drug delivery,[27] molecule stabilisation,[28] molecule isolation,[29] influencing stereochemistry,[26] and molecular machines.[30]

1.4 Self-Assembly

The formation of supramolecular assemblies most commonly occurs through self-assembly processes, where smaller building units come together due to a combination of favourable interactions.[31] For metallo-supramolecular structures this interaction is the coordination between ligands and metal ions but can be modulated by the weaker interactions such as hydrogen bonds and π-π forces.[32] This allows for the variation in the structure and properties of these architectures through moderation of either the metal ion or ligand used in

the self-assembly process. Drastically different supramolecular outcomes can arise by altering the metal ion, where different metals with the same coordination geometries and ligand have been observed to give different supramolecular structures.[33] An example of this has been provided by Nitschke *et al.*, where five unique supramolecular assemblies were formed using the same ligand, with changes to either the metal ion or anion, (**Scheme. 1.1**).[34] Changing the number or type of donor atoms in the ligand or introducing spacer groups also affects the supramolecular scaffold that is formed.[35-36] The final outcome of the structure can also often be affected by the stoichiometry of metal and ligand, adding to the number of tuneable features available in the synthesis of supramolecular architectures. The ease of synthesis makes self-assembly highly desirable as multiple synthetic steps are not required. Reversibility and lability of the metal-ligand coordination bond is important for creation of supramolecular assemblies due to the possibility of the kinetic and thermodynamic products forming. The formation of the unwanted polymeric kinetic products can be reversed due to coordination bond lability. The thermodynamically stable product can therefore be formed, which due to entropic factors are often discrete molecules as opposed to polymeric structures (**Figure 1.5**).[33] Self-assembly can also be assisted by the other stabilising interactions, including hydrogen bonding, chelation effects and host-guest interactions.

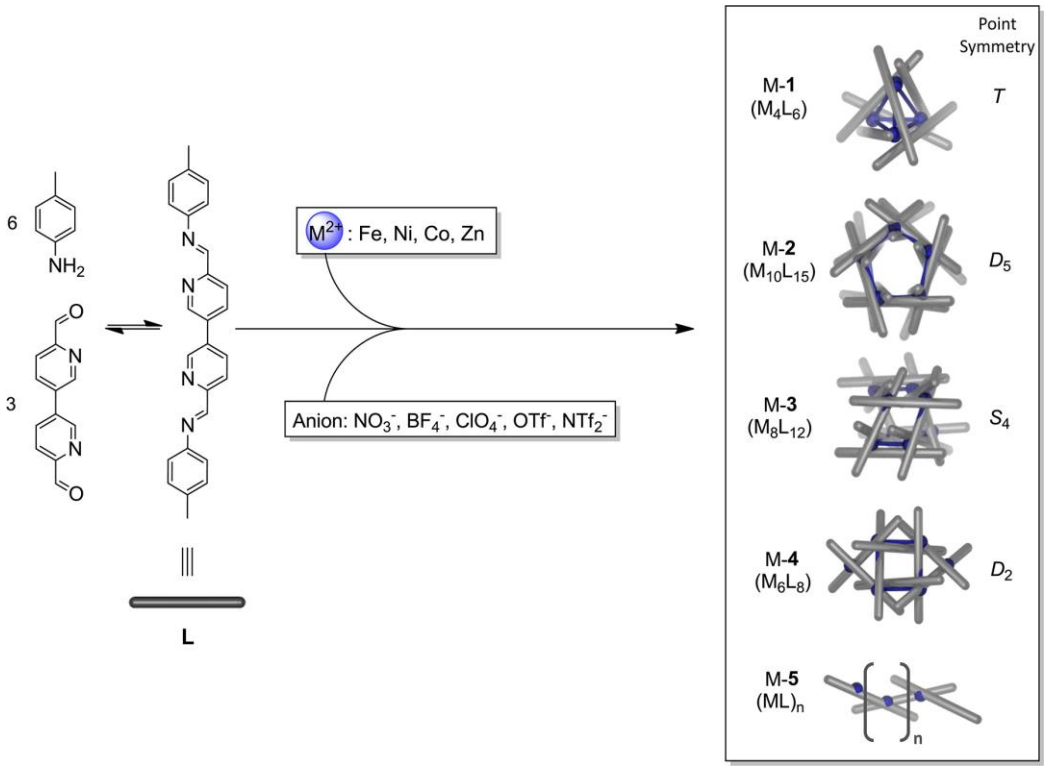

Scheme 1.1: *The subcomponent assembly of five different supramolecular architectures containing the same ligand, formed when exposed to different metal ions and anions.*[34]

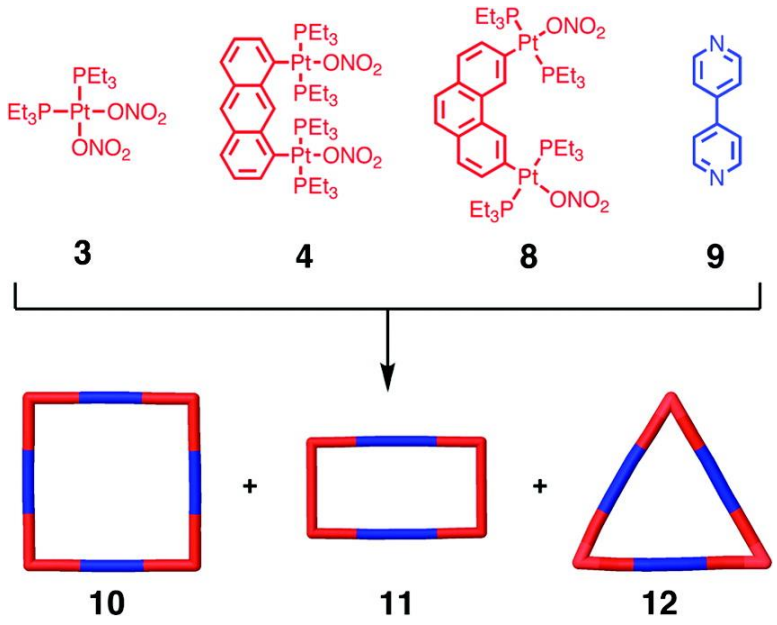

Figure 1.5*: Combinations of the resulting ligands preferably form discrete structures as opposed to polymeric chains due to entropic factors.*[37]

1.5 Metallo-Helicates

Helical molecules have been readily studied in chemistry with the discovery of the helical nature of DNA by Watson and Crick in 1953 increasing the interest in the field.[38] Supramolecular helical structures, or 'helicates', which are comprised of organic based ligands which form helical twists around the metal centres have also been established.[39] Helicates can form with varying number of metal centres, which is dependent on the number of coordinating sites of the ligand (**Fig. 1.6**).

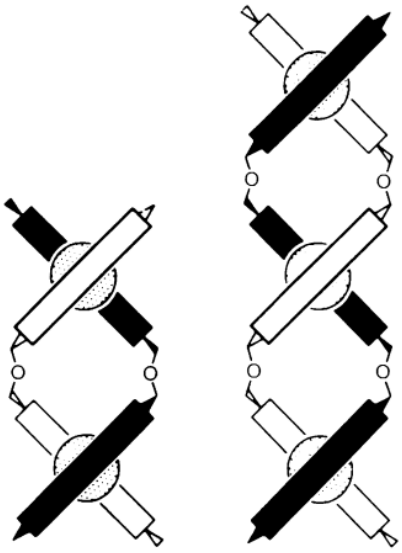

Figure 1.6*: Schematic representation of helicates where the ligands are coordinated to two (left) or three (right) metal centres.*[39]

The term helicates comes from the Greek word *helix*, depicting a 3-D supramolecular spiral or twist. Helicates in which the ligands twist uniformly in one direction gives the supramolecular assembly chirality. The helicate is considered right handed (Δ=P) or left handed (Λ=M) depending on whether the rotation is clockwise or anticlockwise viewing down the pitch of the helicate.[40] Helicates can be characterised and named by a number of terms, describing the structural nature of the helicate (**Fig. 1.7**). The number of ligands that

form the helicate are termed as strands, with the number of strands depicted as either single, double, triple or quadruple stranded when one, two, three or four ligands are coordinated, respectively. The binding sites on these strands which coordinate to the metal centres are either the same or different from one another, labelled homotopic or heterotopic, respectively. The alignment of the heterotopic strands are called either head-to-head or head-to-tail, depending on whether the same binding site is coordinated to the same metal in each strand, or if different binding sites coordinate to one metal. Helicates are termed as saturated when no auxiliary ligands are present and unsaturated when additional ligands are coordinated to the metal centres. The coordination preference of the metals influences whether the helicate formed is a double or triple stranded helicate, saturated or unsaturated. It has been observed that the same ligand forms a double stranded helicate when complexed with a metal centre favouring tetrahedral coordination, and a triple stranded helicate when complexed with a metal that prefers an octahedral arrangement.[41] The denticity of the ligand will therefore influence the number of strands required to fulfil the coordination requirements of the metal centres geometry, with exception to unsaturated helicates were ligands other than the helicate strands are coordinated to the metal.

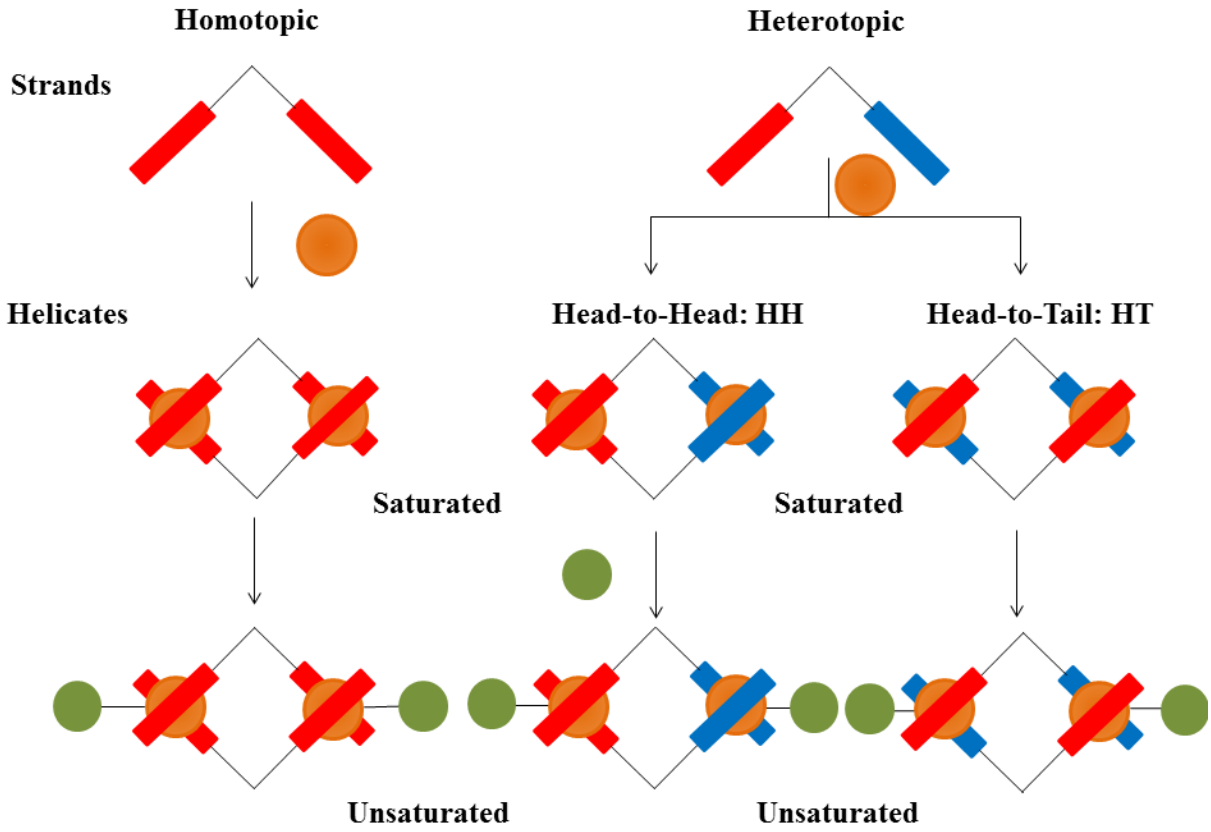

***Figure 1.7**: Schematic diagram of different terms used to describe helicates.*[40]

Mesocates can share the metal and ligand stoichiometry of helicates; however, they do not exhibit a helical twist of the ligands and are more cage-like in their arrangement (**Fig. 1.8**). The control over the stereochemistry and whether chiral helicates or achiral mesocates are formed preferentially is largely unknown. Some research has however, found that ligand rigidity and properties have an influence over the stereochemistry of the resultant $[M_2L_3]$ architecture.[42] The shape of the ligand influences the architecture which is formed, with linear ligands preferably forming helicates and those with increased flexibility have the ability to form either. The supramolecular assemblies discussed within this thesis are $[M_2L_3]^{2-}$ helicates and $[M_2L_3]^{4+}$ mesocates.

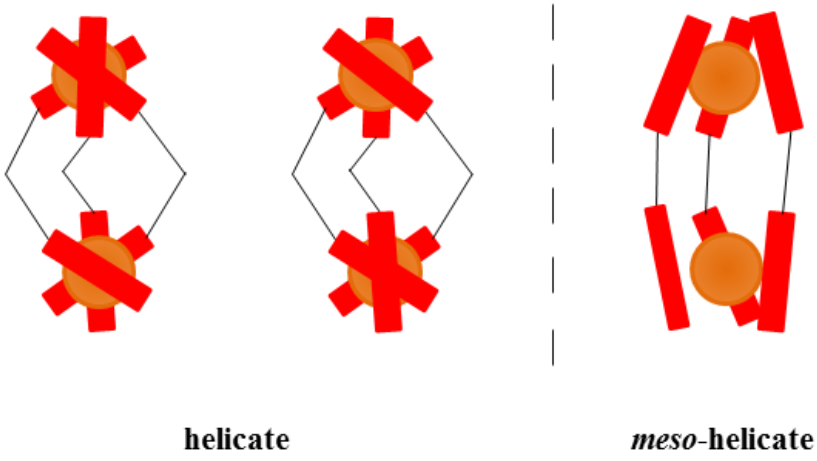

***Figure 1.8**: The schematic depiction of the [M_2L_3] helicate chiral enantiomers compared with the achiral mesocate.*[42]

1.6 Spin Crossover

Spin-crossover is a phenomenon where switching can occur between the high-spin (HS) and low spin (LS) spin states in metal centres.[43-44] This occurrence is seen in $3d^4$-$3d^7$ transition metal complexes, when the energies of the HS and LS states are close enough to one another to permit spin state switching.[45] In complexes containing transition metals with octahedral geometry the d-orbitals split into the subsets t_{2g} and e_g,[45] where the energy between these states is determined by the ligand field strength, with weaker field ligands having a smaller energy gap and therefore favouring the HS state (**Fig. 1.9**).

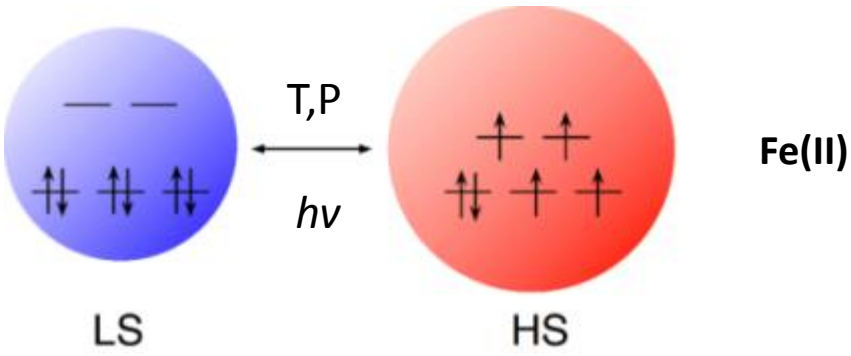

***Figure 1.9**: Reversible spin-state switching of octahedralFe(II) between high spin (HS) and low spin (LS), facilitated by temperature (T), pressure (P) or light (hv).*

Magnetisation is when a solid material is induced with a magnetic dipole. The magnetic dipole moment is measured per unit volume when a magnetic field is applied to the molecule. The extent as to which a molecule reacts to an applied magnetic field is measured through magnetic susceptibility.[46] This provides information on whether the molecule is attracted or repelled from the magnetic field, whether it is diamagnetic or paramagnetic. Diamagnetic molecules have paired dipole moments, and when present the magnetic moment acts against the external magnetic field. In paramagnetic molecules there are unpaired dipole moments, which results in a permanent magnet dipole moment. The susceptibilities of paramagnetic molecules are temperature dependant with the susceptibility varying inversely with temperature.[47]

1.7 Communication in Supramolecular Assemblies

First sphere coordination is the direct coordination of a ligand to a metal centre. Non coordinating interactions are called second sphere coordination.[48] Second sphere coordination has been shown to be able to alter magnetic, electronic, geometric and optical properties of metal complexes in the solid state.[48] Spin-crossover has been shown to be significantly affected through intermolecular second sphere hydrogen bond interactions,[49] therefore the introduction of hydrogen bonds could alter the spin-crossover properties of a complex. Introduction of communication can lead to cooperativity of metal centres' spin switching which can lead to a hysteresis effect. When spin crossover occurs abruptly or within a small temperature range, which is often a result of high cooperativity, thermal hysteresis can occur. Thermal hysteresis is when the temperature at which half the metal centres are HS and half are LS is lower upon cooling than on heating the outcome of which is a memory effect.[50]

1.8 Previous work on metallo-helicates with SCO

Previous research within the Kruger group has included investigations into supramolecular metallo-helicates including those with SCO properties. The link between the number of strands in a formed helicate and the steric bulk of a ligand was demonstrated *via* modulation of a novel dipyridyl-bispyrazole ligand. The formation of a double stranded helicate was the result of the sterically demanding ligand as opposed to the triple stranded helicate otherwise formed.[51-52] Investigations into anion binding and directing roles in supramolecular entities were also conducted, finding that particular helicates are formed through anion direction or were found to be capable of anion encapsulation.[53-54] Design strategies towards achieving particular supramolecular assemblies in relation to helicates were additionally demonstrated through a ligand which formed either molecular boxes or helicates

depending on the oxidation state of the metal it was complexed to.[55] Among many other helicate systems researched, the formation of SCO helicates was achieved through complexation of an imidazole based ligand (**Fig. 1.10**).[56] SCO was observed between the temperatures of 300 K and 80 K with slight thermal hysteresis being observed. Differences in SCO during heating and cooling modes suggest that the Fe(II) spin switching is occurring through a two-step process. Modulation of the ligand could potentially lead to altered SCO properties and metal cooperativity, which is discussed further below.

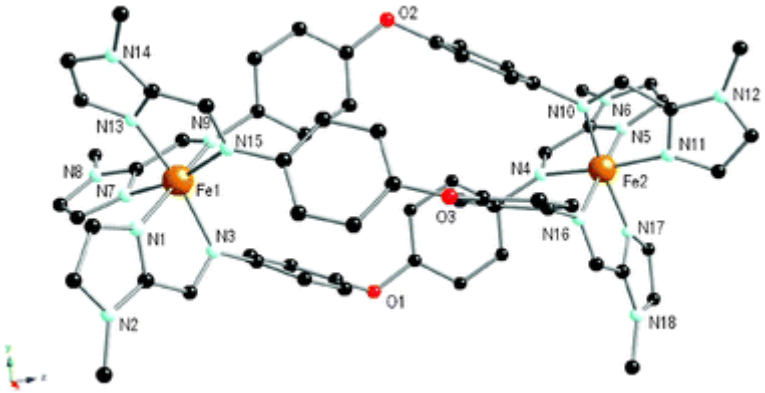

Figure 1.10: *Molecular structure of* $[Fe_2L_3]^{4+}$ *helicate which exhibits SCO properties* [56]

1.9 Aims of study

1.9.1 Design Strategies

The aim of this study was to introduce communication between spin crossover active metal centres to potentially introduce cooperativity between the spin switching metal centres. SCO often occurs in step transitions and communication of spin switching within the crystal lattice is frequently limited. To increase communication between supramolecular units, weak

non-covalent interactions are introduced through the ligands. Non-covalent interactions such as π-π interactions and H bonding can potentially bring order and intermolecular interactions between supramolecular entities. To achieve communication ligands with either strong hydrogen bonding or π-π interaction potentials were synthesised and accessed for supramolecular SCO capabilities.

1.9.2 Sulfonated helicates

Triple stranded helicates formed from the pro-ligand 6,6'oxybis(3-aminobenzenesulfonate), **L** (**Fig. 1.11**), reacted with 2-pyridinecarboxyaldehyde and Fe(II) metal centres, have previously been reported in the literature.[57-58] The complete complex, forms through *in situ* sub-component self-assembly. The ligand forms *via* an imine condensation between amines and aldehydes, resulting in the *bis*-bidentate ligands which form the complex. Pyridine imines are relatively strong field ligands, favouring low spin Fe(II) centres, in these $[M_2L_3]^{2-}$ structures. The sulfonated functionality on the helicate ligand introduces the potential for hydrogen bonding and second sphere coordination between helicate units, which could encourage communication and cooperativity between them. Work conducted within the Kruger group previously focused on helicates with the non-sulfonated analogue, 4,4'-oxyaniline, which formed the ligands with 1-methyl-2-imidazolecarboxyaldehyde. This ligand formed dinuclear triple stranded helicates with Fe(II) that exhibited spin-crossover properties which were discussed earlier.[56, 59] It would therefore be of additional interest to see whether this similar ligand could also create spin-crossover active helicates, such as those already observed.

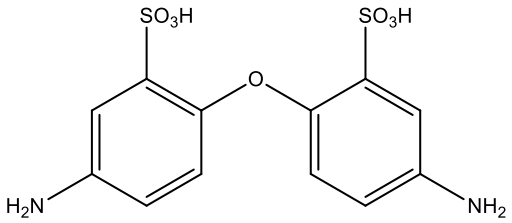

***Figure 1.11**: Structure of the pro-ligand, **L**.*

1.9.3 Organophosphate helicates

Introduction of a phosphate group into a ligand introduces a polar functional group, which has a lower water affinity than sulfonated ligands. Organic molecular cages have been constructed with phosphate functionalities incorporated within them.[60] Selective capture of CO_2 over other potential guests within this cage in particular has been observed. This cages selectivity for CO_2 has been associated to the appropriate size of the cavities but also the polarity of the P=O bond, showing that the incorporation of phosphate groups into supramolecular architectures could potentially lead to interesting applications. Previous work within our group has included incorporating a phosphate containing ligand, tris(4-((E)-(pyridim-2-ylmethylene)amino)phenyl) phosphate, into a metallosupramolecular tetrahedral cage (**Fig. 1.12**).

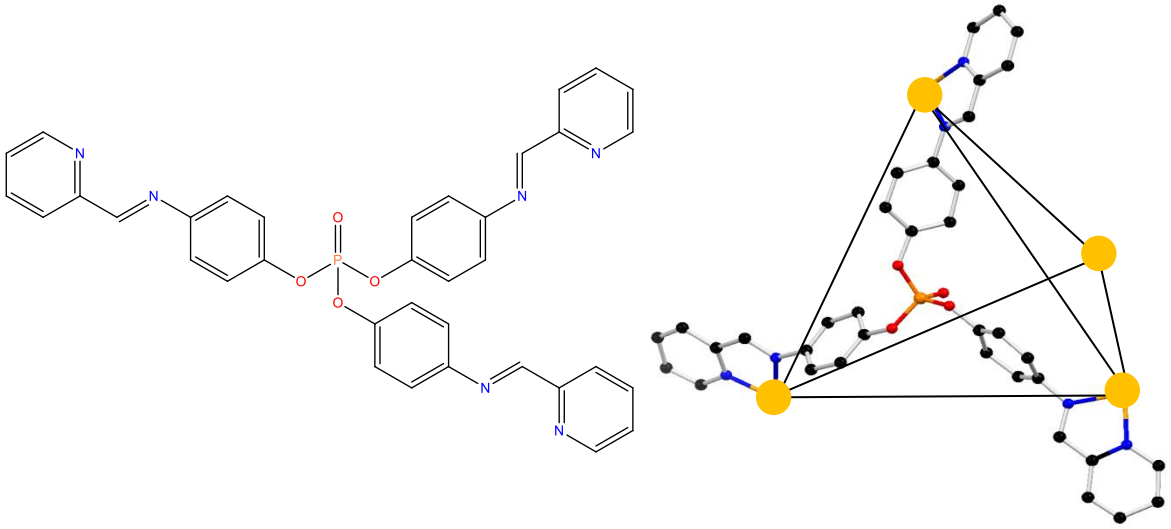

***Figure 1.12**: Phosphorus ligand tris(4-((E)-(pyridim-2-ylmethylene)amino)phenyl) phosphate(left),the tetrahedral cage formed with phosphate ligands tris(4-((E)-(pyridim-2-ylmethylene)amino)phenyl) phosphate capping the faces of the tetrahedron (right, solvents and other faces of cage omitted for clarity).*

An extension of the phosphate supramolecular chemistry will be the second aim of this project. Modification of the pro-ligand used to construct the tetrahedral cages from the *tris*-amino ligand to a *bis*-amino ligand will be pursued. The target ligand in question is *bis*(4-aminophenyl) phenyl phosphate has the possibility to form helicates (**Fig. 1.13**). Organophosphates are at risk of hydrolysis,[61] therefore making it imperative that reaction conditions are water free. Supramolecular structures created with this ligand have the potential for communication and cooperativity with one another through the potential π-π stacking that could occur from the non-functionalised phenyl group on the phosphate.

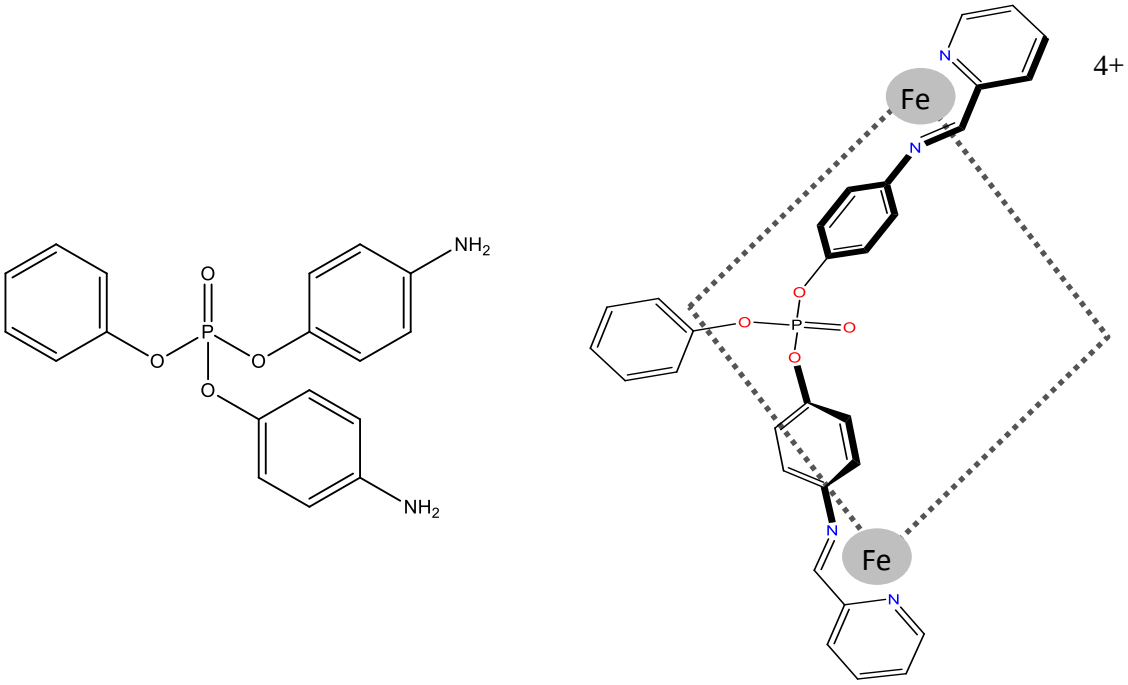

***Figure 1.13**: Pro-ligand bis(4-aminophenyl)phenylphosphate, **L2** (left), and the schematic representation of the helicate potentially formed from the pro-ligand and pyridine-2-carboxyaldehyde (right).*

Chapter 2:

Structural investigations into sulfonated $[M_2L_3]^{2-}$ helicates formed from 6,6'-oxybis(3-aminobenzenesulfonic acid) and imidazolecarboxyaldehydes.

2.1 Sulfonate chemistry

Sulfonate anions are formed by the deprotonation of sulfonic acid (RSO_3H).[62] For the majority of transition metal ions, sulfonates are considered to be non-coordinating or weakly interacting, and are therefore not often utilised in coordination complexes.[63] The incorporation of sulfonated groups into transition metal complexes is commonly as the counter anion to the complex,[64] with the intention of increasing aqueous media solubility. Sulfonate groups are known to hydrogen bond readily,[62] therefore introducing sulfonate groups onto a ligand could result in hydrogen bonding interface between helicates.

2.2 Ligand Synthesis

The precursor ligand 6,6'-oxybis(3-aminobenzenesulfonic acid), was prepared according to literature methods (**Scheme 2.1**).[19, 57] The precursor 4,4'-oxydianiline was dissolved in sulfuric acid, to which fuming sulfuric acid was added dropwise over ice. The solution was left to stir at 0°C for two hours before the temperature was raised to 80°C. The resulting pro-ligand was purified through hydrochloric acid/sodium hydroxide purification to separate starting material from the desired product.

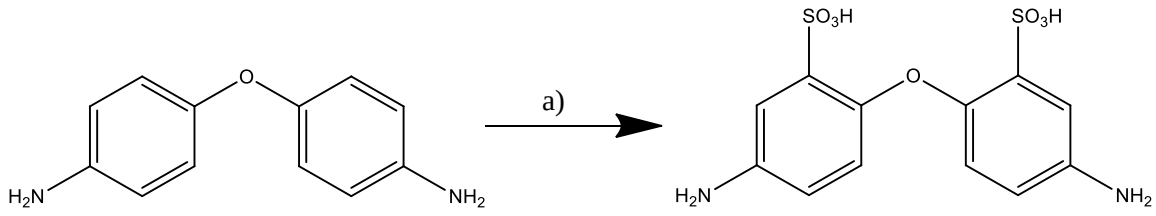

Scheme 2.1: *Synthetic route to ligand precursor 6,6'-oxybis(3-aminobenzenesulfonic acid). Reaction conditions and yield: a)H_2SO_4, Oleum, 0°C - 80°C, 4h, 73%.*

2.3 Alteration of the head group

Modification of the 'head group' from a pyridine-2-carboxyaldehyde to weaker field strength imidazolecarboxyaldehydes has the potential to produce Fe(II) metallo-helicates that possess SCO.[65] The imidazolecarboxyaldehydes chosen to react *in situ* with the pro-ligand and Fe(II) metal centres include: 2-imidazolecarboxyaldehyde, 4-imidazolecarboxyaldehyde, 1-methyl-2-imidazolecarboxyaldehyde and 4-methyl-5-imidazolecarboxyaldehyde (**Scheme 2.2**). When coordinated with the Fe(II) metal centres, the ligands produced with 4-imidazolecarboxyaldehyde and 4-methyl-5-imidazolecarboxyaldehyde gave orange coloured solutions which is consistent with the presence of metallo-helicates with Fe(II) centres in the H.S. state.[66-67] When ligands are formed with 2-imidazolecarboxyaldehyde or 1-methyl-2-imidazolecarboxyaldehyde and are complexed with Fe(II) centres, the colour at room temperature is purple, characteristic of LS metal centres.[68] All of the complexes synthesised from these head groups were successfully crystallised *via* vapour diffusion,[69] however, only those containing 4-methyl-5-imidazolecarboxyaldehyde or 1-methyl-2-imidazole carboxyaldehyde were of a suitable quality for single crystal X-ray diffraction.

Suitable crystals were obtained through vapour diffusion of acetonitrile into the water solution containing a ratio of 3:6:3, ligand **L**, 4-methyl-5-imidazolecarboxyaldehye and $Fe(SO_4)_2.7H_2O$ respectively, resulting in the formation of crystals within 1 week (**Fig. 2.1**). The crystal data were solved and refined in the orthorhombic *Pbca* space group (full refinement data in Table 1, Appendix 2). Six equivalents of triethylamine act as the base in this reaction, enhancing the solubility of the ligand through deprotonation of the sulfonate group. Electrospray Ionisation Mass Spectrometry (ESMS) results were obtained directly from the reaction mixture showing further evidence of the $[Fe_2L_3]^{2-}$ helicates (**A1**-**A2**).

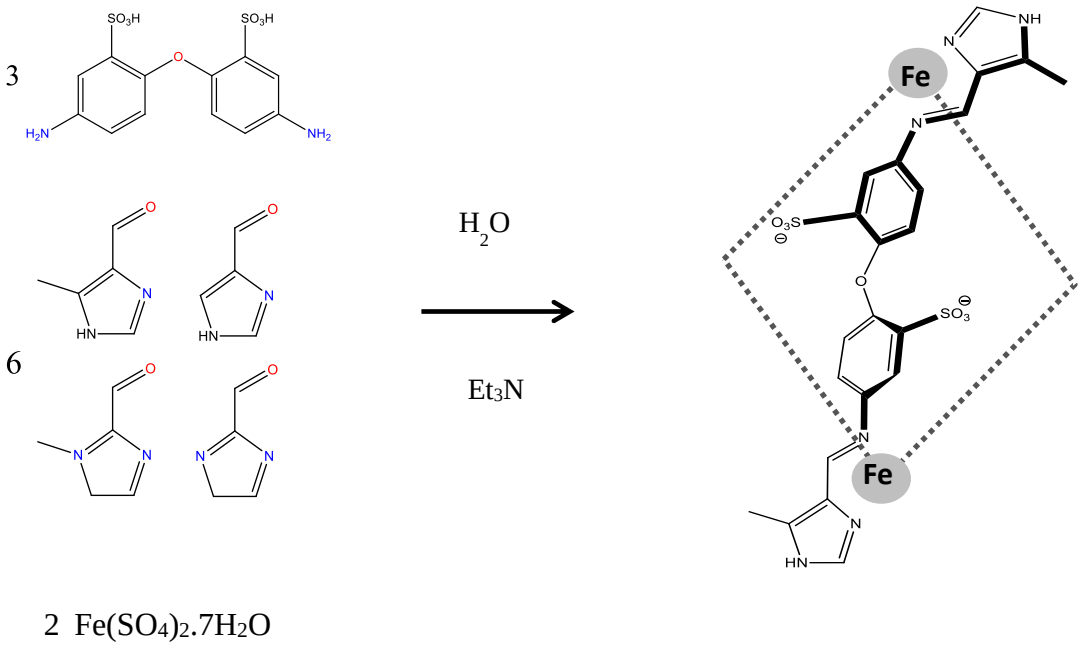

***Scheme 2.2**: In situ formation of triple stranded helicates formed from either 4-methyl-5-imidazolecarboxyaldehyde,4-imidazolecarboxyaldehyde, 1-methyl-2-imidazolecarboxyaldehyde or 2-imidazolecarboxyaldehyde, with bonding of the ligand shown in the schematic representation of the $[Fe_2\mathbf{L3}_3]^{2-}$ helicate.*

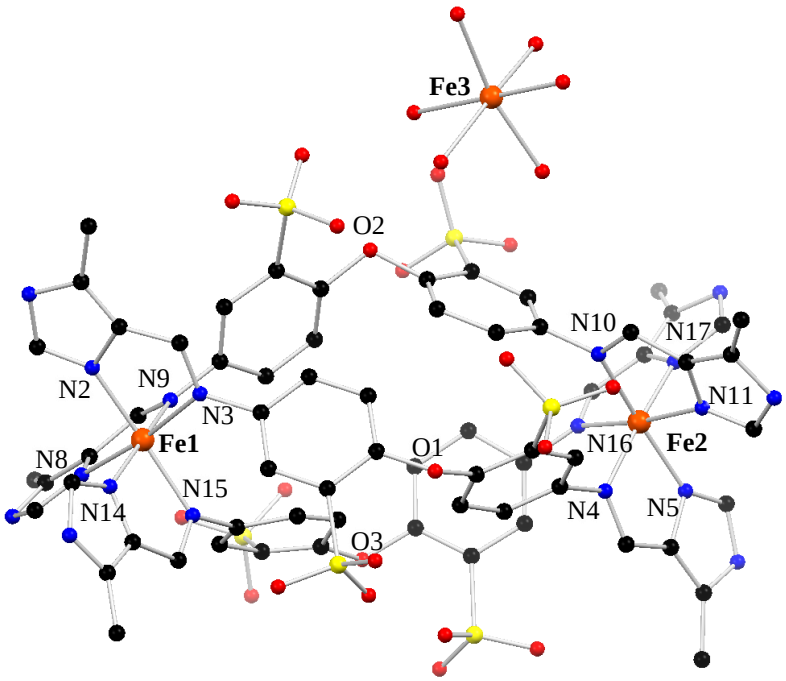

***Figure 2.1**: The synthesised supramolecular helicate $[Fe(OH_2)_6][Fe_2\mathbf{L3}_3]$ (hydrogen atoms and solvate molecules omitted for clarity, collected at 120 K)*

The molecular structure shows that the two metal centres are crystallography different exhibiting varied bond lengths and angles (**Table 2.1**). The geometry of the metal centres are distorted octahedral shown by the angles (N2-Fe1-N15) 173.1(3)°, (N3-Fe1-N8) 171.0(3)°and (N9-Fe1-N14) 174.0(3)° for the Fe(1). The second metal centre also exhibits distorted angles of 171.6(3)°, 172.1(3)° and 173.2(3)° for (N4-Fe2-N17), (N5-Fe2-N10) and (N11-Fe2-N16). These angles are significantly different from the expected angle for octahedral complexes of 180°, suggesting the distorted octahedral geometry. The *cis* angels in both metal centres exhibit a deviation from the expected 90° for a perfect octahedral geometry (Fe1, 79.5(3)°-98.1(2)° and Fe2, 79.6(3)°-98.1(2)°) with a degree of distortion shown by the Σ values of 60.8 (Fe1) and 60.7 (Fe2), which is a substantial degree of variation compared to the ideal value of 0 for a perfect octahedral structure.[70] The overall charge of these $[M_2L_3]$ helicates is (-2) due to the deprotonated sulfonate groups and Fe(II) ions. The countercation, seen in the structure above, is a hexa-aqua Fe(II) species formed during the self-assembly reaction. This helicate exhibits both right and left-handed helicates (P and M) within the crystal lattice. The pitch of the helicate (Fe-Fe distance), is 11.265(2) Å between which the three *bis*-bidentate ligands are coordinated. Bond lengths between coordinated nitrogen atoms and Fe(II) centres are indicative of the spin state of the Fe(II) metal ion centre.[71] The empirical trend is that Fe-N bond lengths over 2.1 Å are associated with high spin Fe(II), whereas bond lengths approximately equal to or lower than 2.0 Å are characteristic of a LS Fe(II) centre.[68] The bond lengths of $[Fe(OH_2)_6][Fe_2\mathbf{L3}_3]$ show that the Fe(II) are LS in the solid state at 120 K (**Table 2.1**). As the colour of the solution at room temperature for this complex is indicative of HS Fe(II) (orange), this result suggests that there may be a spin switch occurring between these two temperatures. No evidence of π-π interactions were observed within the crystal lattice. Hydrogen bonds can be observed between the hexaaqua countercation and the sulfonate groups within the crystal lattice. The complex is heavily hydrated due to the hydrophilicity of

the sulfonates which has resulted in the isolation of the molecules from one another within the crystal lattice.

***Table 2.1**: X-ray crystallography determined bond lengths of Fe-N in [Fe(OH$_2$)$_6$][Fe$_2$**L3**$_3$]*

Fe 1	Imine (Å)		Imidazole (Å)
N3	2.061(6)	N2	1.982(8)
N9	2.008(8)	N8	1.949(9)
N15	2.061(7)	N14	1.994(7)
Fe 2	Imine (Å)		Imidazole (Å)
N4	2.022(9)	N5	1.988(8)
N10	2.046(6)	N11	1.965(9)
N16	2.036(7)	N17	1.970(8)

2.4 Alteration of the Metal Ion:

The incorporation of different metal centres can influence the properties and structure of the supramolecular assembly formed, due to differing electronic and geometric properties favoured by the chosen metal centre. The incorporation of Co(II) and Ni(II) metal centres into $[M_2L_3]^{2-}$ helicates with pro-ligand **L** and imidazolecarboxyaldehydes was successfully achieved using $Co[ClO_4]_2.6H_2O$ and $Ni[ClO_4]_2.6H_2O$ metal salts. The imidazole head group in which single crystals suitable for X-ray diffraction were formed, in both cases was 1-methyl-2-imidazolecarboxyaldehyde, which differs from the previously discussed Fe(II) example (**Fig. 2.2, 2.3**). The formation of helicates using $ZnSO_4.7H_2O$, $Zn[OAc]_2$ and $Cu[ClO_4]_2.6H_2O$ as the metal source were additionally attempted although they were unsuccessful.

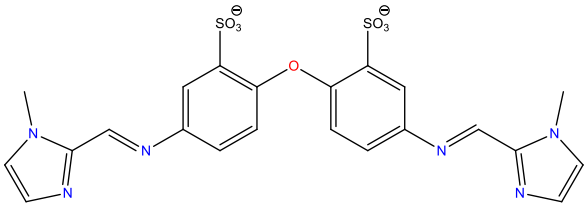

L4

Figure 2.2 *: Ligand **L4** formed in situ imine formation between pro-ligand **L** and 1-methyl-2-imidazolecarboxyalde*

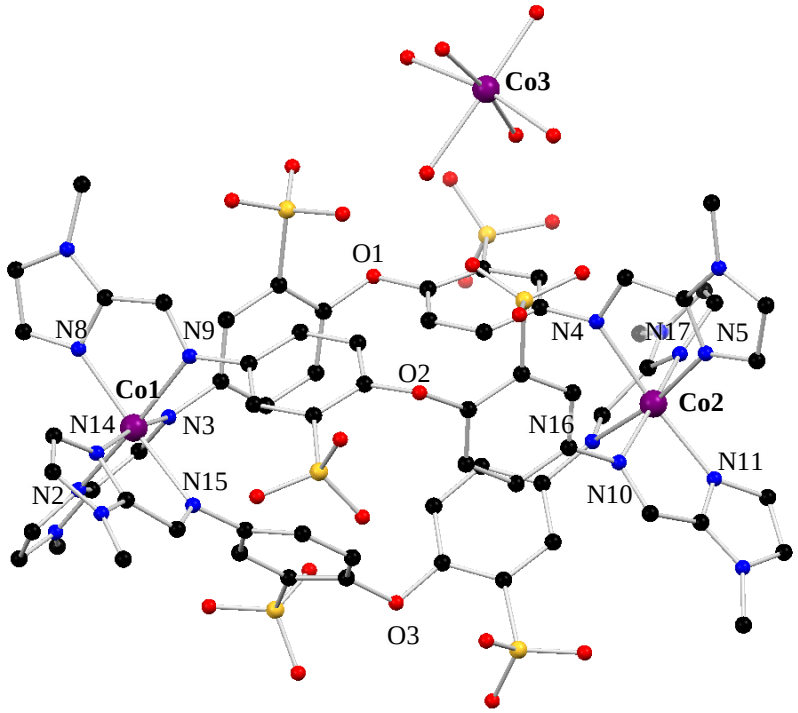

Figure 2.3*: The synthesised helicate [Co(OH₂)₆][Co₂**L4**₃] (hydrogen atoms and solvate molecules omitted for clarity, collected at 120 K).*

Metallo-helicate $[Co(OH_2)_6][Co_2\mathbf{L4}_3]$ crystals were formed through vapour diffusion of either methanol or ethanol into a solution of water containing a 3:6:3 ratio of ligand **L**, 1-methyl-2-imidazolecarboxyaldehyde and $Co[ClO_4]_2.6H_2O$ respectively, forming crystals after a week. As seen with the Fe(II) helicate, the Co(II) helicates crystallises with the presence of

its respective hexa-aquametal countercation. The molecular structure was solved in the monoclinic $P2_1/c$ space group as opposed to the orthorhombic Fe(II) helicate (full refinement data in Table 1, Appendix 2). The two metal centres are crystallography different with distorted octahedral geometries as demonstrated by the coordination angles. The angles of the first cobalt metal coordination sphere are 169.4(3)°, 170.3(3)° and 174.1(3)° for (N8-Co1-N15), (N3-Co1-N14) and (N2-Co1-N9) respectively. The second metal demonstrates similar distortion with (N10-Co2-N17), (N5-Co2-N16) and (N4-Co2-N11) giving angles of 173.1(3)°, 169.8(4)° and 171.3(3)°. The *cis* angles of the metals centres show significant distortion (Co1 76.8(3)°-99.0(3)° and Co2 76.6(4)°-101.4(3)°) giving Σ values of 80.1 and 93.1 for Co1 and Co2, respectively. The pitch of the helicate, defined by metal-metal distance is 11.346(4) Å which is slightly longer than the Fe(II) helicates. Once again both P and M helicates are observed within the crystal lattice. The Co(II)-nitrogen bond lengths are observed to be around 2.111(9), 2.072(9) and 2.202(9) Å which fall within the range that Co(II)-N bond lengths can be observed, shows that the cobalt centres are HS at 120 K (**Table 2.2**).[72-73] No π-π interactions were observed between the Co(II) helicates. Hydrogen bonds can be observed between the hexaaqua countercation and the sulfonate groups within the crystal lattice. The helicates due to their hydrophilicity are heavily hydrated which has resulted in the isolation of the complexes within the crystal lattice.

***Table 2.2**: X-ray crystallography determined bond lengths of Co-N in $[Co(OH_2)_6][Co_2\mathbf{L4}_3]$*

Co 1	Imine (Å)		Imidazole (Å)
N3	2.241(8)	N2	2.194(8)
N9	2.196(8)	N8	2.175(9)
N15	2.202(9)	N14	2.215(9)
Co 2	Imine (Å)		Imidazole (Å)
N4	2.099(8)	N5	2.072(9)
N10	2.097(8)	N11	2.094(8)
N16	2.111(9)	N17	2.091(9)

The $[Ni(OH_2)_6][Ni_2\mathbf{L4}_3]$ helicates were formed through vapour diffusion of ethanol into the water solution containing a ratio of 3:6:3, ligand **L**, 1-methyl-2-imidazolcarboxyaldehyde and $Ni[ClO_4]_2.6H_2O$ respectively (**Fig. 2.4**). Crystals of suitable quality to perform X-ray diffraction on were formed within one week.

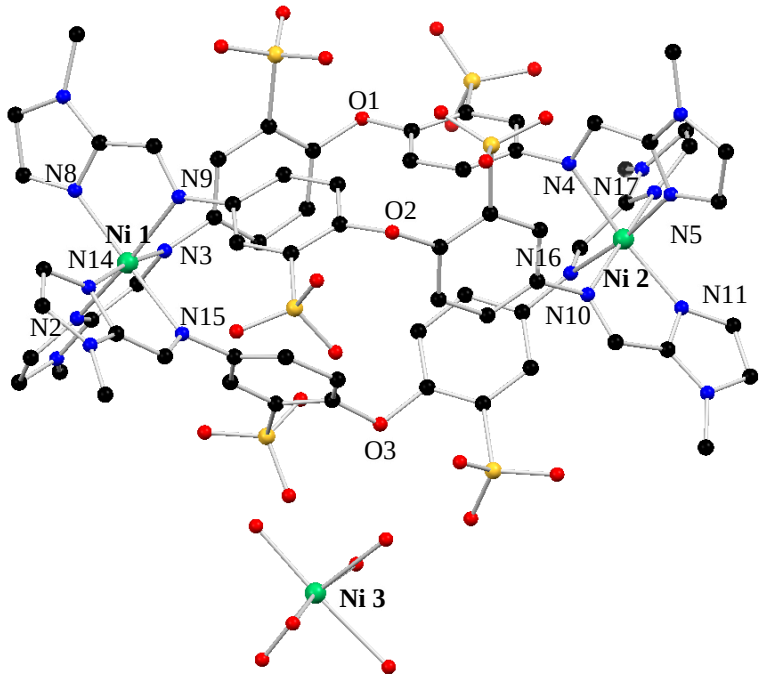

Figure 2.4: *The synthesised supramolecular helicate [Ni(OH$_2$)$_6$][Ni$_2$**L4**$_3$] (hydrogen atoms and solvate molecules removed for clarity, data collected at 120 K).*

The Ni(II) helicates crystallise with the presence of their respective hexa-aquametal countercation as seen with the other metallo-helicates. The molecular structure was solved in the monoclinic P2$_1$/*c* space group as with the Co(II) helicate (full refinement data in Table 1, Appendix 2). The pitch of 11.473(4) Å is observed between the Ni(II) ions. Both P and M helicates were observed within the crystal lattice. The two metal centres are crystallography different as seen by the bond lengths between the nickel ion and nitrogen atom and the metal coordination angles (**Table 2.3**). The geometry of the metal centres are distorted as seen by the angles which are distinctively different to the expected 180° for octahedral geometries, with (N2-Ni1-N9), (N3-Ni1-N14) and (N8-Ni1-N15) angles of 174.2(3)°, 170.6(3)° and 170.7(3)° for the first metal ion. The other metal ion shows similar distortion of coordination angles with 171.1(3)°, 170.5(3)° and 174.3(3)° for (N4-Ni2-N11), (N5-Ni2-N16) and (N12-Ni2-N17) respectively. The *cis* angles show distortion from the perfect octahedral geometry (Ni1 78.5(3)°-98.1(2) and Ni2 78.3(3)°-99.1(3)°) with Σ values of 68.4 (Ni1) and 80.8 (Ni2).

No π-π interactions were observed for the Ni(II) helicates. Hydrogen bonds between the hexaaqua countercation and the sulfonate groups are present once again within the crystal lattice with isolation of helicate molecules due to high hydration.

***Table 2.3**: X-ray crystallographic determined bond lengths of Ni-N in $[Ni(OH_2)_6][Ni_2\mathbf{L4}_3]$*

Ni 1	Imine (Å)		Imidazole (Å)
N3	2.211(7)	N2	2.034(7)
N9	2.162(6)	N8	2.054(7)
N15	2.213(7)	N14	2.065(8)
Ni 2	Imine (Å)		Imidazole (Å)
N4	2.146(7)	N5	2.029(7)
N10	2.135(7)	N11	2.053(6)
N16	2.169(7)	N17	2.026(8)

2.5 Crystal Packing

The helicates constructed with the two ligands discussed above, pack within the crystal lattice in significantly different manners. This is due to the crystals forming in different crystal systems with the Fe(II) helicates in the orthorhombic crystal system and the Co(II) and Ni(II) helicates in the monoclinic crystal system. No π-π interactions were evident within the crystal lattices of the molecular structures in either crystal system. Hydrogen bonding between the sulfonate groups on the metallo-helicate and the hexa-aqua countercation are observed in all of the structures. The main difference between the packing of the crystal lattices is the relationship between helicate units with one another. In the case of the Co(II) and Ni(II) helicates align parallel to one another, as seen when looking at the b axis and down the axis of the helicate of the Co(II) lattice (**Fig 2.5, Fig. 2.6**).

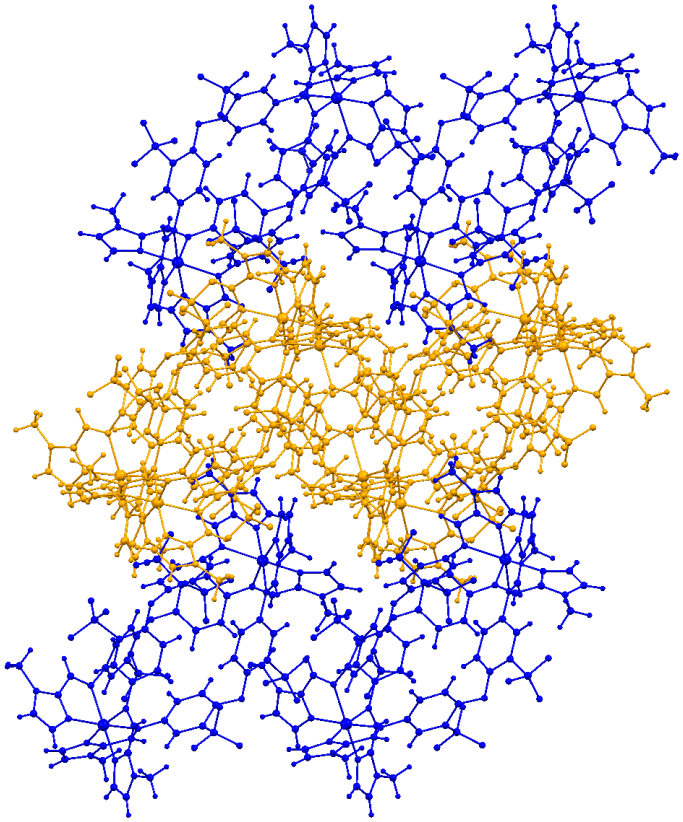

Figure 2.5*: The crystal packing of the Co(II) helicate as seen looking down the b-axis showing parallel alignment of helicate units, shown in orange and blue (solvates and countercations removed for clarity, collected at 120 K).*

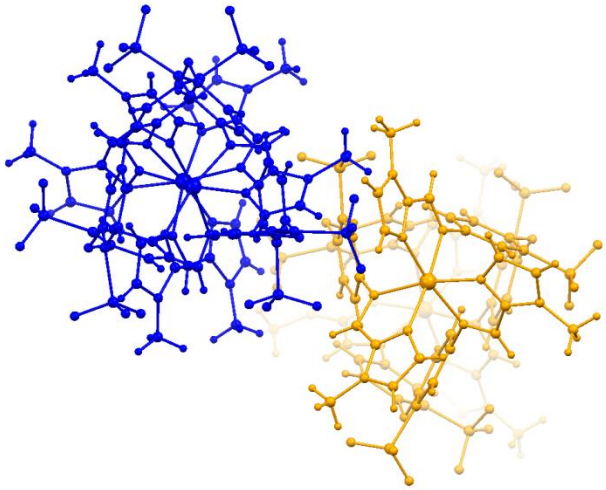

Figure 2.6*: The crystal packing of the Co(II) helicate as seen looking down the axis of the helicate showing parallel alignment(solvates and countercations removed for clarity, collected at 120 K).*

The Fe(II) helicates which form in the orthorhombic crystal system align within the lattice in a perpendicular fashion to one another (**Fig. 2.7, Fig 2.8**). As with the Co(II) and Ni(II) helicates hydrogen bonding between the sulfonate groups and countercations were seen. Notably different however is the occurrence of a hydrogen bond (2.096 Å) that lies between the N-H of the imidazole group on the ligand of one helicate and the sulfonate group of a neighbouring helicate (**Fig. 2.8**). This could potentially allow communication throughout the crystal lattice and influence possible spin crossover properties. The helicates are however, heavily hydrated resulting in difficulty in handling the crystals as they are fragile and loss of solvent results in loss of crystallinity.

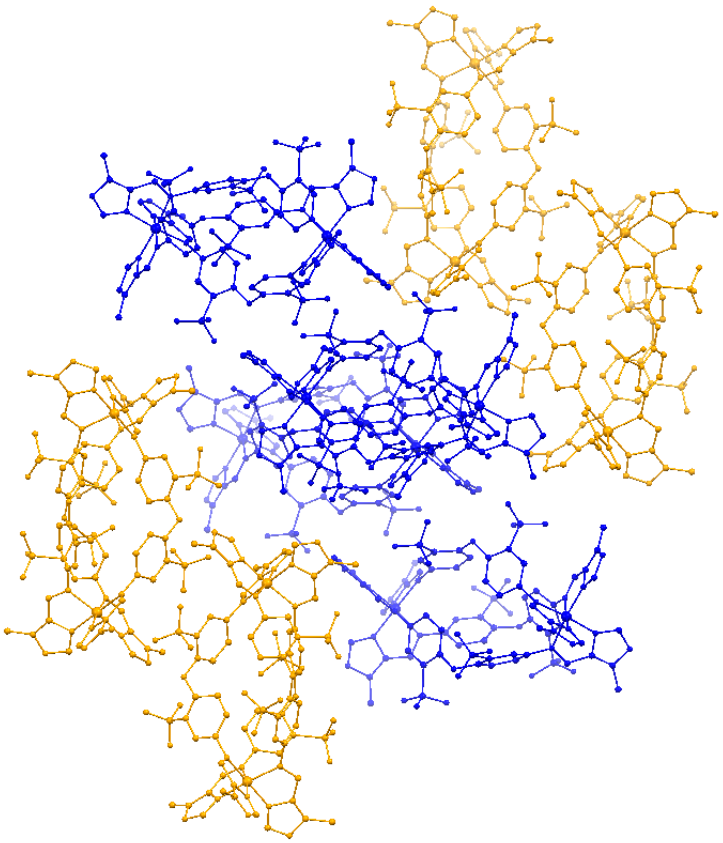

***Figure 2.7**: The crystal packing of the Fe(II) helicate showing the perpendicular association (hydrogen atoms and solvate molecules removed for clarity, collected at 120 K)*

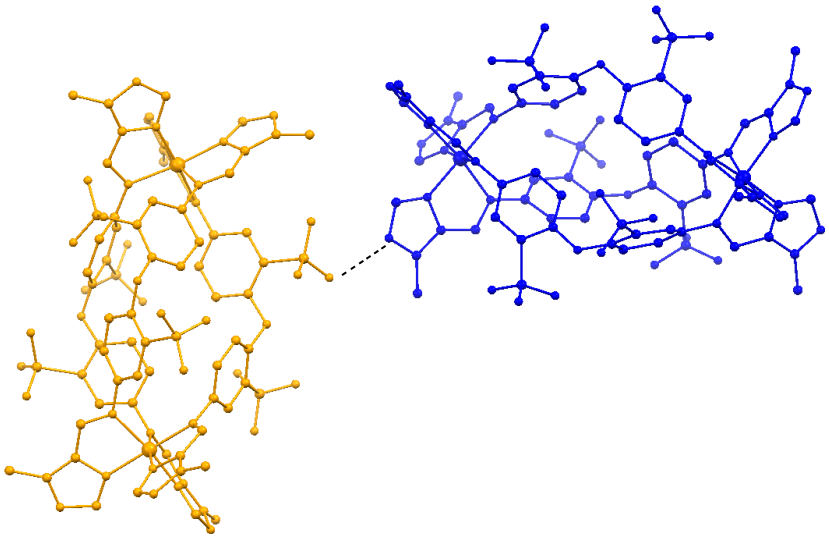

***Figure 2.8**: The crystal packing of the Fe(II) helicate looking at the perpendicular fashion of crystal packing (hydrogen atoms and solvate molecules removed for clarity, collected at 120 K).*

2.6 Interchanging the counter cation:

Altering the countercation present within the crystal lattice is another method in which interaction could be introduced into the crystal lattice. In the absence of base the countercation present is a dicationic hexa-aquametal complex as seen in the examples already discussed, where these countercations are interacting with the adjacent sulfonate groups through hydrogen bonds. Interchanging the countercation present in the lattice to other cations will provide information about the countercations' importance in the crystal packing. Alteration of the base in the self-assembly reaction to KOH, RbOH and $Ca(OH)_2$ resulted in the corresponding structures with countercations $2K^+$, $2Rb^+$ and Ca^{2+} respectively (**Fig. 2.9, Fig. 2.10, Fig 2.11**).

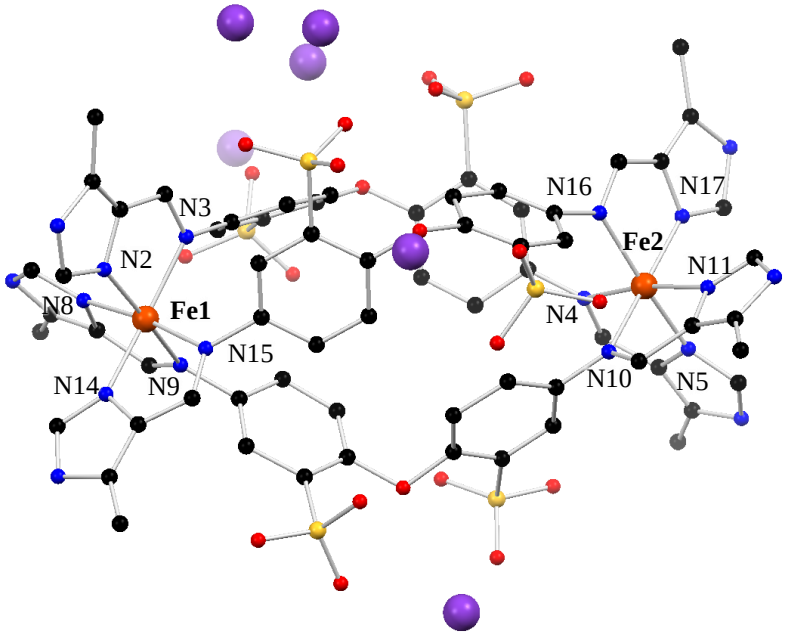

***Figure 2.9**: The supramolecular helicate $K_2[Fe_2\mathbf{L3}_3]$ (hydrogen atoms and solvate moleculaes omitted for clarity, collected at 120 K, K^+ cations in purple).*

The crystals of $K_2[Fe_2\mathbf{L3}_3]$ helicate were formed *via* vapour diffusion of either ethanol or acetone into the water solution containing the ratio 3:6:2:6 of ligand **L**, 4-methyl-5-imidazolecarboxyaldehyde, $Fe(SO_4)_2.7H_2O$ and KOH respectively, which crystallised after a period of one week. The structure was solved and refined in the orthorhombic *Pbca* space group (full refinement data in Table 2, Appendix 2). The countercations in $K_2[Fe_2\mathbf{L3}_3]$ are disordered within the channels around the sulfonate groups with occupancies summing up to two countercations per helicate unit. Complete exchange of hexaaquametal counter cation is observed for this case. The metal-metal distance (or pitch) for this helicate is comparable to the $[Fe(OH_2)_6][Fe_2\mathbf{L3}_3]$ helicate with an Fe-Fe length of 11.270(3) Å in the $K_2[Fe_2\mathbf{L3}_3]$ helicates. Analysis of the Fe-N bond lengths for these this helicate shows similar lengths to those in $[Fe(OH_2)_6][Fe_2\mathbf{L3}_3]$, indicating that $K_2[Fe_2\mathbf{L3}_3]$ have LS metal centres at 120 K (**Table 2.4**). The metal centres have a distorted octahedral geometry, as shown by the angles 172.0(5)°, 173.2(5)° and 171.1(5)° for (N3-Fe1-N14), (N8-Fe1-N15) and (N2-Fe1-N9) respectively. The second metal centre shows similar angles with (N4-Fe2-N11) 171.1(5)°, (N10-Fe2-N17) 172.2(5)° and (N5-Fe2-N16) 172.5(5)°. The *cis* angles also shows deviation from the expected 90° (Fe1 79.4(5)°-98.3(5)° and Fe2 78.8(5)-97.2(4)°) with Σ values of 65.6 (Fe1) and 67.4 (Fe2).

***Table 2.4**: X-ray crystallography determined bond lengths of Fe-N in $K_2[Fe_2\mathbf{L3}_3]$*

Fe 1	Imine (Å)		Imidazole (Å)
N3	2.009 (13)	N2	1.996(12)
N9	2.022(11)	N8	1.968(13)
N15	2.063(10)	N14	1.972(12)
Fe 2	Imine (Å)		Imidazole (Å)
N4	2.058(11)	N5	1.986(11)
N10	2.052(10)	N11	1.961(11)
N16	2.028(11)	N17	1.948(12)

Crystals of $Ca[Fe_2\mathbf{L3}_3]$ helicates were formed when methanol was diffused into the water solution containing ligand **L**, 4-methyl-5-imidazolecarboxyaldehyde, $Fe(SO_4)_2.7H_2O$ and calcium hydroxide in a 3:6:2:6 respectively, resulting in crystal formation within one week. The crystal were solved and refined in the orthorhombic *Pbca* space group (full refinement data in Table 2, Appendix 2).

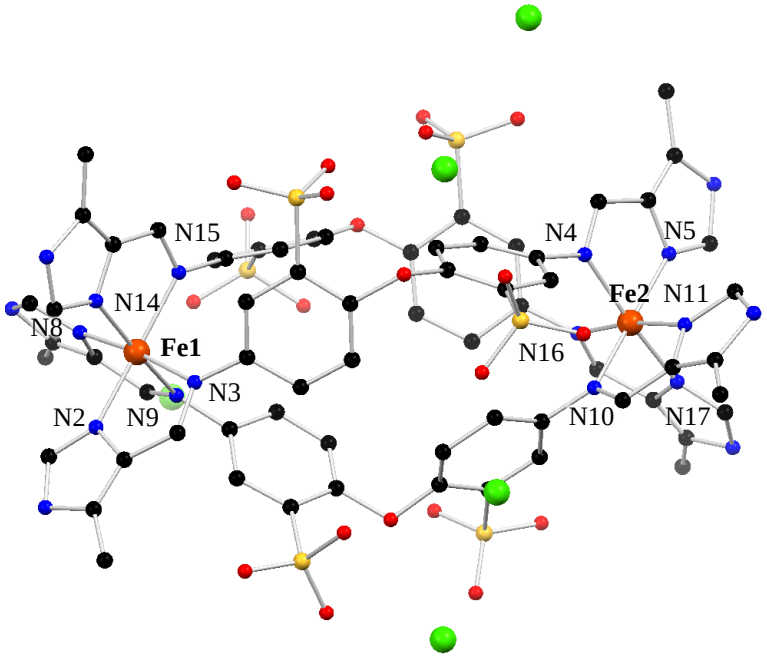

***Figure 2.10**: The helicate Ca[Fe_2**L3**$_3$] (hydrogen atoms and solvate molecules omitted for clarity, collected at 120 K, Ca^{2+} cations in green)*

The Ca^{2+} countercation is disordered over a number of positions, adjacent to the sulfonate groups with occupancies that add up to one countercation per helicate unit. The geometry of the Fe(II) metal centres are distorted octrahedra, around which the three *bis*-bidentate ligands are coordinated. The pitch of the helicate is 11.295(2) Å long, comparable to the other Fe(II) helicates formed. The metal ion-nitrogen atom distance of this metallo-helicate shows that it is LS at 120 K as with the previous Fe(II) helicates (**Table 2.5**). This helicate has metal geometries that are distorted octahedrons, with the Fe(1) exhibiting angles of 171.8(3)° (N9-Fe1-N14), 173.5(3)° (N3-Fe1-N8) and 173.7(3)° (N2-Fe1-N15). Angles of 172.1(3)° (N5-Fe2-N10), 170.9(3)° (N11-Fe2-N16) and 172.9(3)° (N4-Fe2-N17) are observed for Fe(2). The *cis* angles show distortion of the octahedral geometry with (Fe1 78.8(3)°-97.1(3)° and Fe 2 78.8(3)°-98(3)°) giving Σ values of 65.7 (Fe1) and 67.2 (Fe2).

Table 2.5: X-ray crystallography determined bond lengths of Fe-N in Ca[Fe_2**L3**$_3$]

Fe 1	Imine (Å)		Imidazole (Å)
N3	2.090(7)	N2	1.998(8)
N9	2.088(8)	N8	1.999(7)
N15	2.053(9)	N14	2.015(10)
Fe 2	Imine (Å)		Imidazole (Å)
N4	2.035(10)	N5	1.995(8)
N10	2.037(8)	N11	1.932(5)
N16	2.064(7)	N17	1.976(9)

The metallo-helicate $[Fe(OH_2)_6]_{0.2}Rb_{1.6}[Fe_2$**L3**$_3]$ is formed through vapour diffusion of methanol into a solution of water containing ligand **L**, 4-methyl-5-imidazolecarboxyaldehyde, $Fe(SO_4)_2.7H_2O$ and $Rb(OH)_2$ in a 3:6:2:6 ratio. Single crystals suitable for X-ray diffraction were obtained after a period of a week. The molecular structure was solved and refined in the orthorhombic *Pbca* space group (full refinement data in Table 2, Appendix 2).

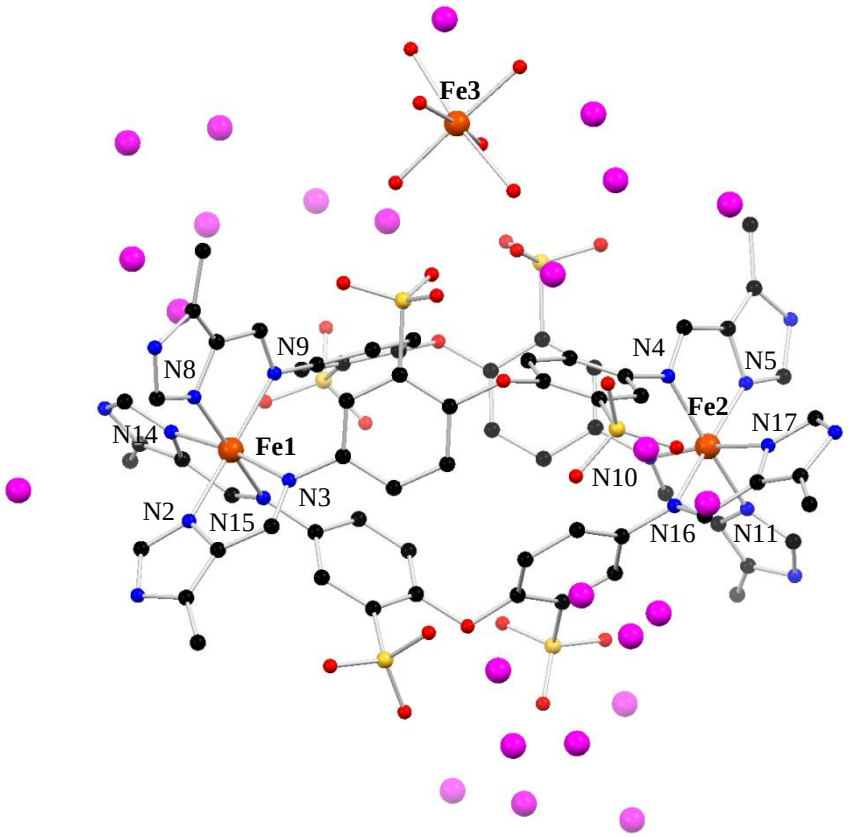

***Figure 2.11**: The supramolecular helicate $[Fe(OH_2)_6]_{0.2}Rb_{1.6}[Fe_2\mathbf{L3}_3]$ (hydrogen atoms and solvate molecules omitted for clarity, collected at 120 K, Rb^+ cations in purple)*

The helicate formed with rubidium hydroxide, however, forms with 0.2 equivalents of $[Fe(OH_2)_6]^{2+}$ still present and only 1.6 equivalents of Rb^+ disordered around the sulfonate groups. The geometry of the metal centres, shown by the coordination angle is a distorted octahedron. The angles created through coordination to the *bis*-bidentate ligands are 172.1(2)° (N2-Fe1-N9), 172.4(2)° (N3-Fe1-N14), 171.6(2)° (N8-Fe1-N15) for the first metal. The second metal centre gave very similar angles of 172.8(2)° (N4-Fe2-N11), 171.0(2)° (N5-Fe2-N16) and 172.6(2)° (N10-Fe2-N17). All of the angles are significantly different from 180° angle expected in an octahedral arrangement. The *cis* angles show distortion from the expected 90° (Fe1 79.0(2)°-97.4(2)° and Fe2 79.7(2)°-98.6(2)°) with Σ values of 67.3 (Fe1) and 63 (Fe2). The metal-metal distances for the $[Fe(OH_2)_6]_{0.2}Rb_{1.6}[Fe_2\mathbf{L3}_3]$ helicates are

11.281(1) Å which is comparable to the $[Fe(OH_2)_6][Fe_2\mathbf{L3}_3]$ metal-metal distance. The Fe-N bond lengths for these three helicates show they have LS metal centres at 120 K (**Table 2.6**).

***Table 2.6**: X-ray crystallography determined bond lengths of Fe-N in $[Fe(OH_2)_6]_{0.2}Rb_{1.6}[Fe_2\mathbf{L3}_3]$*

Fe 1	Imine (Å)		Imidazole (Å)
N3	2.107(5)	N2	2.018(6)
N9	2.084(6)	N8	2.018(7)
N15	2.109(5)	N14	2.026(6)
Fe 2	Imine (Å)		Imidazole (Å)
N4	2.050(6)	N5	1.990(6)
N10	2.062(5)	N11	1.997(6)
N16	2.051(6)	N17	1.982(17)

It was anticipated that these helicate assemblies, with altered countercations, could affect the packing of the crystal lattice. However, they all crystallised in the same crystal system and space group (orthorhombic, *Pbca*) as the hexa-aquametal iron helicate and pack in the same way. As with the $[Fe(OH_2)_6][Fe_2\mathbf{L3}_3]$ helicate, no π-π interactions were found within any of the crystal lattices. Distances between helicate units, measured by metal-metal distances, found that all four Fe(II) helicate complexes gave comparable shortest intermolecular distances around 9.903(2) Å. The Ni(II) and Co(II) helicates have different intermolecular distances due to their different crystal packing system and space group (monoclinic, $P2_1/c$) with the shortest distances approximately 7.525(3) Å.

A range of other bases were used in the attempt to introduce other countercations into the system, in conjunction with the bases which successfully introduced differing countercations into the crystal lattice. To introduce increased or differing interaction

throughout the crystal lattice system, countercations with increased or differing hydrogen bond potential to $[Fe(OH_2)_6]^{2+}$ were investigated. The other bases trialled included; pyridine, benzene-1,4-diamine, pyrazine, guanidine carbonate, guanidinium chloride and phosphonium chloride (**Fig 2.12**). These compounds can all act as bases or hydrogen bond acceptors with the potential to form hydrogen bonding networks between helicate units. These potential countercations would differ from the $[Fe(OH_2)_6]^{2+}$ cations due to geometries formed from the 3-fold hydrogen bond extension that comes from the shape of guanidinium, or the coordination number for the phosphonium chloride which could affect the crystal packing outcome of the crystal lattice.

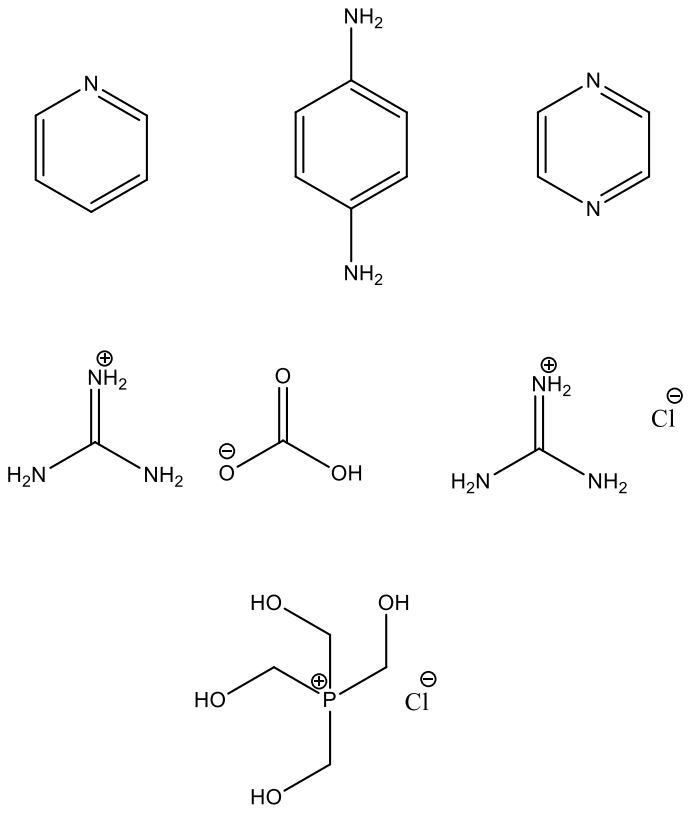

***Figure 2.12**: Alternative bases used which have hydrogen bonding potential if present as a countercation in the lattice (left to right, top to bottom); pyridine, benzene-1,4-diamine, pyrazine, guanidine carbonate, guanidinium chloride and phosphonium chloride.*

Unfortunately although many of the helicates using these differing bases gave crystals of X-ray quality, the resulting structures showed no interchange of countercation and were observed as the hexaaqua-metal dication stabilised helicates. As the sulfonated ligand is only readily soluble in water, the creation of the hexaaqua metal countercation cannot be readily avoided. Attempts were made using the stoichiometry to limit the amount of metal used in this self-assembly reaction, however, this yielded a lower concentration of helicate crystals formed instead of limiting the creation of the countercation.

2.7 Spin Crossover

The investigation into whether these helicates exhibit spin crossover behaviour has already been discussed earlier when investigating the M-N bond lengths of the various helicates formed. From these bond lengths the conclusion was drawn that the Fe(II) helicates have bond lengths corresponding to LS Fe(II) at 120 K, whereas the colour of the solution at room temperature (bright orange) is linked to a HS metal centre. Although these findings are indicative of potential spin crossover behaviour, this is not definitive as the crystallisation process and formation of a crystal lattice could be locking the metal centres into the LS state, resulting in no dynamic spin state change. Variable temperature experiments were conducted to see whether dynamic spin crossover is occurring.

One crystal was mounted and data collections were performed at different temperatures. The crystal data was initially collected at 298 K (room temperature) and the crystal was then gradually cooled at 1 $Kmin^{-1}$ to 100 K with a 5 minute adjustment period to allow any spin switching at the target temperature to proceed to completeness. The crystals were weakly diffracting with rapid fall-off of data at high resolution, a commonly seen phenomenon in crystallography, therefore, only the unit cell data was collected at each temperature. The unit cell data for each collection gave approximately the same unit cell, with

a 3.8% volume loss of the crystal seen between 298 K and 100 K (**Fig. 2.13**). Volume loss can be attributed to either spin-crossover or to thermal contraction of the crystal lattice. Crystallinity of the complex was lost when collection was attempted at 82 K.

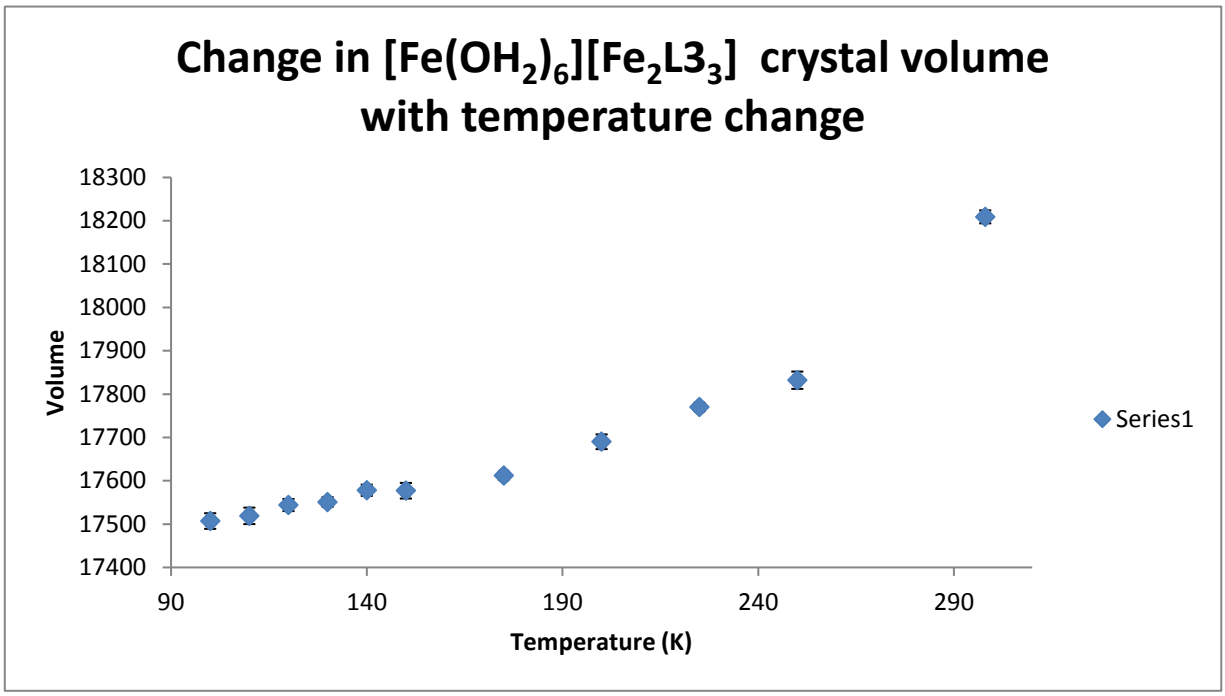

***Figure 2.13**: Volume change of the crystallographic unit cell of [Fe(OH$_2$)$_6$][Fe$_2$**L3**$_3$] over the variable temperature experiment from 298 K to 100 K.*

*2.7.1 Magnetic characterisation of [Fe(OH$_2$)$_6$][Fe$_2$**L3**$_3$] and [Co(OH$_2$)$_6$][Fe$_2$**L4**$_3$]*

Magnetic susceptibility measurements were conducted on both of the [Fe(OH$_2$)$_6$][Fe$_2$**L3**$_3$] and [Co(OH$_2$)$_6$][Co$_2$**L4**$_3$] helicates. The measurements were performed upon freshly isolated samples that were transferred to a gelatine capsule which was then enclosed within a straw, along with a little mother liquor to suppress desolvation, and then located within the SQUID chamber. The molecular weights for each was that based on the degree of solvation observed from the crystallography data which amounted to 29 water molecules per helicate complex.

*2.7.1.1 Magnetic characterisation of [Fe(OH$_2$)$_6$][Fe$_2$**L3**$_3$]*

Magnetic susceptibility measurements were carried out on the [Fe(OH$_2$)$_6$][Fe$_2$**L3**$_3$] complex and the data is presented within **Fig. 2.14**. The sample was cooled from 260 to 10 K (cycle 1), then heated from 10 to 300 K before being cooled back down to 10 K. The initial cycles show reproducible magnetic behaviour below 260 K. Once heated to 300 K it is evident that some desolvation has occurred as a sharp increase in susceptibility is observed. Complex [Fe(OH$_2$)$_6$][Fe$_2$**L3**$_3$] has a χ_MT value of 4.2 cm^3 mol^{-1} K at 300 K. The χ_MT value then gradually decreases with decreasing temperature to a value of 2.3 cm^3 mol^{-1} K at 10 K. The χ_MT value at 150 K of around 3.2 is consistent to 2:1 LS/HS metal centres, which corroborates the structure obtained from X-ray diffraction where the two helicate metal centres are LS at 120 K. The different path followed after 300 K is most likely attributed to desolvation. The cooling to 270 K from 300 K possibly shows a gradual spin transition occurring before the helicate metals return to LS states. This data is additionally consistent to the variable X-ray diffraction experiment where the crystal cell volume decreased in size by 3.8 % on decreasing from 300 K which is consistent with the onset of spin crossover.

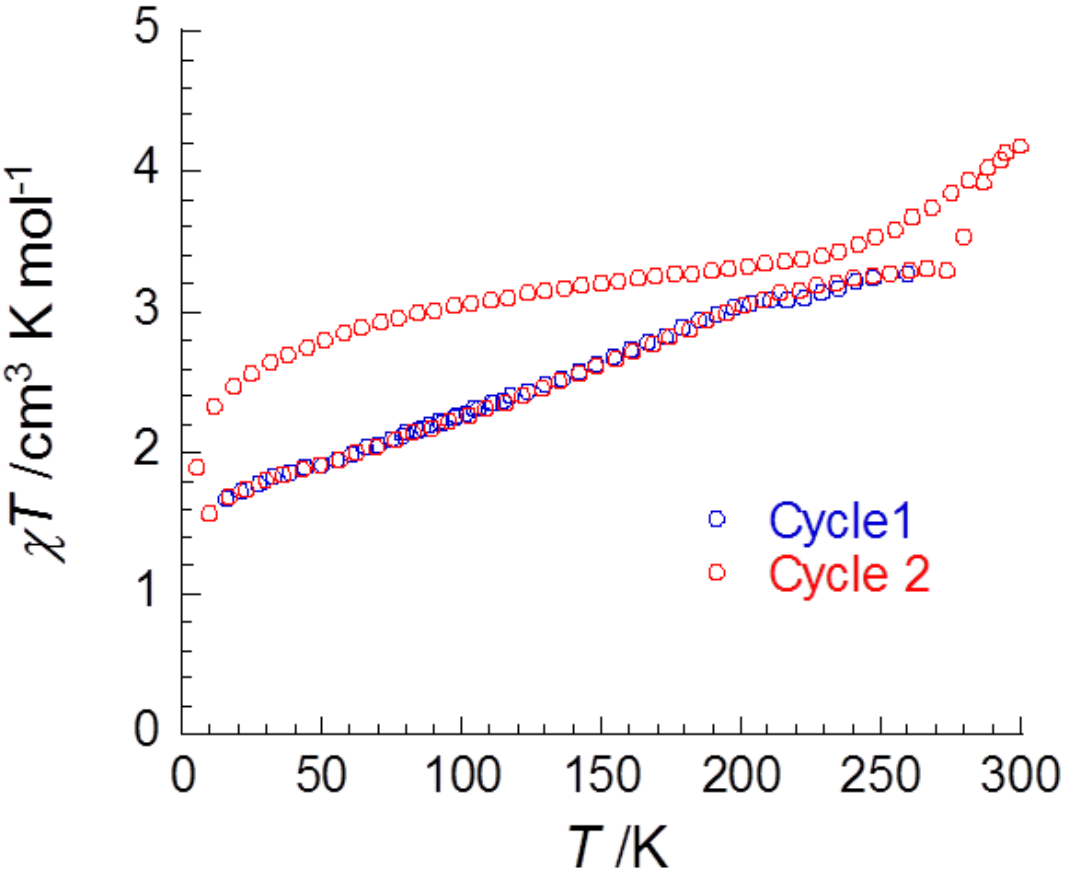

Figure 2.14: *The plot of $\chi_M T$ vs T with an applied dc field of 0.5 T for the complex [Fe(OH$_2$][Fe$_2$**L3**$_3$], with cycle 1(blue) cooling from 260 to 10 K and cycle 2(red) corresponding to heating from 10 to 300 K then cooling back down to 10 K.*

*2.7.1.2 Magnetic characterisation of [Co(OH$_2$)$_6$][Co$_2$**L4**$_3$]*

Magnetic susceptibility measurements were carried out on the [Co(OH$_2$)$_6$][Co$_2$**L4**$_3$] complex and are presented in **Fig. 2.15**. The sample was cooled from 250 to 5 K, then heated from 5 to 300 K then finally cooled from 300 back down to 5 K. [Co(OH$_2$)$_6$][Co$_2$**L4**$_3$] has a χ_MT value of 8.5 cm^3 mol^{-1} K at 300 K. This value agrees with the expected value of around 9 cm^3 mol^{-1} K for 3 HS cobalt metal centres. The χ_MT value gradually decreases with decreasing temperature to a value of 4.9 cm^3 mol^{-1} K at 5 K. The shape and magnitude of this curve is shown to repeat during the cycling experiments. This data is in agreement with the X-ray diffraction data in which the metal centres within the helicate are in the HS state. No

evident spin transitions are evident from this data for this complex, evident from the gradual slope.

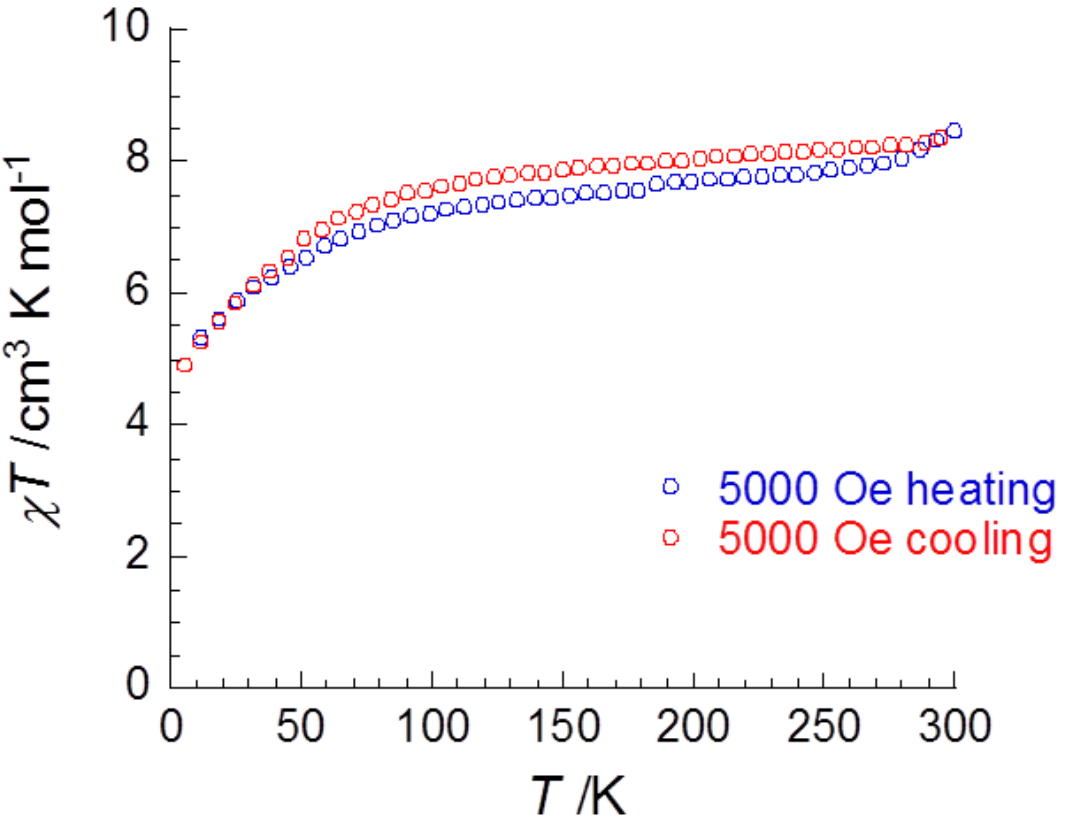

***Figure 2.15**: The plot of $\chi_M T$ vs T with an applied dc field of 0.5 T for the complex $[Co(OH_2)_6][Co_2\mathbf{L4}_3]$*

2.8 Thermogravimetric Analysis on $[Fe(OH_2)_6][Fe_2L3_3]$

To evaluate the loss of solvent (in this instance water) from the complex, a thermogravimetric analysis (TGA) experiment was performed (**Fig. 2.16**). Preparation of the sample included drying of the crystals briefly in an oven set to 333 K so that they are appropriately dry to place on the pan of the TGA apparatus, which is required to the heavy hydration of the crystals. This preparative process could result in loss of solvent before the TGA was undertaken. Drying of the sample was required prior to TGA analysis due to the hydrophilic nature of these complexes, making the substance hard to handle without removal

of some water. The TGA shows a rapid loss of solvent initially, and that the helicate then remains stable until decomposition close to 400 K. The first significant weight loss is seen up to 60 °C were the weight percentage is reduced by around 10 %. This can be attributed to solvent and water loss from the crystal lattice, however it can be seen that loss of water is occurring immediately which is likely due to the preparation process. The weight percentage is then seen to plateau until around 350 °C where 60 % of product weight is lost, corresponding to decomposition of the helicate.

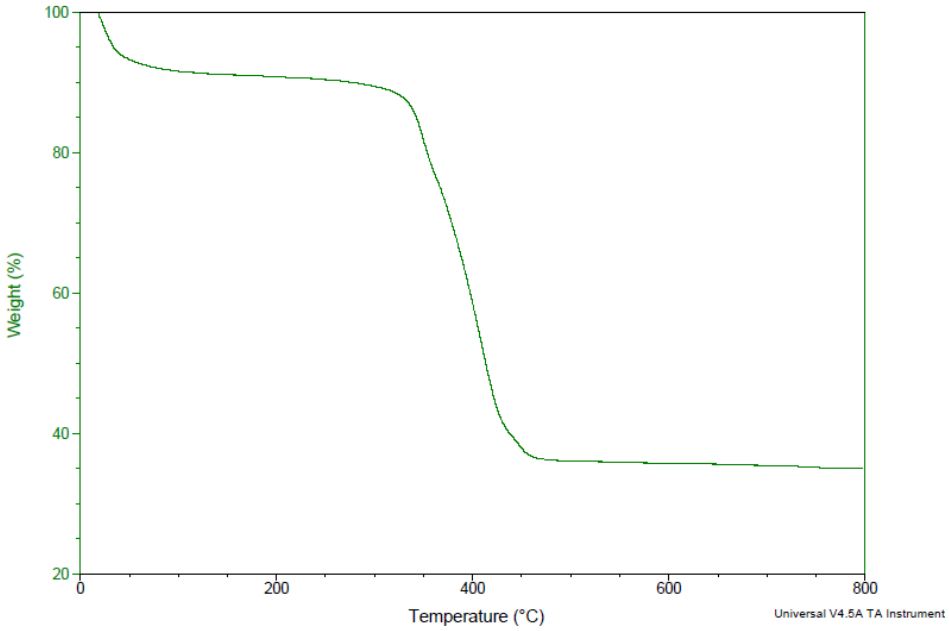

***Figure 2.16**: TGA analysis of complex [Fe(OH$_2$)$_6$][Fe$_2$**L3**$_3$]*

2.9 Conclusion

The synthesis of a series of $[M_2L_3]^{2-}$ helicates has been demonstrated, either by varying combinations of the base, metal salt or the head group used in the self-assembly synthesis. By varying the base used, the countercation of the helicates formed could also be changed. The alterations made to the helicates were done with the intention of introducing communication and tailoring spin-crossover behaviour. The potential of communication has been realised in

the complexes made with ligand **L3** which forms hydrogen bonds, altering the crystal packing compared to helicates formed in the absence of a hydrogen bond donor. The investigations into whether they exhibit spin-crossover properties are however preliminary due to the difficulties of studying this system. Crystal structure bond lengths and unit cell volume changes during variable temperature experiments suggests spin-crossover occurs. The magnetic measurements conducted on the $[Fe(OH_2)_6][Fe_2\mathbf{L3}_3]$ and $[Co(OH_2)_6][Co_2\mathbf{L4}_3]$ helicates do not show significant SCO for these helicates. The aim to influence to introduce communication was hindered by the hydrophilicity which isolated the helicates from one another in the crystal lattice.

Chapter 3:

Phosphate-based supramolecular $[M_2L_3]^{4+}$ assemblies formed from the pro-ligand *bis*(4-aminophenyl)phenyl phosphate

3.1 Phosphate chemistry

Organophosphate esters have been studied in chemistry for their function as fire retardants, plasticisers and insecticides.[74] Phosphate groups are made up of a pentavalent phosphorus atom surrounded by four oxygens atoms which are arranged in a tetrahedral fashion and are esters of phosphoric acid.[75] Phosphoric acid has been known to complex with metal centres, having been shown to form both clusters and discrete assemblies including double helicates.[76-78] Organophosphates, though readily formed, are sensitive to bases and in particular hydroxide ions which facilitate hydrolysis of the phosphate ester.[61] Phosphate monoesters metal centres aggregate together through coordinate bonds creating structures that are zeolitic in nature.[75] The structures formed with diesters have been found to form smaller discrete structures containing only one or two metal centres as opposed to clusters.[79] In these cases, however, the structures formed are often through direct coordination of the phosphates to metal centres as opposed to a coordination site on the organic ester component. Communication between supramolecular assemblies comprised with phosphate containing ligands could be introduced, due to the uncoordinated P=O group which has the potential to provide secondary sphere coordination through hydrogen bonds.[80-81] *Bis*(4-aminophenyl)phenyl phosphate, the ligand of interest has been synthesised previously, however, its coordination chemistry has not been previously reported.[82] The aim of the work in this Chapter is to construct supramolecular assemblies of containing phosphate ligands comprising of bidentate chelating sites created *via* imine condensation of *bis*(4-aminophenyl)phenyl phosphate with appropriate aldehydes.

3.2 Ligand synthesis

The precursor ligand *bis*(4-aminophenyl)phenyl phosphate was synthesised using an adapted preparation that was modified for previous phosphorus work conducted within the

Kruger group (**Scheme 3.1**). In a Schlenk tube, 4-nitrophenol was stirred in dry acetonitrile under an argon atmosphere. To this, dry triethylamine was added dropwise via an evacuated syringe at 0°C. Phenyl dichlorophosphate diluted in dry acetonitrile is then added dropwise to the deprotonated nitrophenol. Single crystals of *bis*(4-nitrophenyl)phenyl phosphate were obtained through slow evaporation of the reaction solution (**Fig. 3.1**).

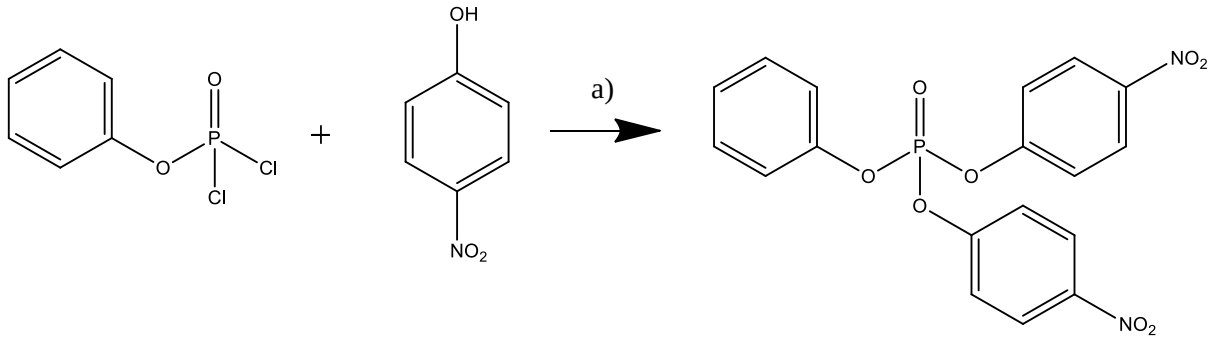

Scheme 3.1: *Synthetic route to bis(4-nitrophenyl)phenyl phosphate. Reaction yields and conditions: a) NEt_3, MeCN, 0°C – RT, 1h, 81%.*

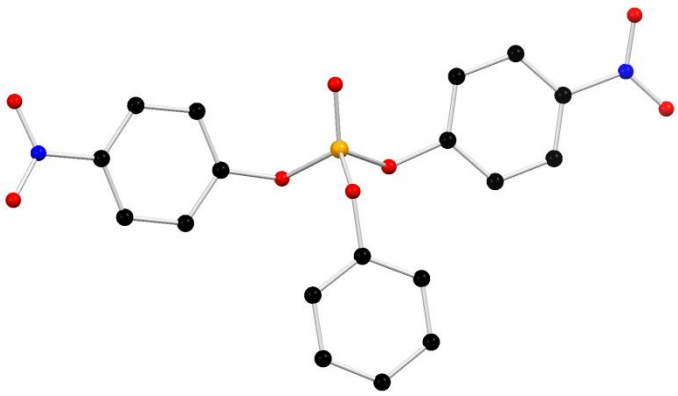

Figure 3.1*: The molecular structure of bis(4-nitrophenyl)phenyl phosphate (hydrogen atoms omitted for clarity).*

The crystal data was solved in the triclinic P-1 space group with the unit cell containing one complete ligand molecule (full refinement data in Table 3, Appendix 2). The *bis*(4-nitrophenyl)phenyl phosphate molecules stack on top of one another with off centre

parallel π-π interaction separated by 3.431 Å between the benzene rings (**Fig. 3.2**). No apparent hydrogen bonding is seen within this system.

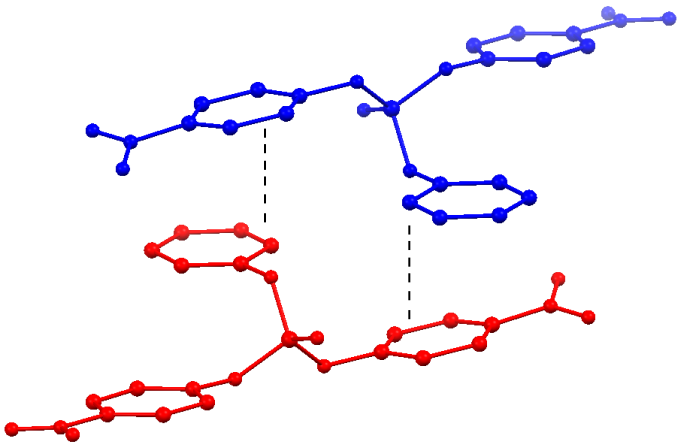

Figure 3.2*: Crystal structure of precursor bis(4-nitrophenyl)phenyl phosphate showing weak π-π interactions between molecule units.*

The *bis*(4-nitrophenyl)phenyl phosphate was then reduced *via* a hydrogen gas reduction over 10% Pd/C as a catalyst, which proceeded to completion over 19 hours (**Scheme 3.2**). After being filtered through Celite, single crystals of *bis*(4-aminophenyl)phenyl phosphate were obtained through slow evaporation of a concentrated methanol solution (**Fig. 3.3**). The amine groups are found displaced over the three benzene rings with occupancies of 0.9, 0.85 and 0.25. This 4-aminophenyl-substituted ligand was capable of forming supramolecular structures, creating *bis*-bidentate ligands when reacted with aldehydes, through the formation of imine groups.

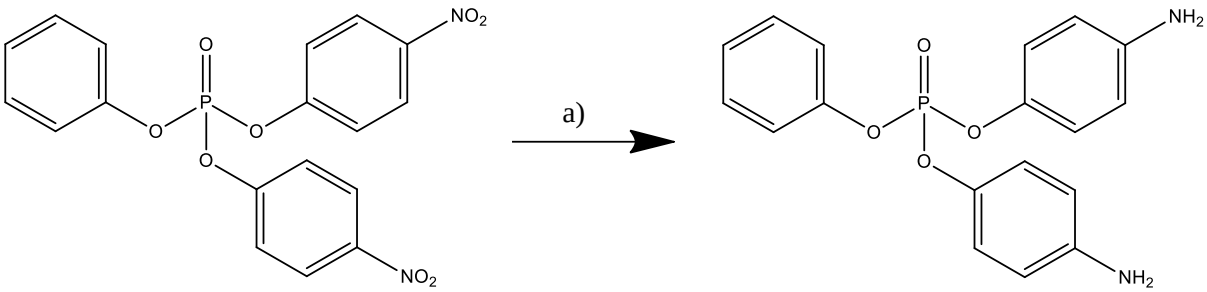

Scheme 3.2: *Synthetic route to pre cursor ligand bis(4-aminophenyl)phenyl phosphate. Reaction yields and conditions: a) H_2, 10% Pd/C, MeOH, RT, 22h, 88%.*

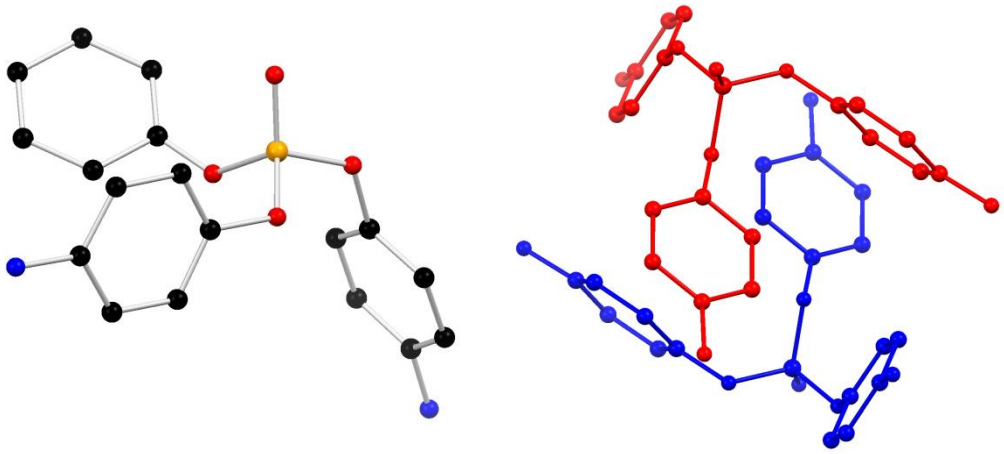

Figure 3.3*: The molecular structure of the pro-ligand* ***L2****, bis(4-aminophenyl)phenyl phosphate (left, hydrogen atoms omitted for clarity, the amine with 0.25 occupancy has been omitted for clarity), crystal packing of ligand bis(4-aminophenyl)phenyl phosphate, showing edge to face π-π interactions between two molecules (right).*

The crystal data was solved in the triclinic P-1 space group, (full refinement data in Table 3, Appendix 2). There is one ligand molecule present within the unit cell. Investigations into the crystal packing of ligand *bis*(4-aminophenyl)phenyl phosphate reveal an alteration of π-π interactions opposed to its nitro precursor. Edge to face π-π interactions with a separation of 3.338 Å is seen between the pendant phenyl ring and aminophenyl rings on adjacent molecules (**Fig. 3.3**). Hydrogen bonding between amine groups is seen relating the π-π interacting units to others within lattice.

3.3 Complex formation

To form $[M_2L_3]^{4+}$ supramolecular assemblies containing the phosphate pro-ligand **L2,** subcomponent self-assembly was attempted using the pro-ligand, appropriate aldehydes and metals ions. The aldehydes used in the self-assembly reaction included; 2-pyridinecarboxyaldehyde, 2-imidazolecarboxyaldehyde, 4-imidazolecarboxyaldehyde, 1-methyl-2-imidazolecarboxyaldehyde and 4-methyl-5-imidazolecarboxyaldehyde. The low stability and sensitivity of the phosphate bonds to acid and base, which is needed to catalyse the imine bond formation needs to be taken into consideration.[83] Stabilisation of the imine bond formation, however, allows for supramolecular structures to be formed *in situ*. The self-assembly reaction using 4-imidazolecarboxyaldehyde or 2-imidazolecarboxyaldehyde as the head groups was unsuccessful when attempted with Fe^{2+}, Co^{2+}, Ni^{2+}, Cu^{2+} and Zn^{2+} metal ions. No solid-state or MS data were obtained for any of these combinations. Creation of $[M_2L_3]^{4+}$ architectures was however achieved using 2-pyridinecarboxyaldehyde, 4-methyl-5-imidazolecarboxyaldehyde and 1-methyl-2-imidazolecarboxyaldehyde as the head groups with a variety of metal ions. Evidence of the formation of supramolecular assemblies is seen in MS analysis performed on the solutions after the self-assembly reactions.

3.4 Studies of *bis*(4-(E)-(pyridine-2-ylmethylene)amino)phenyl) phosphate, L5

The reaction between $Fe(ClO_4)_2.3H_2O$, the pro-ligand and 2-pyridinecarboxyaldehyde forms the ligand phenyl *bis*(4-(E)-(pyridine-2-ylmethylene)amino)phenyl) phosphate (**L5**) *in situ* (**Fig. 3.4**). This produced a solution of dark purple colour, which is expected for low spin Fe(II) metals.[84] The MS results for the $[Fe_2\mathbf{L5}_3]^{4+}$ supramolecular assembly show evidence for $[M_2L_3]^{4+}$ formation, with evidence of perchlorate anions being associated with the complex (**Fig. 3.5, A3**). Multiply charged peaks containing Fe(II) ions can be identified, with the peaks at 428 m/z corresponding to the $[Fe_2\mathbf{L5}_3]^{4+}$ (M^{4+}) supramolecular species. The peaks at 604

corresponds to a $[M_2L_3]^{4+}$ supramolecular assembly with an perchlorate anion associated to it, (M^{3+}) $[Fe_2\mathbf{L5}_3][ClO_4]^{3+}$. The $[Fe_2\mathbf{L5}_3][ClO_4]_2^{2+}$ supramolecular assembly (M^{2+}) is seen with peaks at 956 m/z. This reaction was also attempted using a range of other metal centres including, Co^{2+}, Zn^{2+}, Ni^{2+}, Cu^{2+} but only MS peaks corresponding to complex formation were observed for the $[Zn_2\mathbf{L5}_3]^{4+}$ helicates (**A4-A5**). Peaks at 456 are indicative of the (M^{4+}), $[Zn_2\mathbf{L5}_2]^{4+}$ supramolecular species.

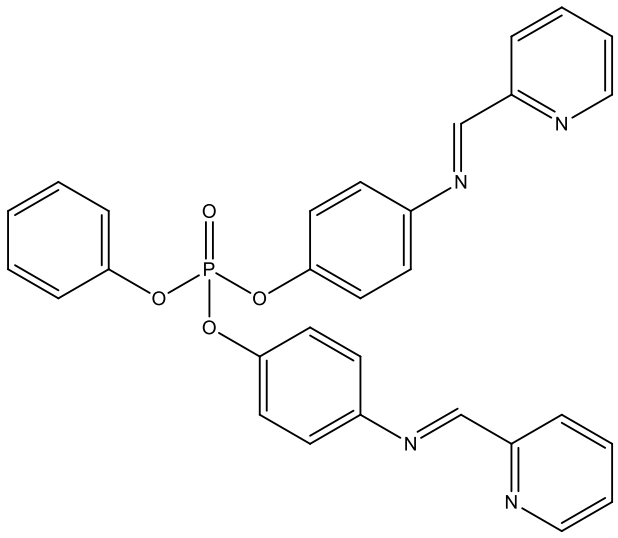

Figure 3.4**: Phenyl bis(4-(E)-(pyridine-2-ylmethylene)amino)phenyl) phosphate, **L5.

.

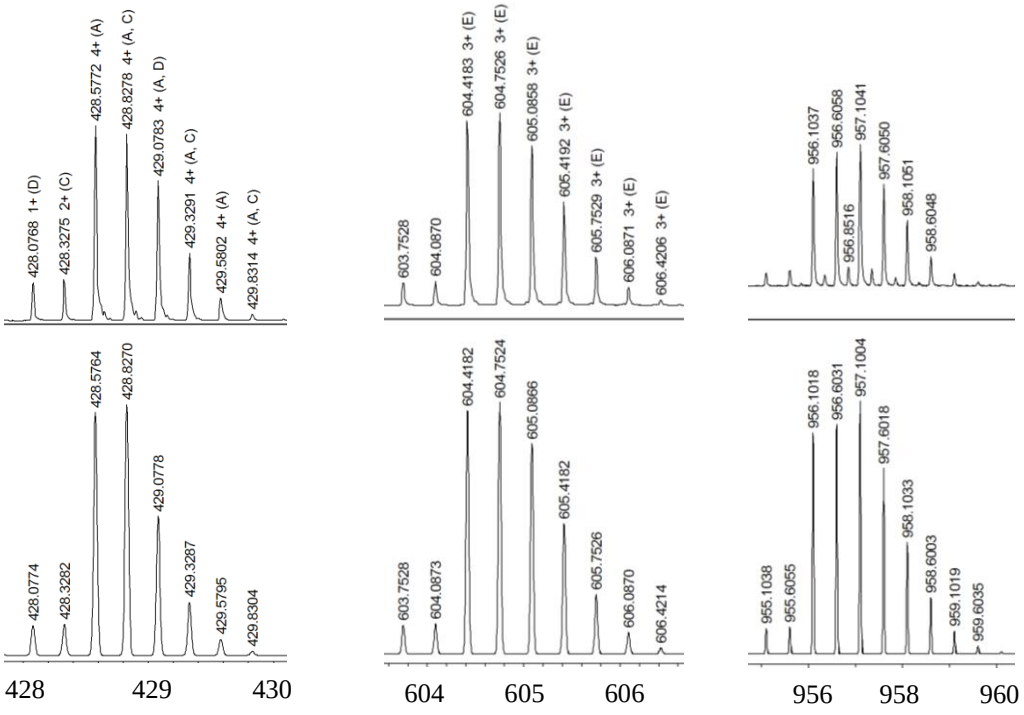

Figure 3.5*: The experimental (top) and simulated (bottom) MS spectra showing evidence of* $[Fe_2\mathbf{L5}_3]^{4+}$, $[Fe_2\mathbf{L5}_3][ClO_4]^{3+}$, $[Fe_2\mathbf{L5}_3][ClO_4]_2^{2+}$ *species shown left to right respectively.*

Attempts to produce X-ray quality single crystals by vapour diffusion using a variety of antisolvents and slow evaporation were unsuccessful. Vapour diffusions were conducted at room temperature and below 273 K, with benzene doping of solutions also being attempted to facilitate crystallisation through favourable π-π interactions, however, no suitable single crystals were observed. The ^{1}H NMR spectra taken from the $[Fe_2\mathbf{L5}_3]^{4+}$ precipitate shows evidence of the fully assembled ligand formation by the imine peak at δ_H 8.87, identified pyridine peaks at 8.50, 8.38, 7.75 and the peaks of the pre-cursor ligand (A). Although no crystals were formed for this complex, the results from the MS analysis and the ^{1}H-NMR spectroscopy suggest the presence of the desired $[M_2L_3]^{4+}$ assembly.

3.5 Studies of *bis*(4-((E)-((4-methyl-4*H*-imidazol-5-yl)methylene)amino)phenyl)phenyl phosphate, L6:

The ligand *bis*(4-((E)-((4-methyl-4*H*-imidazol-5-yl)methylene)amino)phenyl)phenyl phosphate, **L6**, is created *in situ* during the sub-component self-assembly with 4-methyl-5-imidazolecarboxyaldehyde and precursor ligand, **L2**, in the presence of metal ions (**Fig. 3.6**). Formation of the desired $[M_2\mathbf{L6}_3]^{4+}$ complexes is seen in the MS spectra for the sub-component reaction with Co^{2+} metal ions (**Fig. 3.7, A6-A7)**. Multiply charged peaks are seen with those at 434 m/z corresponding to the $[Co_2\mathbf{L6}_3]^{4+}$ (M^{4+}) supramolecular species. The (M^{3+}) supramolecular species $[Co_2\mathbf{L6}_3]^{3+}$ species is additionally observed with peaks seen at 579 m/z. $[Co_2\mathbf{L6}_3][ClO_4]^{3+}$ is observed through (M^{3+}) peaks at 612 m/z. The data shows evidence of the complex including association to perchlorate anions. Supramolecular assemblies are also shown in the MS spectra for self-assembly reactions involving Ni^{2+} and Fe^{2+} metal ions (**A8-A13**). No peaks for supramolecular helicates were found with Cu^{2+} or Zn^{2+} metal ions which were also attempted.

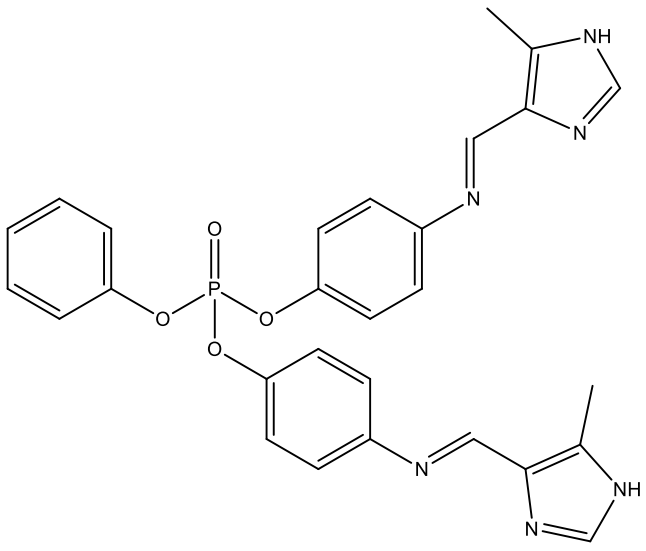

***Figure 3.6**: The ligand bis(4-((E)-((4-methyl-4H-imidazol-5-yl)methylene)amino)phenyl)phenyl phosphate, **L6**, created in situ.*

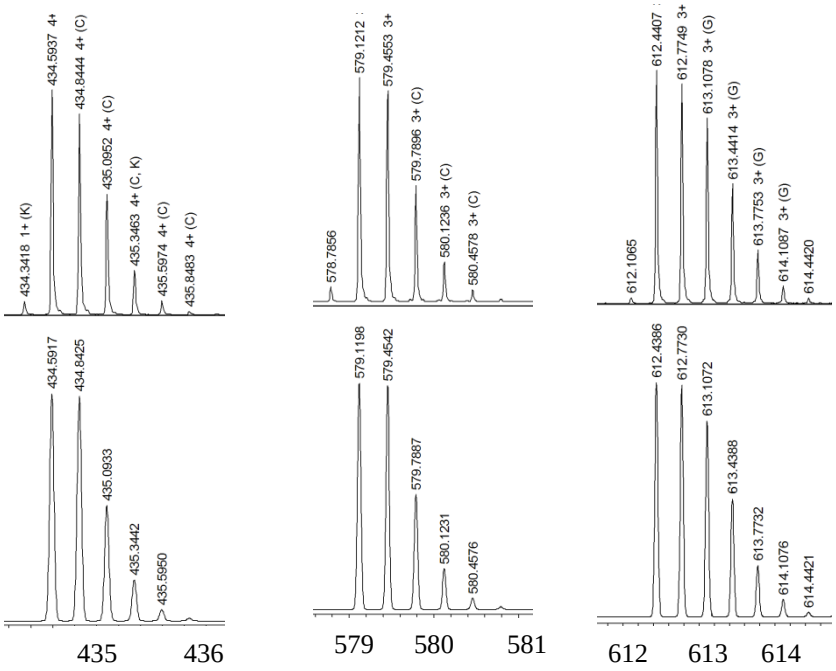

***Figure 3.7**: The experimental (top) and simulated (bottom) MS showing evidence of $[Co_2\mathbf{L6}_3]^{4+}$, $[Co_2\mathbf{L6}_3]^{3+}$, $[Co_2\mathbf{L6}_3][ClO_4]^{3+}$ species.*

3.6: Structural Investigations into $[M_2L_3]^{4+}$ assemblies formed with L6:

As with the supramolecular helicates using **L5**, a wide range of crystallisation methods were used to try to obtain X-ray diffraction quality single crystals. The majority of the samples, as with the last case, yielded no suitable results. One case however, resulted in crystals of sufficient quality: $[Co_2\mathbf{L6}_3]^{4+}$ crystallised when tetrahydrofuran was diffused into the acetonitrile solution containing a 3:6:2 ratio of ligand, 4-methyl-5-imidazolecaroxaldehyde and $Co[ClO_4]_2.6H_2O$, respectively, at room temperature (**Fig. 3.8**). The structure was solved and refined in the hexagonal P-62*c* space group (full refinement data in Table 3, Appendix 2). The unit cell of the crystal structure is of one cobalt centre and half of one ligand. The geometry of the metal centres is a distorted octahedral, seen in the *cis* angle (Co1 82.2°-96.6°) with a Σ value of 49.1 which is significantly different to the expected value of 0 for octahedral geometries. The Co-Co distance is 13.315 Å. The Co-N distances were 1.984(10) Å and 1.879(11) Å for the imine and imidazole nitrogen atoms, respectively.

This is suggestive LS Co(II), the MS of the dissolved crystals shows that the supramolecular species is formed with Co(II) metal ions due to the charge of the species. Upon closer inspection of the structure it is observed that this is not the suspected helicate but rather a mesocate. The ligands stretch between the two metal centres, however, they do not twist around one another and are coordinated in a linear fashion.

As can be seen in the structure below, the pendant phenyl group on the phosphate is absent from the molecular structure, which is believed to be due to disorder (complicated by the high symmetry hexagonal space group) and the low quality data collected (with the associated rapid fall off of crystallographic data at higher resolutions). In the crystal structure, high flexibility and mobility could cause disorder of the phenoxy group over a number of positions, making solving of the structure difficult. This is seen in the structure below, as the phenoxy oxygen atoms are disordered over two positions, both having a 50% occupancy (as dictated by symmetry). An alternative possibility as to why the phenyl ring is absent is that this structure is a decomposition product of the initial $[M_2L_3]^{4+}$ structure, where exchange of the pendant phenoxy group for water or the hydroxide anion might aid crystallisation. The ESMS spectrum taken of the dissolved crystals, however, match the data taken from the solution, which contains the complete ligand (including the pendant phenoxy substituents). This is evidence that high symmetry and disorder could be the cause for the missing phenyl rings in the solid-state structure. The presence is additionally inferred from the P-O bond length of 1.64(2) Å, which is consistent with a P-O single bond rather than a delocalised anionic oxygen atom.[85-87] Although the structure shown does not show the whole ligand, one can see the novel $[M_2L_3]^{4+}$ structures that have been formed.

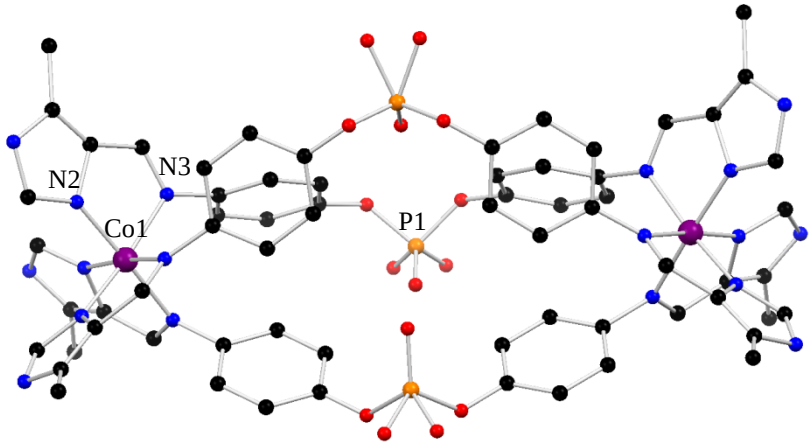

***Figure 3.8**: Molecular structure of $[Co_2\mathbf{L6}_3]^{4+}$, collected at 120 K (solvents, hydrogens and anions omitted for clarity)*

3.7 Crystal packing

The high symmetry of these mesocates is further observed in the crystal lattice. Viewing down the c-axis, the mesocates are seen to pack in a manner that forms hexagonal channels (**Fig. 3.9**). The position in which the pendant phenyl substituent should be observed in the crystal structure is within in the centre of the hexagonal channels formed by the mesocate units. The symmetry elements within the hexagonal channels disorder anything that resides within that space in the crystal lattice, potentially removing it from being seen. No obvious π-π interactions are seen within the crystal structure, though as the pendant phenoxy groups are unable to be observed, the presence of π-π interactions cannot be disregarded completely. The Co-Co distance between a mesocate and its nearest neighbour is 10.522 Å which is larger than the smallest packing distance of the sulfonated cobalt helicate, likely due to hydrogen bonding which is present in the mesocate. The mesocate units are aligned in a parallel fashion and exhibit hydrogen bonding of 2.714 Å between the imidazole N-H groups of two neighbouring mesocate assemblies (**Fig. 3.10**). These non-coordinating nitrogen atoms

were modelled with 0.5 hydrogen occupancy, making three out of the six imidazole rings anionic.

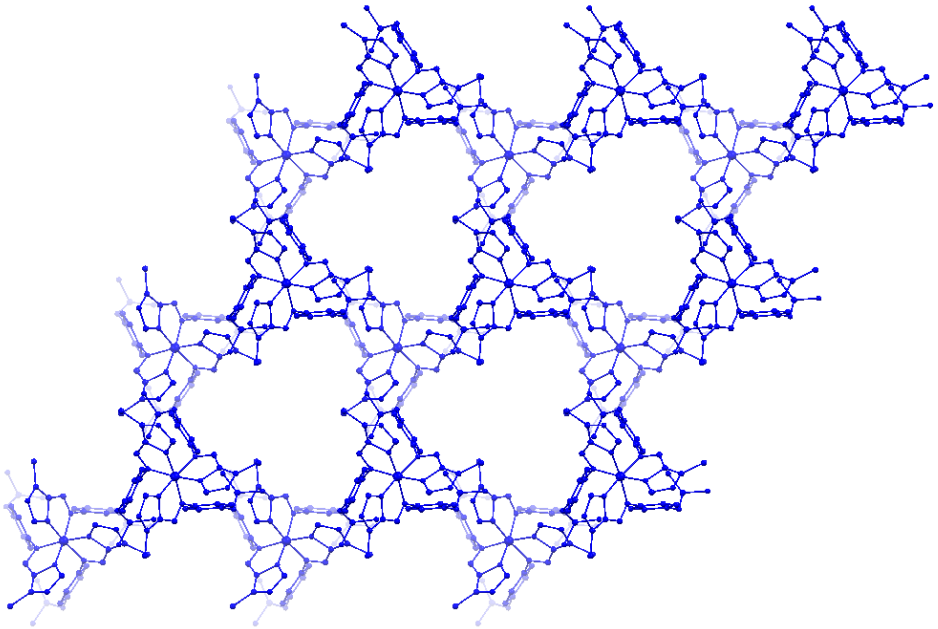

Figure 3.9: *Crystal packing of* $[Co_2\mathbf{L6}_3]^{4+}$*, looking down the c-axis, showing hexagonal channels formed in the crystal structure.*

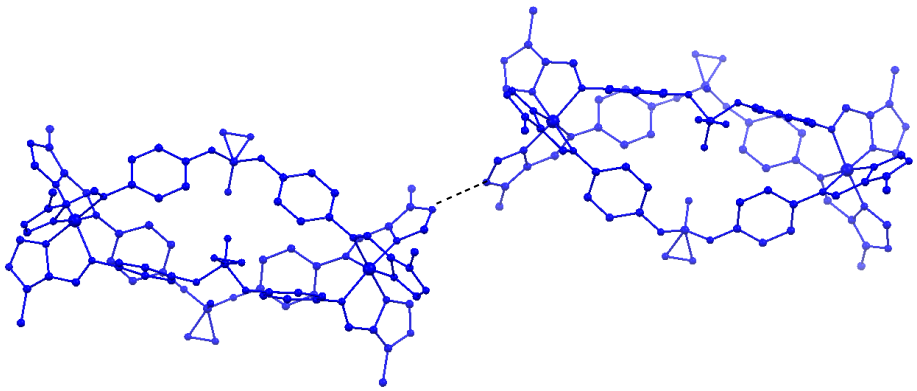

Figure 3.10: *Molecular structures within the crystal lattice of* $[Co_2\mathbf{L6}_3]^{4}$ *showing hydrogen bonding of 2.714 Å between two imidazole groups of the neighbouring* $[Co_2\mathbf{L6}_3]^{4+}$*mesocate units, looking down the b-axis.*

3.8 Studies of *bis*(4-((E)-((1-methyl-1*H*-imidazol-2-yl)methylene)amino)phenyl)phenyl phosphate, L7:

The sub-component self-assembly using 1-methyl-2-imidazolecarboxyaldehyde as the head group, with precursor **L2,** forms ligand *bis*(4-((E)-((1-methyl-1*H*-imidazol-2-yl)methylene)amino)phenyl)phenyl phosphate, **L7** (**Fig. 3.11**). Supramolecular $[M_2L_3]^{4+}$ assemblies are observed in the MS spectrum when this self-assembly reaction takes place with Co^{2+} metal ions (**Fig. 3.12, A14**). The multiply charged peaks at 434 m/z correspond to the $[Co_2\mathbf{L7}_3]^{4+}$ supramolecular species and the peaks at 612 m/z are corresponding to the $[Co_2\mathbf{L7}_3]^{3+}$ species. Supramolecular assemblies consisting of the **L7** ligand complexed with Ni^{2+} are shown in the MS spectrum (**A15-A17**). No peaks for supramolecular $[M_2L_3]$ assemblies were found with Fe^{2+}, Cu^{2+} or Zn^{2+} metal ions which were also attempted. Attempts to obtain single crystals of X-ray quality included vapour diffusions under varying conditions and slow evaporation, however, no suitable crystals were obtained for these complexes.

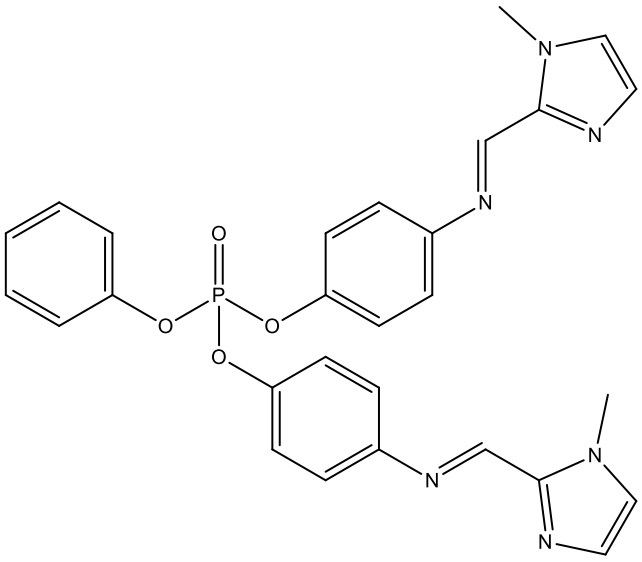

Figure 3.11*: Ligand,* ***L7****, created in situ during a sub-component self-assembly reaction of precursor ligand* ***L2****, 1-methyl-2-imidazolecarboxyaldehyde.*

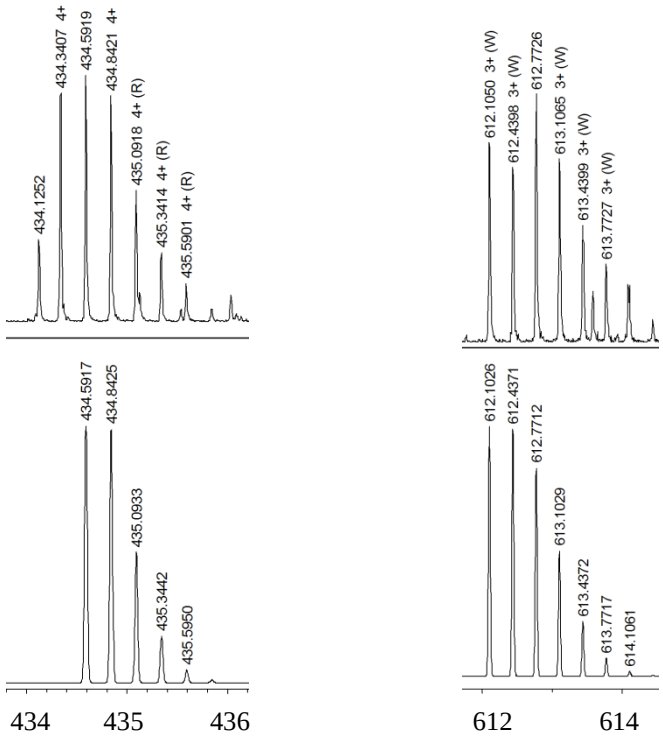

***Figure 3.12**: The experimental (top) and simulated (bottom) MS spectrum of the $[Co_2\mathbf{L7}_3]^{4+}$ and $[Co_2\mathbf{L7}_3]^{3+}$ with an associated ClO_4^- anion, shown left to right respectively.*

3.9 Conclusion:

The precursor ligand *bis*(4-aminophenyl) phenyl phosphate, **L2**, was successfully synthesised using modified literature preparations. Sub-component self-assembly of this ligand with a variety of aldehyde head groups and metal ions have resulted in a series of supramolecular architectures being formed. This has included combinations of 2-pyridinecarboxyaldehyde, 4-methyl-5-imidazolecarboxyaldehyde and 1-methyl-2-imidazolecarboxyaldehyde head groups which *in situ* formed ligands **L5**, **L6** and **L7** with the precursor ligand respectively. The resulting $[M_2L_3]^{4+}$ architectures were identified primarily using MS analysis; $[Fe_2\mathbf{L5}_3]^{4+}$, $[Zn_2\mathbf{L5}_3]^{4+}$, $[Fe_2\mathbf{L6}_3]^{4+}$, $[Co_2\mathbf{L6}_3]^{4+}$, $[Ni_2\mathbf{L6}_3]^{4+}$, $[Co_2\mathbf{L7}_3]^{4+}$, $[Ni_2\mathbf{L7}_3]^{4+}$ and $[Cu_2\mathbf{L7}_3]^{4+}$. The molecular structure of the $[Co_2\mathbf{L6}_3]^{4+}$ mesocate was identified and solved using single crystal X-ray crystallography. Unfortunately, crystallisations of the other systems were unsuccessful.

Conclusions and Future Work

A series of sulfonated helicates were synthesised through sub-component self-assembly using the precursor ligand **L**, 6,6'-oxy-*bis*(3-aminobenzenesulfonic acid). The sulfonated helicates were varied through changing the metal ion, base and aldehyde used in the self-assembly reaction. This resulted in the isolation of six characterised complexes that were; $[Fe(OH_2)_6][Fe_2\mathbf{L3}_3]$, $[Co(OH_2)_6][Co_2\mathbf{L4}_3]$, $[Ni(OH_2)_6][Ni_2\mathbf{L4}_3]$, $K_2[Fe_2\mathbf{L3}_3]$, $Ca[Fe_2\mathbf{L3}_3]$ and $[Fe(OH_2)_6]_{0.2}Rb_{1.6}[Fe_2\mathbf{L3}_3]$. The complexes produced with ligands **L3** and **L4**, which are produced *in situ* by metal complexation, crystallise in multiple space groups; orthorhombic and monoclinic. Hydrogen bonding results in helicates being oriented in a perpendicular fashion through the hydrogen bond between the sulfonate and imidazole head groups of neighbouring helicates, as opposed to the parallel alignment that occurs without this additional bonding. This alteration and potential communication introduced into the crystal lattice could produce cooperativity between different spin-crossover metal centres. Preliminary investigations into the spin-crossover have been conducted through examining the bond lengths observed by SC-XRD and conducting variable temperature X-ray crystallography and UV-vis experiments. The bond lengths suggest that the iron helicates have LS metal centres, however, the other two methods to investigate spin-crossover properties were unsuccessful due to the helicates being weakly diffracting and most soluble in water. The magnetisation results do not show significant SCO occuring, however the uncertainty of the molecular weight hinders the full analysis of the data.

Supramolecular mesocates were isolated using a phosphorus containing precursor ligand, *bis*(4-aminophenyl)phenyl phosphate, **L5.** Self-assembly with head groups 2-pyridinecarboxyaldehyde, 4-methyl-5-imidazolecarboxyaldehyde and 1-methyl-2-imidazolecarboxyaldehyde resulted in the formation of $\mathbf{[}Fe_2\mathbf{L5}_3]^{4+}$, $[Zn_2\mathbf{L5}_3]^{4+}$, $[Fe_2\mathbf{L6}_3]^{4+}$, $[Co_2\mathbf{L6}_3]^{4+}$, $[Ni_2\mathbf{L6}_3]^{4+}$, $[Co_2\mathbf{L7}_3]^{4+}$, $[Ni_2\mathbf{L7}_3]^{4+}$ and $[Cu_2\mathbf{L7}_3]^{4+}$ assemblies. These complexes were all identified through ESMS analysis in solution. Additionally, one crystal structure was

obtained from complex $[Co_2\mathbf{L6}_3]^{4+}$ which confirmed the formation of a supramolecular $[M_2L_3]$ architecture. The ligand shown in the solid-state structure was missing the pendant phenyl rings, thought to be due to the high symmetry of the crystal lattice as the mass spectrum of the dissolved crystals showed the presence of the phenyl ring. Due to the difficulty of crystallisation no other crystal structures were obtained for this series of complexes. The combination of the solid-state structure, the promising ^{1}H-NMR result and various MS solution studies for these complexes established that supramolecular assemblies have been synthesised.

Further work for these mesocates would involve intensive work on their crystallisation to try to procure further solid-state data to examine. The crystallisation process was not successfully explored and optimised for this system, although various techniques were attempted. If successful, the crystallisation would enable the study of the mesocates properties, *e.g.*, spin-crossover. Syntheses of additional phosphate-based ligands are also of interest to expand the series of complexes. The precursor ligand phenylphosphonic dichloride would be of interest to investigate whether the removal of the linking oxygen atom has a significant effect on the supramolecular assemblies' properties and ability to crystallise (**Fig. 4.1**).

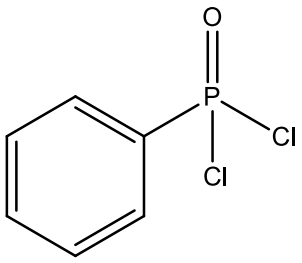

Figure 4.1*: Potential precursor ligand phenylphosphonic dichloride*

To widen the potential phosphorus containing supramolecular structures formed, ligands made with 3-nitrophenol and 2-nitrophenol could also be attempted (**Fig. 4.2**). Preliminary attempts were made to obtain these phosphate analogues, however, more time is required to

refine and optimise their reactions. To synthesise these analogues different synthetic methods can be attempted, including the method described above which successfully synthesised the 4-nitrophenol containing ligand. The other synthetic method that could be attempted involved the initial deprotonation of nitrophenol using sodium hydroxide to which diluted phenyl phosphorodichloridate can be added dropwise afterwards. The synthesis and subsequent reduction to amine funcitionalities would provide pro-ligands with substantially different coordinating angles, providing an opportunity to create diverse supramolecular assemblies.

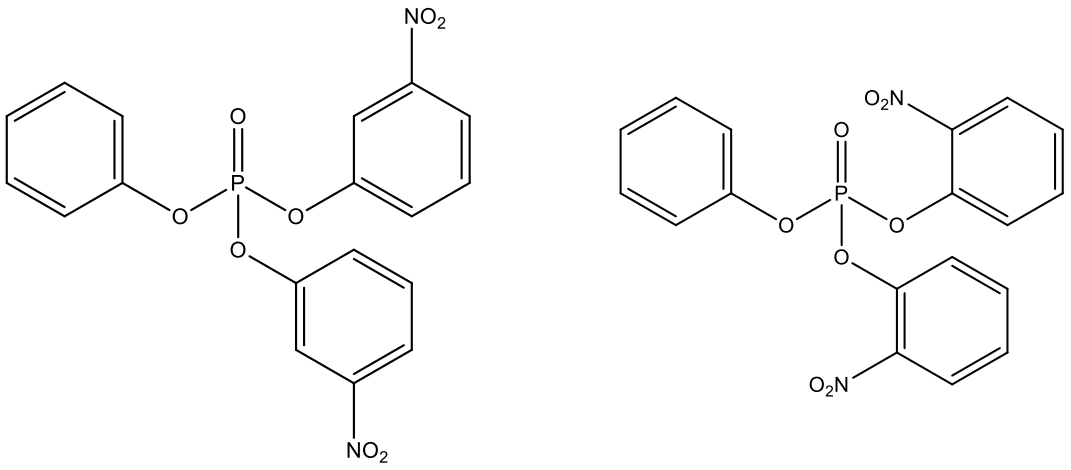

***Figure 4.2**: Potential nitro-phenolphosphate analogues made by using 3-nitrophenol (left) or 2-nitrophenol (right) instead of 4-nitrophenol*

Experimental Methods

All starting materials and reagents were reagent grade and used as received from standard suppliers. Solvents were reagent grade and used as received. Infrared spectra were recorded on a Bruker ALPHA Platinum ATR FT-IR spectrometer. Melting points were recorded on an Electrothermal melting point apparatus and are uncorrected. ^{1}H, ^{13}C and ^{31}P NMR measurements were carried out on an Agilent 400 MR spectrometer with chemical shifts given in parts per million (PPM). Thermogravimetric Analyses for complexes **1** (Supporting Information) were carried out on an AlphaTech SDT Q600 DSC/TGA instrument using alumina crucibles, where samples were heated under nitrogen flow of 100 mL min^{-1} and heated at a rate of 1°C min. The magnetic susceptibilities were measured using a Quantum Design Squid Magnetometer, PPMS, ac and dc field of 1 T, with samples held within gelatin capsules held at the centre of a straw which is fixed at the end of the sample rod. Samples were sent to Monash University and the magnetic susceptibilities were run by Boujemaa Moubaraki and fitted by Professor Keith Murray.

X-Ray Crystallography

Crystallographic data for compounds $K_2[Fe_2(\mathbf{L3})_3]$, $Rb_2[Fe_2(\mathbf{L3})_3]$, $Ca[Fe_2(\mathbf{L3})_3]$ and $[Co_2(\mathbf{L6})_3]$ were collected on an Oxford-Agilent SuperNova instrument with focused micro-source Cu Kα (λ = 1.5418 Å) radiation and ATLAS CCD area detector, with data reduction performed using *CrysAlis PRO*.[88] Structures for $[Fe(OH_2)_6][Fe_2(\mathbf{L3})_3]$, $[Co(OH_2)_6][Co_2(\mathbf{L4})_3]$ and $[Ni(OH_2)_6][Ni_2(\mathbf{L4})_3]$ were collected at the Australian Synchrotron MX1 Beamline with silicon double crystal-monochromatised Mo Kα (λ = 0.71073 Å) radiation and ADSC Quantum 210r detector, with data reduction performed using *BluIce* and *XDS*.[89-90] All structures were solved using direct methods with SHELXT and refined on F^2 using all data by full matrix least-squares procedures with SHELXL within OLEX2.[91-93] Non-hydrogen atoms were refined with anisotropic displacement parameters. Hydrogen atoms were included in calculated positions, or were manually assigned from

residual electron density where appropriate, with isotropic displacement parameters 1.2 times the isotropic equivalent of their carrier atoms.

Ligand synthesis

Synthesis of 6,6'-oxybis(3-aminobenzenesulfonic acid)

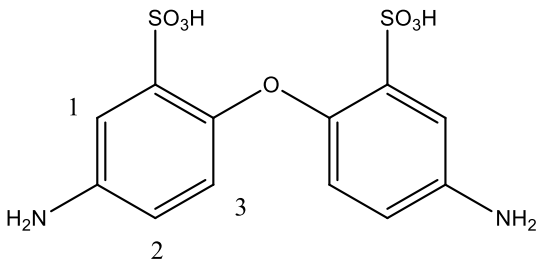

6,6'-oxy*bis*(3-aminobenzenesulfonic acid), **L**, was prepared according to literature methods.[19, 57-58] 4,4'-oxydianiline (1.5 g, 7.46 mmol) was dissolved in concentrated sulfuric acid (95%). After it was completely dissolved excess fuming sulfuric acid (60%) was added dropwise to the reaction mixture. This reaction mixture was stirred at 0°C for 2 hours and then slowly heated to 80°C, where it was kept stirring for another additional 2 hours. After cooling the mixture to room temperature, it was poured over 20 g of ice, which resulted in a white precipitate. This was purified through acid/base purification. Yield 1.96 g (73.0%). MP >300 °C. ^{1}H-NMR (DMSO): δ_H 6.95 (d, 2H, H^1), 6.65 (d, 2H, H^3), 6.34 (dd, 2H, H^2)

Synthesis of bis(4-nitrophenyl)phenyl phosphate

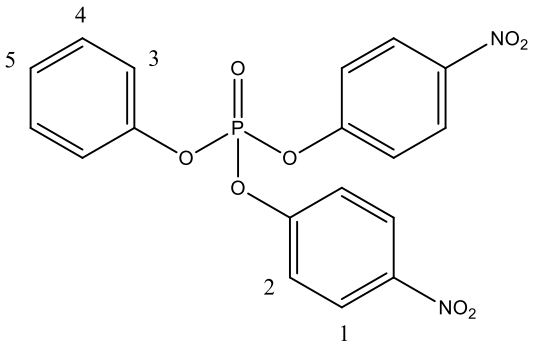

The reaction was carried out under standard Schlenk line conditions. Into a Schlenk tube, 4-nitrophenol (2 g, 14.3 mmol) was added to a solution of dry acetonitrile (30 mL). To this, dry triethylamine (2 mL, 14.3 mmol) was added dropwise *via* syringe at 0°C. Phenyl dichlorophosphate (1 mL, 6.7 mmol) which was diluted in acetonitrile (2 mL) was then added dropwise to the nitrophenol solution and the solution

was left to stir at 0 °C for five minutes and then at room temperature for a further sixty minutes. The solution was filtered and the solvent removed under reduced pressure and then washed with diethyl ether to obtain the product. Yield 2.26 g (81%) MP 110.8-111.0°C ^{1}H-NMR (CD_3CN): δ_H 8.29 (d, 4H, H^1), 7.50 (d, 4H, H^2), 7.45 (t, 2H, H^4), 7.35 (d, 2H, H^3), 7.32 (t, 1H, H^5). ^{13}C-NMR (CD_3CN): δ_C 131.5, 127.8, 127.3, 122.5, 121.2, 79.5, 79.2, 78.9. ^{31}P-NMR (CD_3CN): δ_P -18.84 (s, 1P) ESMS Calculated for $C_{18}H_{14}N_2O_8P$ $[M + H]^+$: 417.05 m/z Found : 417.0488 m/z. IR 853 cm^{-1} (-C-NO_2), 942 cm^{-1} (P-O-Ph symmetric stretch), 1183 cm^{-1} (P-O-Ph asymmetric stretch), 1239 cm^{-1} (-P=O), 1345 cm^{-1} & 1527 cm^{-1} (Ph-NO_2).

Synthesis of bis(4-aminophenyl) phenyl phosphate

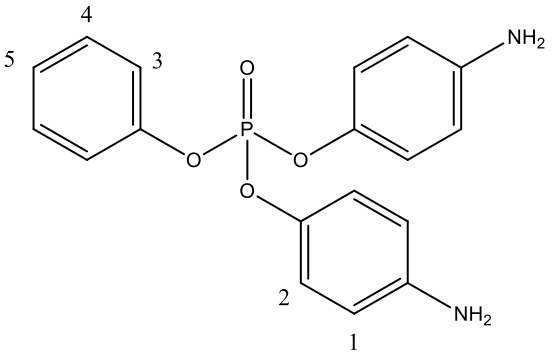

Bis(4-nitrophenyl)phenyl phosphate (1.136 g, 2.73 mmol) was suspended in a solution of dry methanol (50 mL) to which 10% Pd/C was added. A hydrogen balloon was then attached and the reaction was left to stir for 19 hours. The resulting grey suspension was filtered through celite, and the product isolated from the filtrate under reduced pressure. Yield 0.859 (88%). MP 130.1-130.4°C. ^{1}H-NMR (CD_3CN): δ_H 7.42 (t, 2H, H^4), 7.28 (d, 2H, H^3), 7.24 (t, 1H, H^5) 6.96 (d, 4H, H^2) 6.63 (d, 4H, H^1). ^{13}C-NMR (CD_3CN): δ_C 131.3, 126.8, 122.0, 121.3, 116.2, 50.3. ^{31}P-NMR (CD_3CN): δ_P -15.34 (s, 1P) ESMS Calculated for $C_{18}H_{18}N_2O_4P$ $[M + H]^+$: 357.10 m/z Found: 357.0999 m/z, Calculated for $C_{18}H_{19}N_2O_4P$ $[M + 2H]^{2+}$: 179.055 m/z Found: 179.0539 m/z. IR 957 cm^{-1} (P-O-Ph stretch), 1189 cm^{-1} (P-O-Ph asymmetric stretch), 1272 cm^{-1} (-P=O), 3362 cm^{-1} (-Ph-NH_2).

Complex synthesis

Synthesis of $[Fe(OH_2)_6][Fe_2(\mathbf{L3})_3]$

Ligand **L** (15 mg, 41.6 μmol) was added to a solution of triethylamine (11.6 μL, 83.2 μmol) in 15 mL water to give a colourless solution. To this an aqueous solution containing 4-methyl-5-imidazolecarboxyaldehyde (9.2 mg, 83.2 μmol) was added and left to stir at 50°C for 30 minutes. To this solution $FeSO_4.7H_2O$ (7.8 mg, 27.7 μmol) was added and was left to stir at 50°Cfor 19 hours. After this period, the solution turned from colourless to a bright orange colour. Orange plate crystals of suitable quality for single crystal X-ray diffraction were obtained by vapour diffusion of acetonitrile into a concentrated water solution of the product over several days. Yield 7.5 mg (14%) ESMS Calculated for $Fe_2C_{66}H_{58}N_{18}O_{21}S_6$ $[M + 4H]^{2+}$: 581.0376 m/z Found: 581.0376 m/z, Calculated for $Fe_2C_{66}H_{59}N_{18}O_{21}S_6$ $[M + 5H]^{3+}$: 871.0520 Found: 871.0618 m/z. IR 615 cm^{-1} (s), 1021 cm^{-1} (s), 1080 cm^{-1} (s), 1197 cm^{-1} (m), 1244 cm^{-1} (m), 1393 cm^{-1} (m), 1465 cm^{-1} (s), 1622 cm^{-1} (m), 3382 cm^{-1} (s). UV/VIS λmax 484 nm

Synthesis of $[Co(OH_2)_6][Co_2(\mathbf{L4})_3]$

The synthesis of this complex was just as for the synthesis of $[Fe(OH_2)_6][Fe_2(\mathbf{L3})_3]$ with Co^{2+} metal ions obtained from $Co(ClO_4)_2.6H_2O$ (10.2 mg, 27.7 μmol). Colour change from colourless to a bright orange colour was observed. Brown plate single crystals of suitable quality for single crystal X-ray diffraction were obtained by vapour diffusion of methanol or ethanol into a concentrated water solution of the product. Yield 8mg (15%). IR 620 cm^{-1} (s), 1021 cm^{-1} (s), 1079 cm^{-1} (s), 1198 cm^{-1} (m), 1470 cm^{-1} (m), 3315 cm^{-1} (s). UV/VIS λmax 316 nm

Synthesis of $[Ni(OH_2)_6][Ni_2(\mathbf{L4})_3]$

The synthesis of this complex was just as for the synthesis of $[Fe(OH_2)_6][Fe_2(\mathbf{L3})_3]$ with Ni^{2+} metal ions obtained from $Ni(ClO_4)_2.6H_2O$ (10.2 mg, 27.7 μmol) instead of Fe^{2+} being used. A colour change from colourless to a bright orange colour was observed. Orange crystals of suitable quality for single crystal X-ray diffraction were obtained by vapour diffusion of acetone or acetonitrile into a concentrated water solution of the product over several days. Yield 6 mg (11%) IR 620 cm^{-1} (s), 1020 cm^{-1} (s), 1077 cm^{-1} (s), 1187 cm^{-1} (m), 1470 cm^{-1} (m), 1610 cm^{-1} (m), 3443 cm^{-1} (s). UV/VIS λmax 322 nm

Synthesis of $K_2[Fe_2(\mathbf{L3})_3]$

The synthesis of this complex was just as for the synthesis of $[Fe(OH_2)_6][Fe_2(\mathbf{L3})_3]$ with KOH (41.6 μL, 83.2 μmol) being used as the base instead of triethylamine. A colour change from colourless to bright orange was observed. Orange plate of suitable quality for single crystal X-ray diffraction were obtained by vapour diffusion of ethanol into a concentrated water solution of the product over several days. Yield 8.5 mg (18 %) (IR 610 cm^{-1} (s), 1020 cm^{-1} (s), 1079 cm^{-1} (s), 1469 cm^{-1} (m), 1622 cm^{-1} (m), 3141 cm^{-1} (s) UV/VIS λmax 473 nm

Synthesis of $[Fe(OH_2)_6]_{0.2}Rb_{1.6}[Fe_2(\mathbf{L3})_3]$

The synthesis of this complex was just as for the synthesis of $[Fe(OH_2)_6][Fe_2(\mathbf{L3})_3]$ with RbOH (3.33 mL, 83.2 μmol) being used as the base instead of triethylamine. A colour change from colourless to bright orange was observed). Orange plate of suitable quality for single crystal X-ray diffraction were obtained by vapour diffusion of methanol into a concentrated

water solution of the product over several days. Yield 7 mg (13%) IR 615 cm^{-1} (s), 1021 cm^{-1} (s), 1081 cm^{-1} (s), 1471 cm^{-1} (m), 3135 cm^{-1} (s) UV/VIS λmax 310 nm

*Synthesis of Ca[Fe_2(**L3**)$_3$]*

The synthesis of this complex was just as for the synthesis of [$Fe(OH_2)_6$][Fe_2(**L3**)$_3$] with $Ca(OH)_2$ (41.6 μL, 83.2 μmol) being used as the base instead of triethylamine. A colour change from colourless to bright orange was observed. Orange plate of suitable quality for single crystal X-ray diffraction were obtained by vapour diffusion of methanol into a concentrated water solution of the product over several days. Yield 7 mg (14%), IR 615 cm^{-1} (s), 1021 cm^{-1} (s), 1080 cm^{-1} (s), 1471 cm^{-1} (m), 3135 cm^{-1} (s) UV/VIS λmax 473

*Synthesis of [Fe_2**L5**$_3$]$^{4+}$*

Ligand **L2** (15mg, 42.0 μmol) was dissolved in acetonitrile to give a pale brown coloured solution. To this a solution of $Fe(ClO_4)_2.6H_2O$ (7.8 mg, 28.0μmol) and 2-pyridinecarboxyaldehyde (7.99 μL, 84.0 μmol) were added dropwise to the solution of **L2** and left to stir at 50°C for 19 hours. During this time the solution turned from pale brown to a deep purple colour. ESMS Calculated for $Fe_2C_{90}H_{69}N_{12}O_{12}P_3$ $[M]^{4+}$: 428.5764 m/z Found: 428.5772 m/z, Calculated for $Fe_2C_{90}H_{69}N_{12}O_{12}P_3ClO_4$ $[M + ClO_4]^{3+}$: 604.4182 m/z Found: 604.4183 m/z, Calculated for $Fe_2C_{90}H_{69}N_{12}O_{12}P_3Cl_2O_8$ $[M +2ClO_4]^{2+}$: 956.1018 Found: 956.1037 ^{1}H-NMR was obtained from precipitate. ^{1}H-NMR (CD_3CN): δ_H 8.87 (s, 2H) , 8.50 (d, 2H) 8.38 t, 2H), 7.75 (t, 2H) (Pyridine peaks), 7.30 (Multiple peaks under which some pyridine and some of the ligand **L2** fall under), 6.96 (d, 4H) 6.63 (d, 4H). IR 623 cm^{-1} (m),

765 cm^{-1} (m), 841 cm^{-1} (m), 962 cm^{-1} (s), 1094 cm^{-1} (s), 1162 cm^{-1} (s), 1237 cm^{-1} (m), 1494 cm^{-1} (s), 1641 cm^{-1} (m). UV/VIS 568 nm

Synthesis of $[Zn_2\mathbf{L5}_3]^{4+}$

The synthesis of this complex was just as for the synthesis of $[Fe_2\mathbf{L5}_3]^{4+}$ with Zn^{2+} metal ions obtained from $Zn(ClO_4)_2.6H_2O$ (10.5mg, 28.0µmol) instead of Fe^{2+} metal ions being used. Colour change from pale brown to a pale yellow colour was observed. ESMS Calculated for $Zn_2C_{90}H_{69}N_{12}O_{12}P_3$ $[M]^{4+}$: 448.5 m/z Found: 428.5777 m/z. IR 622 cm^{-1} (m), 773 cm^{-1} (m), 841 cm^{-1} (m), 959 cm^{-1} (s), 1088 cm^{-1} (s), 1185 cm^{-1} (s), 1292 cm^{-1} (m), 1492 cm^{-1} (s), 1635 cm^{-1} (m). UV/VIS λmax 326 nm

Synthesis of $[Co_2\mathbf{L6}_3]^{4+}$

Ligand **L2** (15mg, 42.0 µmol) was dissolved in acetonitrile (15mL) to give a pale brown coloured solution. To this a solution of $Co(ClO_4)_2.7H_2O$ (10.3 mg, 28.0µmol) and 4-methyl-5-imidazolecarboxyaldhehyde (9.3 mg, 84.0 µmol) were added dropwise to the solution of **L2** and left to stir at 50°C for 19 hours. After this time the solution turned from a pale brown to a pale yellow colour. Orange hexagonal crystals of X-ray diffraction quality were obtained through vapour diffusion of THF into a concentrated MeCN solution of the complex over several days. ESMS Calculated for $Co_2C_{84}H_{75}N_{18}O_{12}P_3$ $[M]^{4+}$: 434.5917 m/z Found: 434.5937 m/z, Calculated for $Co_2C_{84}H_{74}N_{18}O_{12}P_3$ $[M]^{3+}$: 579.1198 m/z Found: 579.1212 m/z, Calculated for $Co_2C_{84}H_{75}N_{18}O_{12}P_3ClO_4$ $[M + ClO_4]^{3+}$: 612.4386 m/z Found: 612.4407 m/z, Calculated for $Co_2C_{84}H_{73}N_{18}O_{12}P_3$ $[M]^{2+}$: 868.1761 m/z Found: 868.1784, Calculated for $Co_2C_{84}H_{74}N_{18}O_{12}P_3ClO_4$ $[M + ClO_4]^{2+}$: 918.1542 m/z Found: 918.1561 m/z, Calculated for $Co_2C_{84}H_{75}N_{18}O_{12}P_3Cl_2O_8$ $[M + 2ClO4]^{2+}$: 968.1324 m/z Found: 968.1349 m/z. IR 621 cm^{-1} (s), 838 cm^{-1} (m), 958 cm^{-1} (s), 1087 cm^{-1} (m), 1183 cm^{-1} (m), 1489 cm^{-1} (m), 1623 cm^{-1} (m).

Synthesis of $[Ni_2\mathbf{L6}_3]^{4+}$

The synthesis of this complex was just as for the synthesis of $[Co_2\mathbf{L6}_3]^{4+}$ with Ni^{2+} metal ions obtained from $Ni(ClO_4)_2.7H_2O$ (10.3mg, 28.0µmol) instead of Co^{2+} metal ions being used. Colour change from pale brown to pale yellow was observed. ESMS Calculated for $Ni_2C_{84}H_{75}N_{18}O_{12}P_3$ $[M]^{4+}$: 434.0927 m/z Found: 434.0930m/z, Calculated for $Ni_2C_{84}H_{74}N_{18}O_{12}P_3$ $[M]^{3+}$: 578.4546 m/z Found: 578.4548 m/z, Calculated for $Ni_2C_{84}H_{75}N_{18}O_{12}P_3ClO_4$ $[M + ClO_4]^{3+}$: 611.7733 m/z Found: 611.7744 m/z, Calculated for $Ni_2C_{84}H_{73}N_{18}O_{12}P_3$ $[M]^{2+}$: 867.1782 m/z Found: 867.1794 m/z, Calculated for $Ni_2C_{84}H_{74}N_{18}O_{12}P_3ClO_4$ $[M + ClO_4]^{2+}$: 917.1564 m/z Found: 917.1591 m/z, Calculated for $Ni_2C_{84}H_{75}N_{18}O_{12}P_3Cl_2O_8$ $[M + 2ClO_4]^{2+}$: 967.1345 m/z Found: 967.1379 m/z. IR 622 cm^{-1} (s), 695 cm^{-1} (m), 963 cm^{-1} (s), 1094 cm^{-1} (s), 1185 cm^{-1} (s), 1491 cm^{-1} (m), 1625 cm^{-1} (m). UV/VIS λmax 266 nm

Synthesis of $[Fe_2\mathbf{L6}_3]^{4+}$

The synthesis of this complex was just as for the synthesis of $[Co_2\mathbf{L6}_3]^{4+}$ with Fe^{2+} metal ions obtained from $Fe(ClO_4)_2.7H_2O$ (7.8mg, 28.0µmol) instead of Co^{2+} metal ions being used. Colour change from pale brown to an orange colour was observed. ESMS Calculated for $Fe_2C_{84}H_{75}N_{18}O_{12}P_3$ $[M]^{4+}$: 433.5966 m/z Found: 433.5910 m/z, Calculated for $Fe_2C_{84}H_{74}N_{18}O_{12}P_3$ $[M]^{3+}$: 577.7931 m/z Found: 577.7850 m/z. IR 622 cm^{-1} (s), 960 cm^{-1} (s), 1090 cm^{-1} (s), 1185 cm^{-1} (s), 1492 cm^{-1} (m), 1625 cm^{-1} (m).

Synthesis of $[Co_2\mathbf{L7}_3]^{4+}$

Ligand **L2** (15mg, 42.0 µmol) was dissolved in acetonitrile (15 mL) to give a pale brown coloured solution. To this a solution of $Co(ClO_4)_2.7H_2O$ (10.3 mg, 28.0µmol) and 1-methyl-2-imidazolecarboxyaldhehyde (9.3 mg, 84.0 µmol) were added dropwise to the solution of **L2** and left to stir at 50°C for 19 hours. Colour change from pale brown to a pale yellow colour was observed. ESMS Calculated for $Co_2C_{84}H_{75}N_{18}O_{12}P_3$ $[M]^{4+}$: 434.5917 m/z Found: 434.5919 m/z, Calculated for $Co_2C_{84}H_{74}N_{18}O_{12}P_3ClO_4$ $[M + ClO_4]^{3+}$: 612.1026 m/z Found: 612.1050 m/z. IR 958 cm^{-1} (s), 1066 cm^{-1} (s), 1180 cm^{-1} (s), 1487 cm^{-1} (m), 1607 cm^{-1} (m), 1685 cm^{-1} (m).

Synthesis of $[Ni_2\mathbf{L7}_3]^{4+}$

The synthesis of this complex was just as for the synthesis of $[Co_2\mathbf{L7}_3]^{4+}$ with Ni^{2+} metal ions obtained from $Ni(ClO_4)_2.7H_2O$ (10.3mg, 28.0µmol) instead of Co^{2+} metal ions being used. Colour change from pale brown to a light green colour was observed. ESMS Calculated for $Ni_2C_{84}H_{75}N_{18}O_{12}P_3$ $[M]^{4+}$: 434.0927 m/z Found: 434.0944m/z, Calculated for $Ni_2C_{84}H_{75}N_{18}O_{12}P_3ClO_4$ $[M + ClO_4]^{3+}$: 611.7733 m/z Found: 611.7751, Calculated for $Ni_2C_{84}H_{75}N_{18}O_{12}P_3Cl_2O_8$ $[M + 2ClO_4]^{2+}$: 967.1345 m/z Found: 967.1382 m/z. IR 619 cm^{-1} (s), 951 cm^{-1} (s), 1070 cm^{-1} (s), 1185 cm^{-1} (s), 1292 cm^{-1} (m), 1419 cm^{-1} (m), 1443 cm^{-1} (m), 1487 cm^{-1} (m), 1608 cm^{-1} (m). UV/VIS λmax 322 nm

Appendix 1: Supplementary Infomation

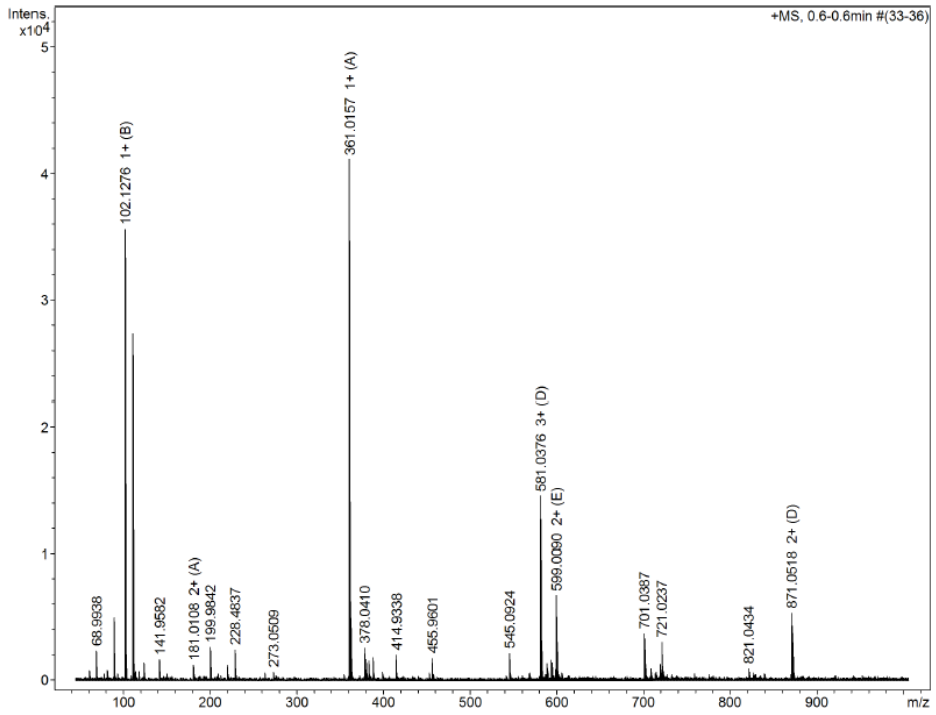

A1: *The MS spectrum of the* $[Fe_2\mathbf{L3}_3]^{2-}$ *helicate.*

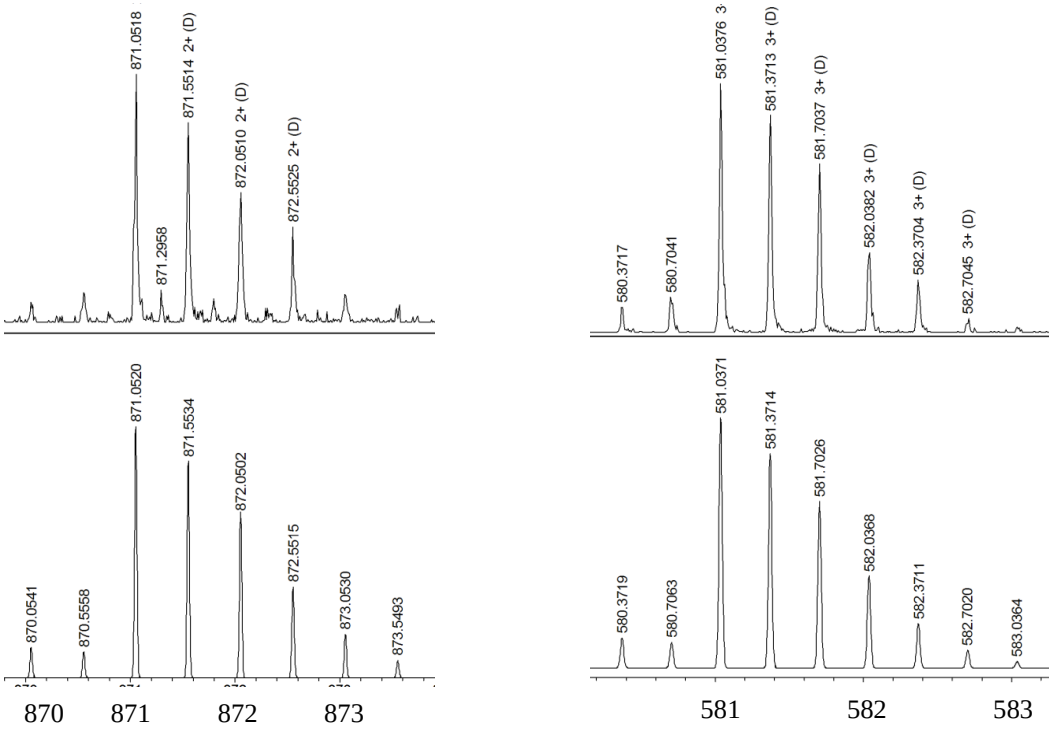

A2: *The experimental (top) and simulated (bottom) MS spectrum showing* $[Fe_2\mathbf{L3}_3]^{2+}$ *and* $[Fe_2\mathbf{L3}_3]^{3+}$ *helicate species shown left to right, respectively.*

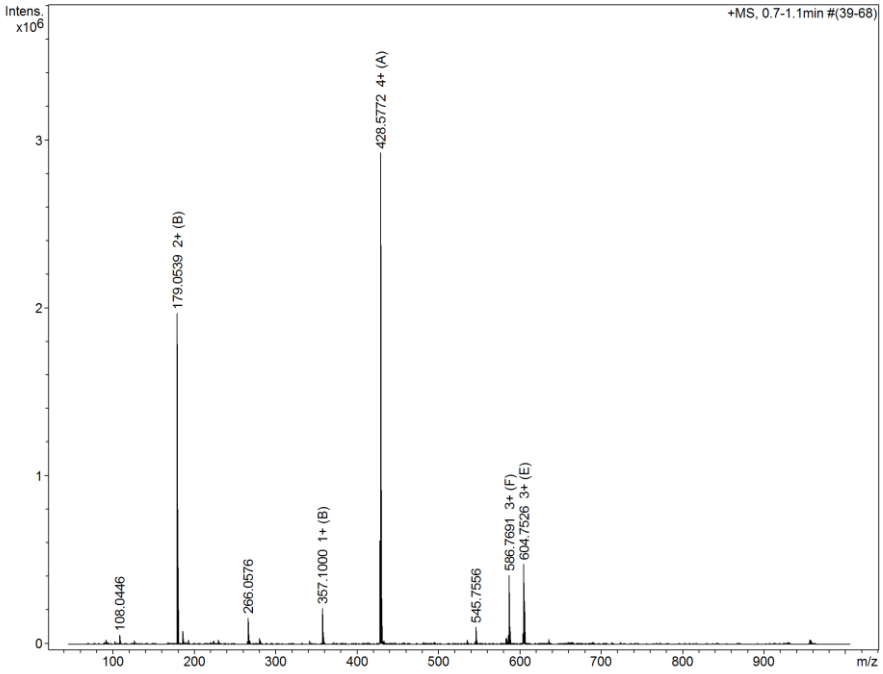

A3: *Complete MS spectrum for* $[Fe_2\mathbf{L5}_3]^{4+}$ *in acetonitrile reaction mixture*

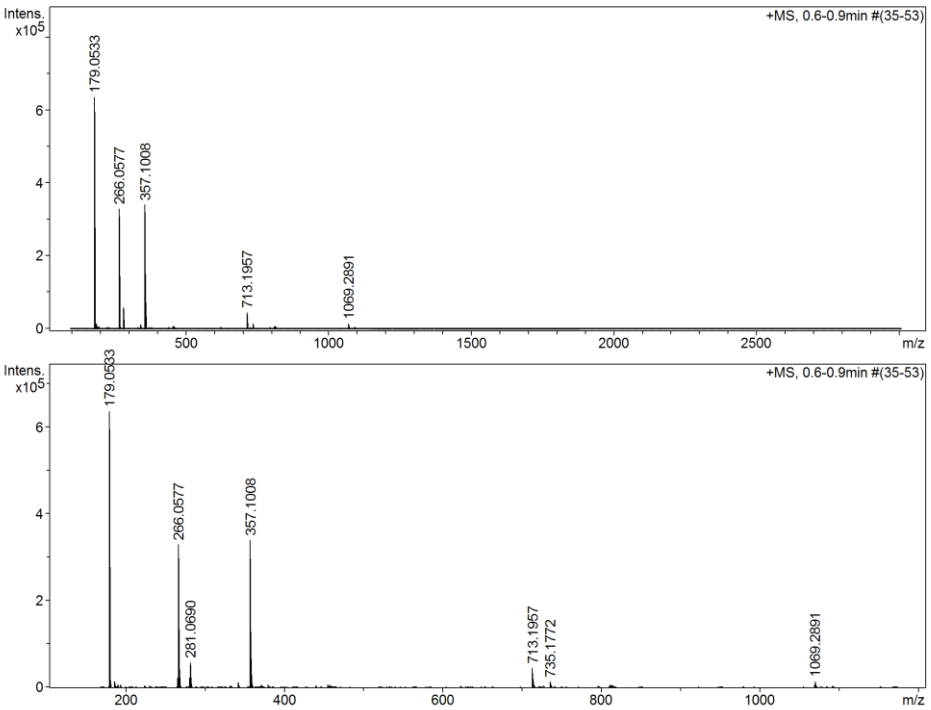

A4: *The MS spectrum for* $[Zn_2\mathbf{L5}_3]^{4+}$ *species.*

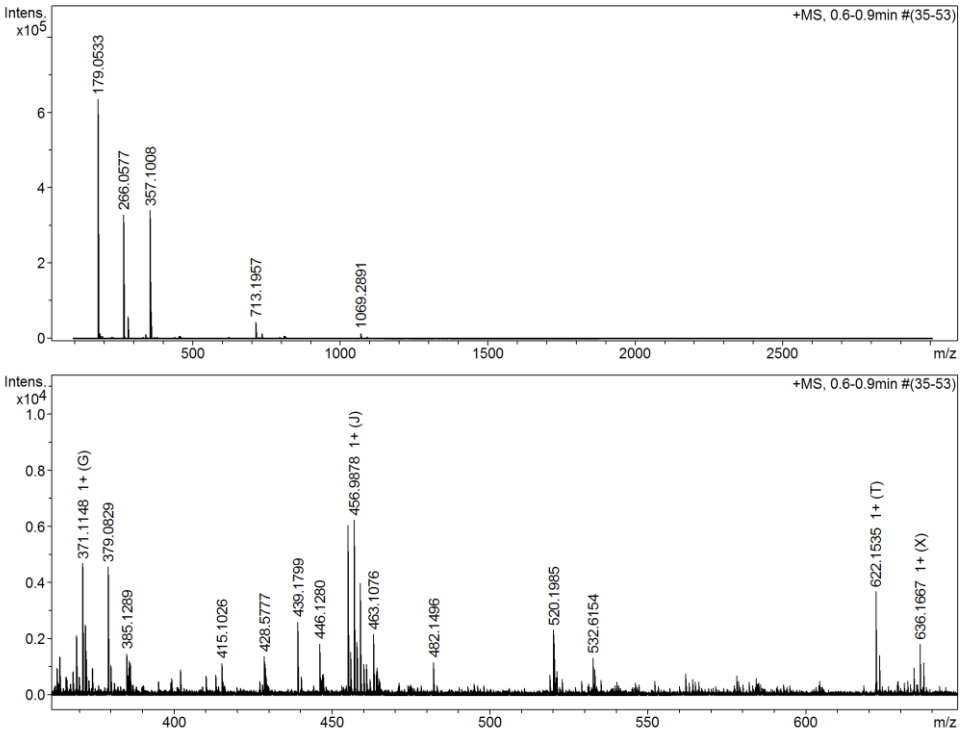

A5: *The MS spectrum for* $[Zn_2\mathbf{L5}_3]^{4+}$ *species*

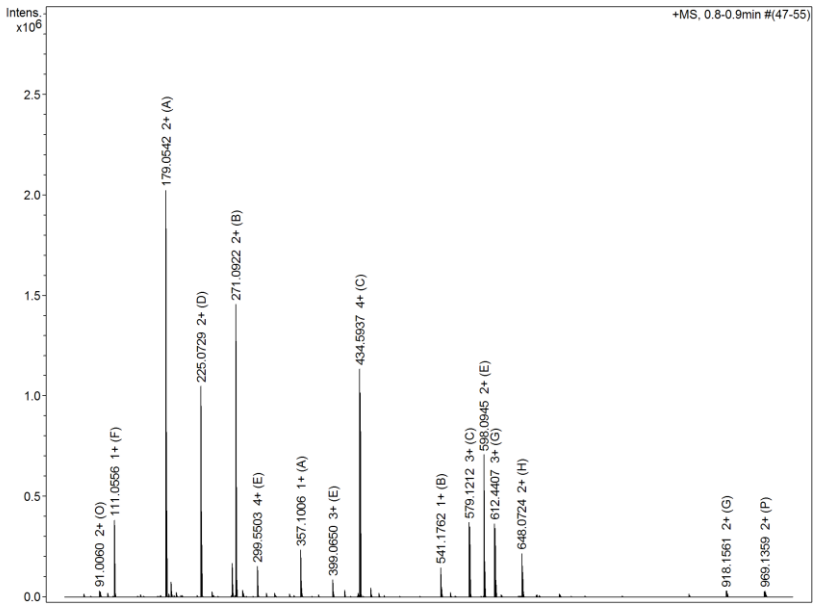

A6*: The MS spectrum of the complex* $Co_2\mathbf{L6}_3$ *collected in acetonitrile.*

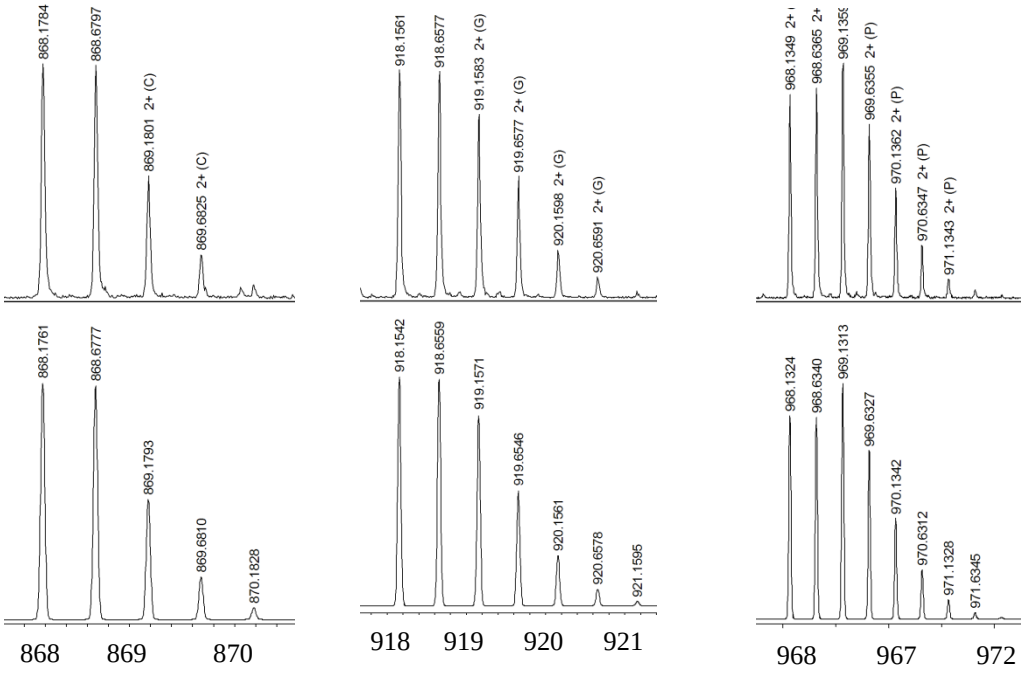

***A7**: The experimental (top) and simulated (bottom) MS showing evidence of $[Co_2\mathbf{L6}_3]^{2+}$, $[Co_2\mathbf{L6}_3][ClO_4]^{3+}$ and $[Co_2\mathbf{L6}_3][ClO_4]_2^{2+}$ species which are shown left to right respectively.*

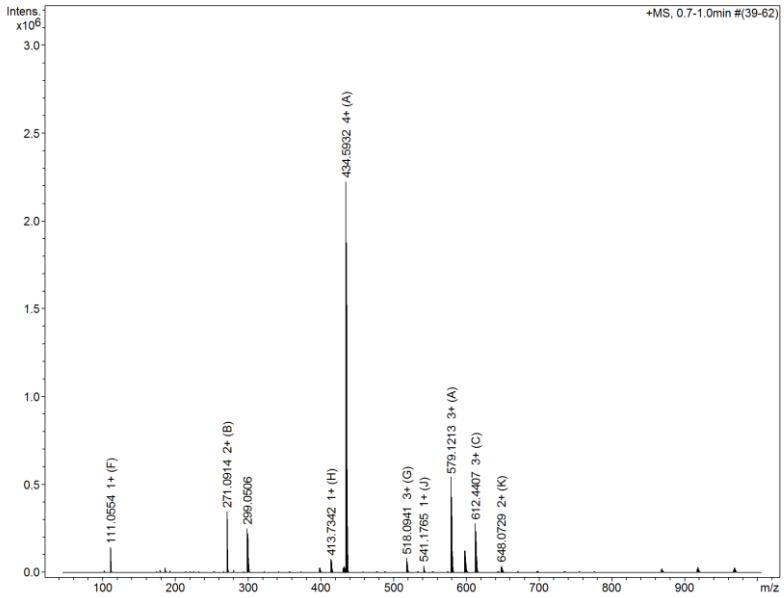

***A8**: The MS spectrum showing $[Ni_2\mathbf{L6}_3]^{4+}$ species*

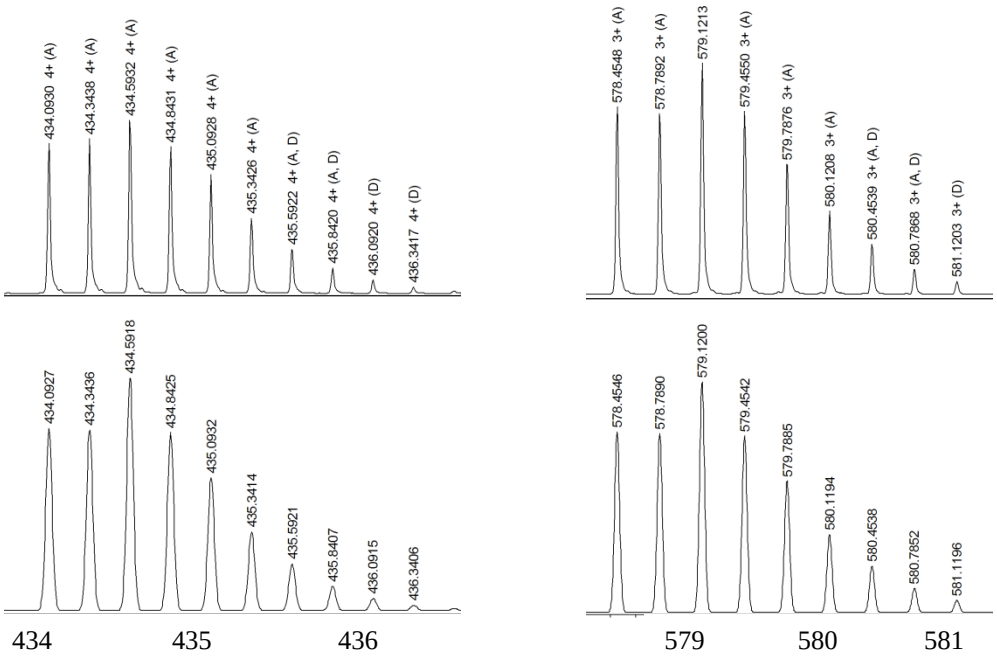

***A9**: The experimental (top) and simulated (bottom) MS showing evidence of $[Ni_2\mathbf{L6}_3]^{4+}$ and $[Ni_2\mathbf{L6}_3]^{3+}$ complexes, shown left to right respectively*

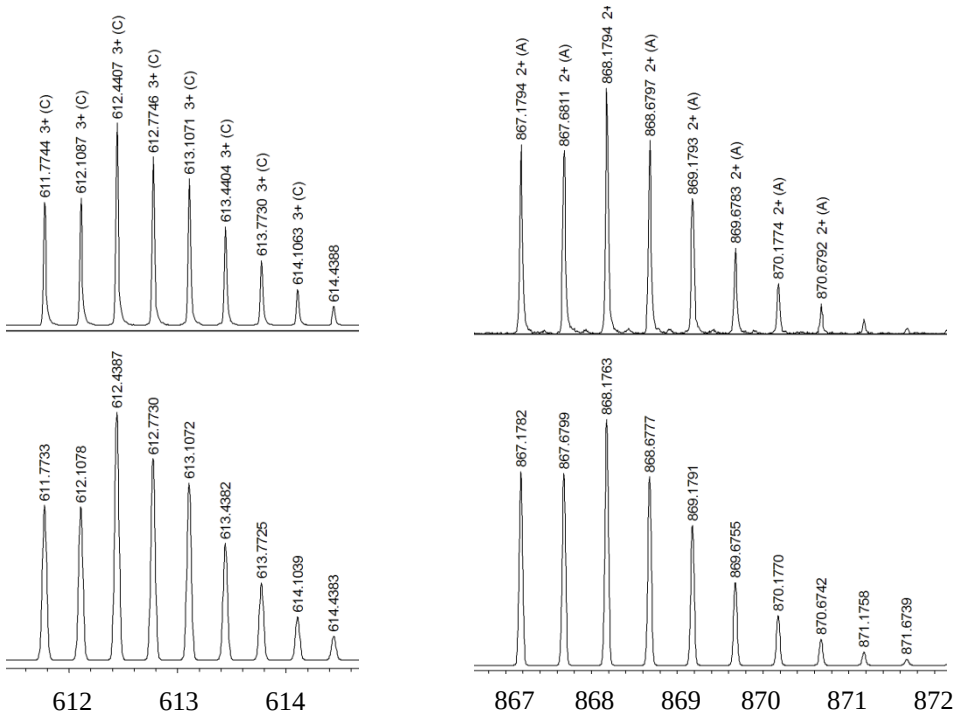

***A10**: The experimental (top) and simulated (bottom) MS showing the $[Ni_2\mathbf{L6}_3][ClO_4]^{3+}$ and $[Ni_2\mathbf{L6}_3]^{2+}$ species, shown left to right respectively.*

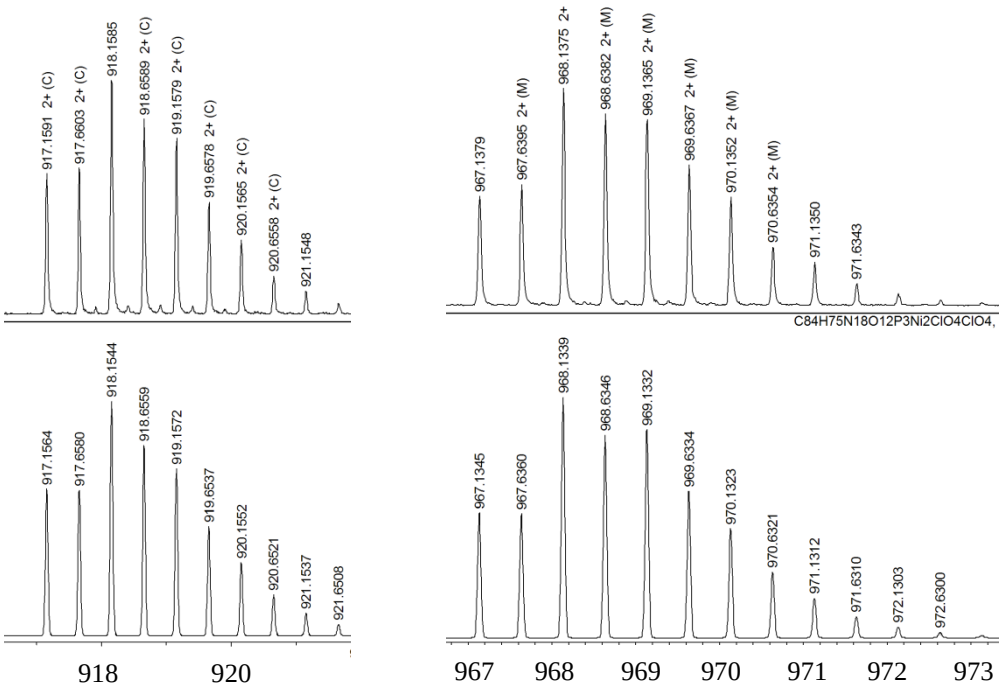

A11: *The experimental (top) and simulated (bottom) MS showing the* $[Ni_2\mathbf{L6}_3][ClO_4]^{3+}$ *and* $[Ni_2\mathbf{L6}_3][ClO_4]_2^{2+}$ *species, shown left to right respectively.*

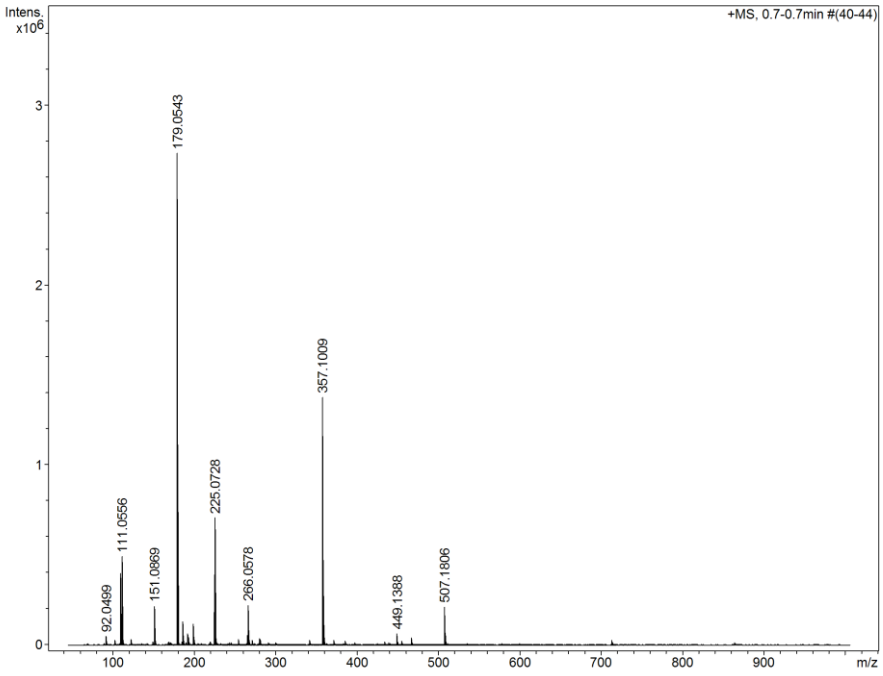

A12*: The MS spectrum of* $[Fe_2\mathbf{L6}_3]^{4+}$

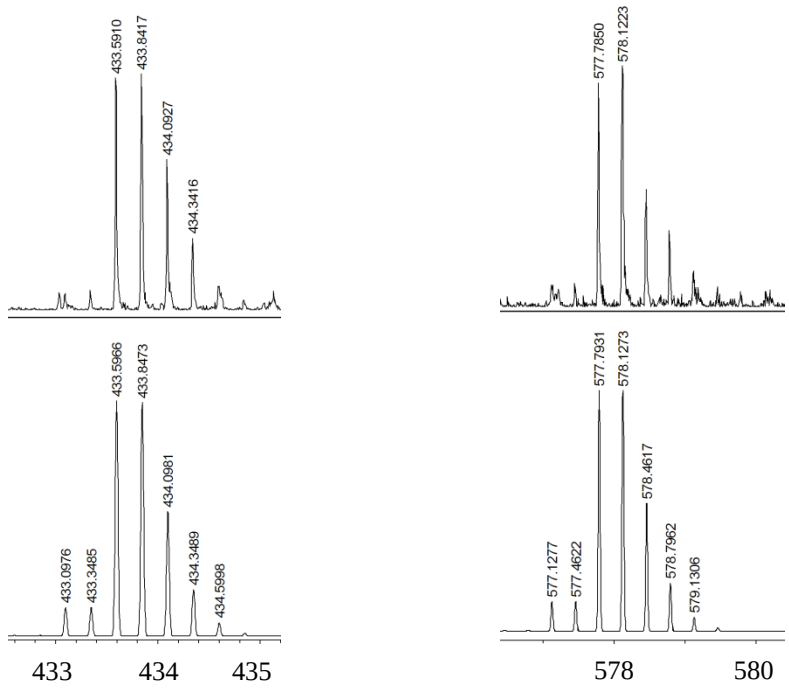

***A13**: The experimental (top) and simulated (bottom) MS peaks showing evidence of $[Fe_2\mathbf{L6}_3]^{4+}$ and $[Fe_2\mathbf{L6}_3]^{3+}$ species, shown left to right respectively.*

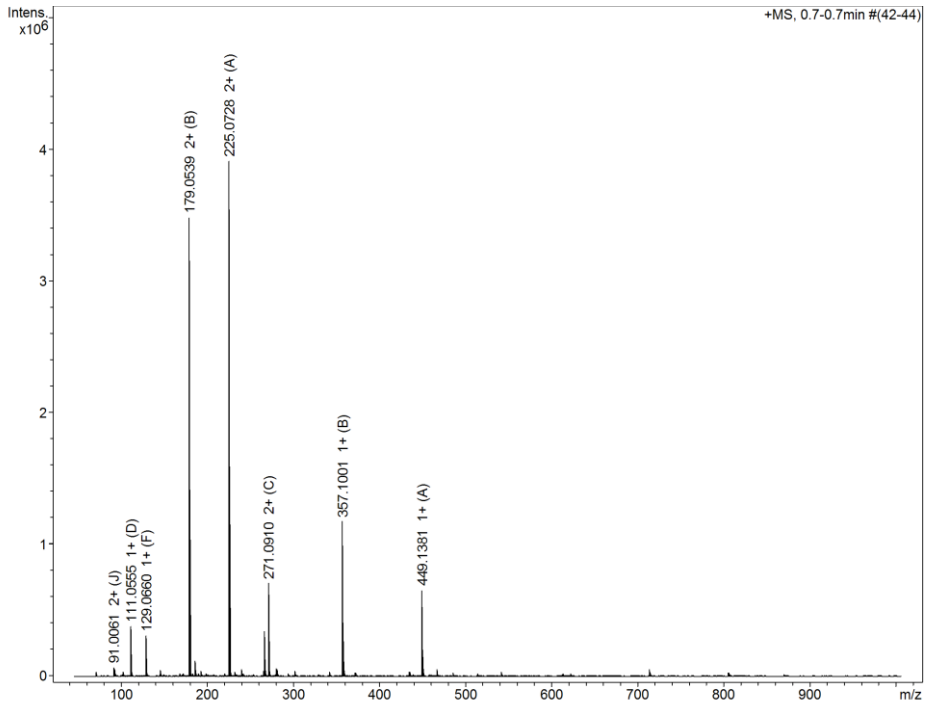

***A14**: The MS spectrum of $[Co_2\mathbf{L7}_3]^{4+}$ collected in acetonitrile.*

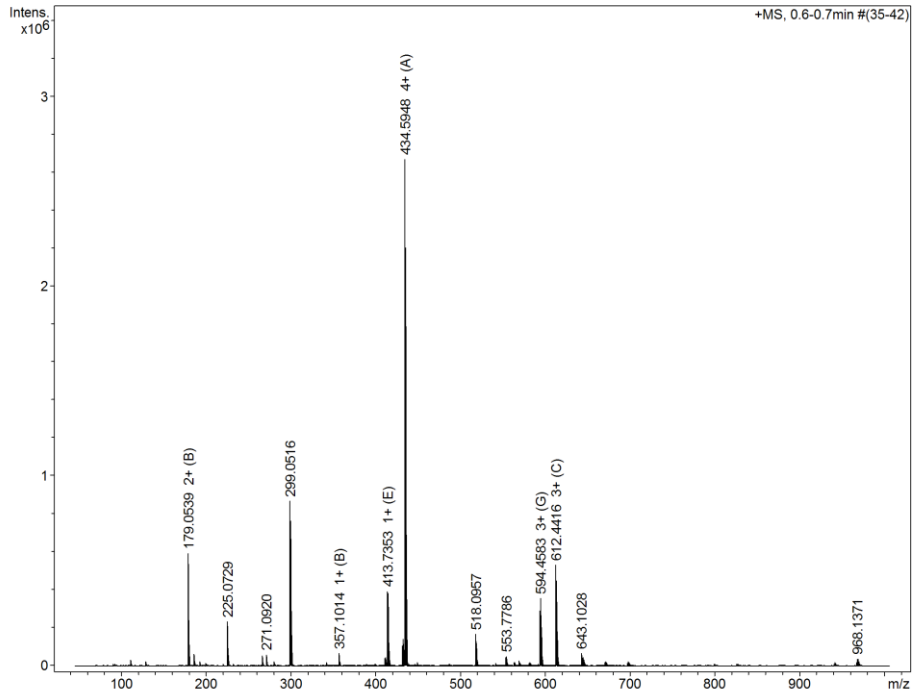

***A15**: The MS spectrum of complex $[Ni_2\mathbf{L7}_3]^{4+}$ complex*

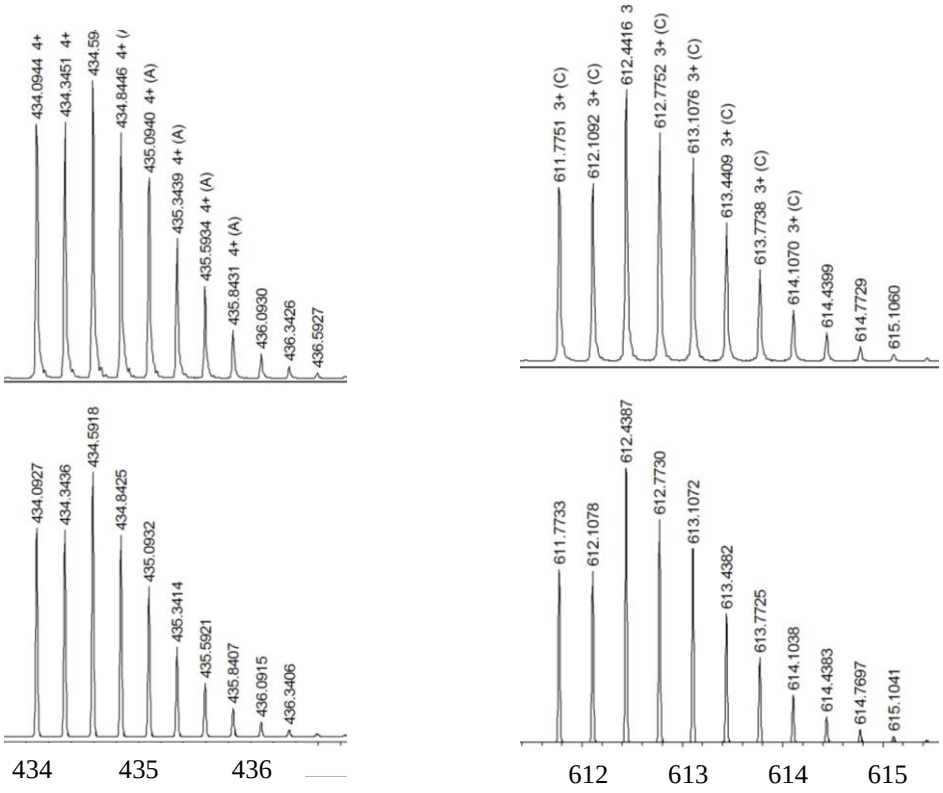

***A16**: The experimental (top) and simulated (bottom) MS spectrum showing evidence of $[Ni_2\mathbf{L7}_3]^{4+}$ and $[Ni_2\mathbf{L7}_3][ClO_4]^{3+}$ species, shown left to right respectively.*

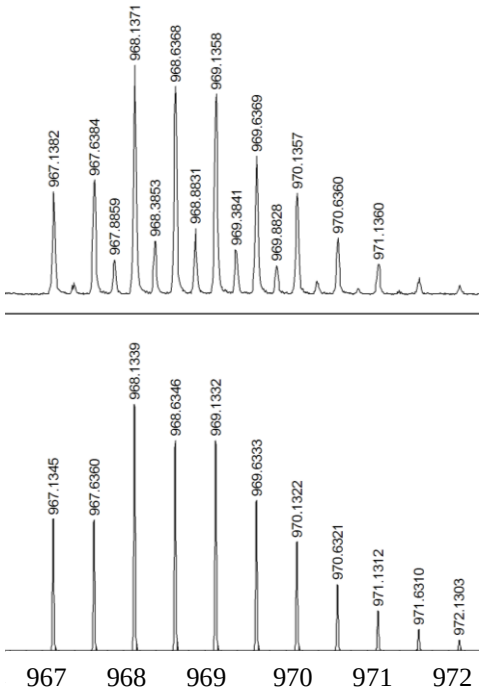

***A17**: The experimental (top) and simulated (bottom) MS spectrum of $[Ni_2\mathbf{L7}_3][ClO_4^-]_2^{2+}$ species.*

Appendix 2: Crystallographic refinement data

Table 1: *Crystallographic refinement data for [Fe(OH$_2$)][Fe$_2$(**L3**)$_3$], [Co(OH$_2$)$_6$][Co(**L4**)$_3$] and [Ni(OH$_2$)$_6$][Ni(**L4**)$_3$]*

Compound	[Fe(OH$_2$)][Fe$_2$(**L3**)$_3$]	[Co(OH$_2$)$_6$][Co(**L4**)$_3$]	[Ni(OH$_2$)$_6$][Ni(**L4**)$_3$]
Chemical formula	[FeO$_6$H$_{12}$] [C$_{66}$H$_{54}$Fe$_2$N$_{18}$O$_{21}$S$_6$]	[CoO$_6$] [C$_{66}$H$_{54}$Co$_2$N$_{18}$O$_{21}$S$_6$]	[NiO$_6$] [C$_{66}$H$_{54}$Fe$_2$N$_{18}$O$_{21}$S$_6$]
Formula mass			
Crystal system	Orthorhombic	Monoclinic	Monoclinic
Space group	*Pbca*	P2$_1$/*c*	P2$_1$/*c*
Crystal size / mm	0.05 x 0.05 x 0.01	0.12 x 0.1 x 0.02	0.05 x 0.05 x 0.01
Crystal colour	Red, plate	Brown, plate	Brown, plate
a/Å	25.441 (5)	26.585 (5)	26.523 (5)
b/Å	24.831 (5)	28.811 (6)	28.404 (6)
c/Å	32.440 (7)	24.342 (5)	24.317 (5)
α/°	90	90	90
β/°	90	94.94(3)	95.31(3)
γ/°	90	90	90
Unit Cell Volume/ Å^3	20493 (7)	18575 (7)	18235 (6)
Temperature/K	120	120	120
Z	8	8	8
Radiation type	Synchrotron	Synchrotron	Synchrotron
Absorption coefficient, μ/mm^{-1}	0.61	0.74	0.83
No. of reflections measured	275406	171508	191816
No. of independent reflections	19929	43482	51542
R_{int}	0.166	0.078	0.100
Final R1 values (I>2σ(I))	0.147	0.198	0.159
Final wR(F2) values (I>2σ(I))	0.394	0.548	0.472

Table 2: *Crystallographic refinement data for $K_2[Fe(\mathbf{L3})_3]$, $[Fe(OH_2)_6]_{0.2}Rb_{1.6}[Fe(\mathbf{L3})_3]$ and $Ca[Fe(\mathbf{L3})_3]$*

Compound	$K_2[Fe(\mathbf{L3})_3]$	$[Fe(OH_2)_6]_{0.2}Rb_{1.6}[Fe(\mathbf{L3})_3]$	$Ca[Fe(\mathbf{L3})_3]$
Chemical formula	K_2 $[C_{66}H_{54}Fe_2N_{18}O_{21}S_6]$	$[FeO_6]_{0.2}Rb_{1.6}$ $[C_{66}H_{54}Fe_2N_{18}O_{21}S_6]$	Ca $[C_{66}H_{54}Fe_2N_{18}O_{21}S_6]$
Formula mass			
Crystal system	Orthorhombic	Orthorhombic	Orthorhombic
Space group	*Pbca*	*Pbca*	*Pbca*
Crystal size / mm	0.16 x 0.04 x 0.01	0.19 x 0.05 x 0.03	0.18 x 0.06 x 0.03
Crystal colour	Red, plate	Red, needle	Orange, needle
a/Å	26.5836 (10)	26.5705 (7)	26.1452 (12)
b/Å	24.9392 (7)	24.9460 (5)	24.9823 (7)
c/Å	32.4238 (13)	32.4460 (8)	32.4684 (6)
α/°	90	90	90
β/°	90	90	90
γ/°	90	90	90
Unit Cell Volume/ $Å^3$	21496.0 (13)	21506.1 (9)	21207.4 (12)
Temperature/K	120	120	120
Z	8	8	8
Radiation type	Cu Kα	Cu Kα	Cu Kα
Absorption coefficient, μ/mm^{-1}	4.47	4.87	4.25
No. of reflections measured	91525	152685	106490
No. of independent reflections	6360	21638	13919
R_{int}	0.193	0.162	0.104
Final R1 values (I>2σ(I))	0.144	0.102	0.116
Final wR(F2) values (I>2σ(I))	0.422	0.333	0.364

Table 3: *Crystallographic refinement data for Bis(4-nitrophenyl) phenyl phosphate, Bis(4-aminophenyl) phenyl phosphate (**L2**) and* $[Co_2\mathbf{L6}_3]^{4+}$

Compound	*Bis*(4-nitrophenyl) phenyl phosphate	*Bis(4-aminophenyl) phenyl phosphate, **L2***	$[Co_2\mathbf{L6}_3]^{4+}$
Chemical formula	$C_{18}H_{13}N_2O_8P$	$C_{18}H_{17}N_2O_4P$	$C_{66}H_{57}Co_2N_{18}O_{12}P_3.3(ClO_4)$
Formula mass	416.27	356.30	1803.41
Crystal system	Trilinic	Triclinic	Hexagonal
Space	*P-1*	*P-1*	*P*-62*c*
Crystal size / mm	0.7 x 0.5 x 0.4	0.77 x 0.44 x 0.33	0.08 x 0.05 x 0.04
Crystal colour	Orange, block	Orange, block	Orange, Block
a/Å	8.3364(5)	9.4256(6)	13.5101(14)
b/Å	9.7124(7)	9.7196(6)	13.5101(14)
c/Å	11.2907(8)	10.1519(6)	40.752(5)
α/°	96.973(6)	66.998(5)	90.0
β/°	110.238(6)	77.600(5)	90.0
γ/°	90.361(5)	83.986(5)	120.0
Unit Cell Volume/ $Å^3$	850.24(11)	835.90(9)	6442(1)
Temperature/K	120.01(10)	120	120
Z	2	2	2
Radiation type	Cu Kα	Mo Kα	Cu Kα
Absorption coefficient, μ/mm^{-1}	1.949	0.19	3.40
No. of reflections measured	5984	6601	46066
No. of independent reflections	3036	3411	4417
R_{int}	0.0648	0.021	0.275
Final R1 values (I>2σ(I))	0.0414	0.041	0.089
Final wR(F2) values (I>2σ(I))	0.0525	0.103	0.368

References:

1. Lehn, J. M. *Angew Chem Int Ed Engl* **1988,** *27*, 89-112.
2. Tunstad, L. M.; Tucker, J. A.; Dalcanale, E.; Weiser, J.; Bryant, J. A.; Sherman, J. C.; Helgeson, R. C.; Knobler, C. B.; Cram, D. J. *J. Org. Chem.* **1989,** *54* (6), 1305-12.
3. Lehn, J. M.; Sauvage, J. P. *J. Am. Chem. Soc.* **1975,** *97* (23), 6700-7.
4. Pedersen, C. J. *Science* **1988,** *241* (4865), 536-40.
5. Steed, J. W.; Atwood, J. L.; Gale, P. A. In *Definition and emergence of supramolecular chemistry*, John Wiley & Sons Ltd.: 2012; pp 3-7.
6. Lopez, N.; Vos, T. E.; Arif, A. M.; Shum, W. W.; Noveron, J. C.; Miller, J. S. *Inorg. Chem.* **2006,** *45* (11), 4325-4327.
7. Ireta, J.; Neugebauer, J.; Scheffler, M. *J. Phys. Chem. A* **2004,** *108* (26), 5692-5698.
8. Seto, C. T.; Whitesides, G. M. *J. Am. Chem. Soc.* **1993,** *115* (3), 905-16.
9. Coulocheri, S. A.; Pigis, D. G.; Papavassiliou, K. A.; Papavassiliou, A. G. *Biochimie* **2007,** *89* (11), 1291-1303.
10. Zarra, S.; Smulders, M. M. J.; Lefebvre, Q.; Clegg, J. K.; Nitschke, J. R. *Angew. Chem., Int. Ed.* **2012,** *51* (28), 6882-6885
11. Russell, V. A.; Etter, M. C.; Ward, M. D. *J. Am. Chem. Soc.* **1994,** *116* (5), 1941-52.
12. Cozzi, F.; Ponzini, F.; Annunziata, R.; Cinquini, M.; Siegel, J. S. *Angew. Chem., Int. Ed. Engl.* **1995,** *34* (9), 1019-20.
13. Hunter, C. A.; Sanders, J. K. M. *J. Am. Chem. Soc.* **1990,** *112* (14), 5525-34.
14. Martinez, C. R.; Iverson, B. L. *Chem. Sci.* **2012,** *3* (7), 2191-2201.
15. Steel, P. J. *Chem. N. Z.* **2003,** *67* (2), 57-60.
16. Garnovskii, A. D.; Sennikova, E. V.; Kharisov, B. I. *Inorg. Chem. J.* **2009,** *3*, 1-20.
17. Barry, N. P. E.; Sadler, P. J. *Pure Appl. Chem.* **2014,** *86* (12), 1897-1910.
18. Housecroft, C. E.; Sharpe, A. G. *Inorganic Chemistry*. Pearson Education Ltd: 3 Ed, 2008.

19. Fang, J.; Guo, X.; Harada, S.; Watari, T.; Tanaka, K.; Kita, H.; Okamoto, K. *Macromolecules* **2002,** *35* (24), 9022-9028.

20. Ward, M. D. *Chem. Commun.* **2009,** (30), 4487-4499.

21. Turega, S.; Whitehead, M.; Hall, B. R.; Haddow, M. F.; Hunter, C. A.; Ward, M. D. *Chem. Commun.* **2012,** *48* (22), 2752-2754.

22. MacGillivray, L. R.; Atwood, J. L. *Angew. Chem., Int. Ed.* **1999,** *38* (8), 1018-1033.

23. Tasiopoulos, A. J.; Vinslava, A.; Werndorfer, W.; Abboud, K. A.; Christou, G. *Angew. Chem., Int. Ed.* **2004,** *43* (16), 2117-2121.

24. Riddell, I. A.; Smulders, M. M. J.; Clegg, J. K.; Hristova, Y. R.; Breiner, B.; Thoburn, J. D.; Nitschke, J. R. *Nat. Chem.* **2012,** *4* (9), 751-756.

25. Seidel, S. R.; Stang, P. J. *Acc. Chem. Res.* **2002,** *35* (11), 972-983.

26. Zhao, C.; Toste, F. D.; Raymond, K. N.; Bergman, R. G. *J. Am. Chem. Soc.* **2014,** *136* (41), 14409-14412.

27. Cullen, W.; Turega, S.; Hunter, C. A.; Ward, M. D. *Chem. Sci.* **2015,** *6* (1), 625-631.

28. Mal, P.; Breiner, B.; Rissanen, K.; Nitschke, J. R. *Science* **2009,** *324* (5935), 1697-1699.

29. Browne, C.; Brenet, S.; Clegg, J. K.; Nitschke, J. R. *Angew Chem Int Ed Engl* **2013,** *52* (7), 1944-8.

30. Jimenez-Molero, M. C.; Dietrich-Buchecker, C.; Sauvage, J.-P. *Chem. Commun.* **2003,** (14), 1613-1616.

31. Ronson, T. K.; Zarra, S.; Black, S. P.; Nitschke, J. R. *Chem. Commun.* **2013,** *49* (25), 2476-2490.

32. Lawrence, D. S.; Jiang, T.; Levett, M. *Chem. Rev.* **1995,** *95* (6), 2229-60.

33. Hasenknopf, B.; Lehn, J.-M.; Boumediene, N.; Leize, E.; Van Dorsselaer, A. *Angew. Chem., Int. Ed.* **1998,** *37* (23), 3265-3268.

34. Riddell, I. A.; Hristova, Y. R.; Clegg, J. K.; Wood, C. S.; Breiner, B.; Nitschke, J. R. *J. Am. Chem. Soc.* **2013,** *135* (7), 2723-2733.

35. Xu, L.; Chen, X. T.; Xu, Y.; Zhu, D. R.; You, X. Z.; Weng, L. H. *J. Mol. Struct.* **2001,** *559* (1-3), 361-368.

36. Jansze, S. M.; Cecot, G.; Wise, M. D.; Zhurov, K. O.; Ronson, T. K.; Castilla, A. M.; Finelli, A.; Pattison, P.; Solari, E.; Scopelliti, R.; Zelinskii, G. E.; Vologzhanina, A. V.; Voloshin, Y. Z.; Nitschke, J. R.; Severin, K. *J. Am. Chem. Soc.* **2016,** *138* (6), 2046-2054.

37. Northrop, B. H.; Zheng, Y.-R.; Chi, K.-W.; Stang, P. J. *Acc Chem Res* **2009,** *42* (10), 1554-63.

38. Watson, J. D.; Crick, F. H. C. *Nature (London, U. K.)* **1953,** *171*, 737-8.

39. Lehn, J. M.; Rigault, A.; Siegel, J.; Harrowfield, J.; Chevrier, B.; Moras, D. *Proc. Natl. Acad. Sci. U. S. A.* **1987,** *84* (9), 2565-9.

40. Piguet, C.; Bernardinelli, G.; Hopfgartner, G. *Chem. Rev.* **1997,** *97* (6), 2005-2062.

41. Hannon, M. J.; Childs, L. J. *Supramol. Chem.* **2004,** *16* (1), 7-22.

42. Albrecht, M. *Chem. - Eur. J.* **2000,** *6* (19), 3485-3489.

43. Bousseksou, A.; Molnar, G.; Salmon, L.; Nicolazzi, W. *Chem. Soc. Rev.* **2011,** *40* (6), 3313-3335.

44. Achim, C. *J. Am. Chem. Soc.* **2005,** *127* (3), 1061.

45. Real, J. A.; Gaspar, A. B.; Munoz, M. C. *Dalton Trans.* **2005,** (12), 2062-2079.

46. Turnbull, M. M.; Sugimoto, T.; Thompson, L. K. *Molecule-Based Magnetic Materials*. American Chemical Society 1996.

47. Carlin, R. L. *Magnetochemistry*. Springer-Verlag: 1986.

48. Raymo, F. M.; Stoddart, J. F. *Chem. Ber.* **1996,** *129* (9), 981-990.

49. Sunatsuki, Y.; Ohta, H.; Kojima, M.; Ikuta, Y.; Goto, Y.; Matsumoto, N.; Iijima, S.; Akashi, H.; Kaizaki, S.; Dahan, F.; Tuchagues, J.-P. *Inorg. Chem.* **2004,** *43* (14), 4154-4171.

50. Kulmaczewski, R.; Olguin, J.; Kitchen, J. A.; Feltham, H. L. C.; Jameson, G. N. L.; Tallon, J. L.; Brooker, S. *J. Am. Chem. Soc.* **2014,** *136* (3), 878-881.

51. Hawes, C. S.; Kruger, P. E. *Polyhedron* **2013,** *52*, 255-260.

52. Hawes, C. S.; Fitchett, C. M.; Kruger, P. E. *Supramol. Chem.* **2012,** *24* (8), 553-562.

53. Goetz, S.; Kruger, P. E. *Dalton Trans.* **2006,** (10), 1277-1284.

54. Keegan, J.; Kruger, P. E.; Nieuwenhuyzen, M.; O'Brien, J.; Martin, N. *Chem. Commun.* **2001,** (21), 2192-2193.

55. Keegan, J.; Kruger, P. E.; Nieuwenhuyzen, M.; Martin, N. *Cryst. Growth Des.* **2002,** *2* (5), 329-332.

56. Archer, R. J.; Hawes, C. S.; Jameson, G. N. L.; McKee, V.; Moubaraki, B.; Chilton, N. F.; Murray, K. S.; Schmitt, W.; Kruger, P. E. *Dalton Trans.* **2011,** *40* (45), 12368-12373.

57. Giri, C.; Sahoo, P. K.; Puttreddy, R.; Rissanen, K.; Mal, P. *Chem. - Eur. J.* **2015,** *21* (17), 6390-6393.

58. Mal, P.; Nitschke, J. R. *Chem. Commun. (Cambridge, U. K.)* **2010,** *46* (14), 2417-2419.

59. Pelleteret, D.; Clerac, R.; Mathoniere, C.; Harte, E.; Schmitt, W.; Kruger, P. E. *Chem. Commun.* **2009,** (2), 221-223.

60. Feng, G.; Liu, W.; Peng, Y.; Zhao, B.; Huang, W.; Dai, Y. *Chem. Commun.* **2016,** *52* (59), 9267-9270.

61. Lipmann, F.; Tuttle, L. C. *J. Biol. Chem.* **1944,** *153*, 571-82.

62. Onoda, A.; Yamada, Y.; Doi, M.; Okamura, T.-a.; Ueyama, N. *Inorg. Chem.* **2001,** *40* (3), 516-521.

63. Cote, A. P.; Shimizu, G. K. H. *Coord. Chem. Rev.* **2003,** *245* (1-2), 49-64.

64. Dalrymple, S. A.; Shimizu, G. K. H. *Chem. Commun.* **2002,** (19), 2224-2225.

65. Ren, D.-H.; Sun, X.-L.; Gu, L.; Qiu, D.; Li, Z.; Gu, Z.-G. *Inorg. Chem. Commun.* **2015,** *51*, 50-54.

66. Wei, R.-J.; Li, B.; Tao, J.; Huang, R.-B.; Zheng, L.-S.; Zheng, Z. *Inorg. Chem.* **2011,** *50* (4), 1170-1172.

67. Agusti, G.; Belen Gaspar, A.; Munoz, M. C.; Real, J. A. *Inorg. Chem.* **2007,** *46* (23), 9646-9654.

68. Hamon, P.; Thepot, J.-Y.; Le Floch, M.; Boulon, M.-E.; Cador, O.; Golhen, S.; Ouahab, L.; Fadel, L.; Saillard, J.-Y.; Hamon, J.-R. *Angew. Chem., Int. Ed.* **2008,** *47* (45), 8687-8691.

69. Spingler, B.; Schnidrig, S.; Todorova, T.; Wild, F. *CrystEngComm* **2012,** *14* (3), 751-757.

70. Halcrow, M. A. *Chem. Soc. Rev.* **2011,** *40* (7), 4119-4142.

71. Oliver, J. D.; Mullica, D. F.; Hutchinson, B. B.; Milligan, W. O. *Inorg. Chem.* **1980,** *19*, 165-169.

72. Kremer, S.; Henke, W.; Reinen, D. *Inorg. Chem.* **1982,** *21* (8), 3013-22.

73. Kime, N. E.; Ibers, J. A. *Acta Cryst.* **1969,** *B25*, 168.

74. van der Veen, I.; de Boer, J. *Chemosphere* **2012,** *88* (10), 1119-1153.

75. Murugavel, R.; Choudhury, A.; Walawalkar, M. G.; Pothiraja, R.; Rao, C. N. R. *Chem. Rev.* **2008,** *108* (9), 3549-3655.

76. Yu, K.; Wan, B.; Yu, Y.; Wang, L.; Su, Z.-h.; Wang, C.-m.; Wang, C.-x.; Zhou, B.-B. *Inorg. Chem.* **2013,** *52* (1), 485-498.

77. Zhang, X.; Yi, Z.; Zhao, L.; Chen, Q.; Wang, X.; Xu, J.; Xia, W.; Yang, C. *CrystEngComm* **2010,** *12* (2), 595-603.

78. Yamada, H.; Maeda, K.; Yashima, E. *Chem. - Eur. J.* **2009,** *15* (28), 6794-6798.

79. Williams, N. H.; Cheung, W.; Chin, J. *J. Am. Chem. Soc.* **1998,** *120* (32), 8079-8087.

80. Kosolapoff, G. M.; McCullough, J. F. *J. Am. Chem. Soc.* **1951,** *73*, 5392-3.

81. Li, F.; Yang, X.; Li, X.; Li, R.; Zhao, J.; Wu, H. *Chem. Res. Toxicol.* **2014,** *27* (11), 1918-1925.

82. Zhang, T.-t.; Men, W.-w.; Liu, Y.; Lu, Z.-j. *Chin. J. Polym. Sci.* **2012,** *30* (2), 250-257.

83. Mastalerz, M. *Angew. Chem., Int. Ed.* **2010,** *49* (30), 5042-5053.

84. Ayme, J.-F.; Beves, J. E.; Leigh, D. A.; McBurney, R. T.; Rissanen, K.; Schultz, D. *J. Am. Chem. Soc.* **2012,** *134* (22), 9488-9497.

85. Zhou, P.; Wang, C.; Qiu, Q.-m.; Yao, J.-f.; Sheng, C.-f.; Li, H. *Dalton Trans.* **2015,** *44* (40), 17810-17818.

86. Wu, B.; Huo, C.; Li, S.; Zhao, Y.; Yang, X.-J. *Z. Anorg. Allg. Chem.* **2015,** *641* (10), 1786-1791.

87. Harvey, B. G.; Chafin, A. C.; Garrison, M. D.; Cambrea, L. R.; Groshens, T. J. *RSC Adv.* **2015,** *5* (91), 74712-74719.

88. Agilent. *CrysAlis PRO. Agilent Technologies Ltd, Yarnton, Oxforshire, England* **2014**.

89. McPhillips, T. M.; McPhillips, S. E.; Chiu, H. J.; Cohen, A. E.; Deacon, A. M.; Ellis, P. J.; Garman, E.; Gonzalez, A.; Sauter, N. K.; Phizazkerley, R. P.; Soltis, S. M.; Kuhn, P. *J. Synchrotron Rad.* **2002,** *9*, 401-406.

90. Kabsch, W. *J. Appl. Cryst* **1993,** *26*, 795-800.

91. Sheldrick, G. M. *Acta Cryst.* **2015,** *A71*, 3-8.

92. Sheldrick, G. M. *Acta Cryst.* **2015,** *C71*, 3-8.

93. Dolomanov, O. V.; Bourhis, L. J.; Gildea, R. J.; Howard, J. A. K.; Puschmann, H. *J. Appl. Cryst.* **2009,** *42*, 339-341.